PREPARATION AND CHARACTERIZATION OF STARCH NANOPARTICLES FOR DELIVERY OF HISTONE DEACETYLASE INHIBITOR CG-1521 IN BREAST CANCER TREATMENT

MEME KANSERİ TEDAVİSİ İÇİN CG-1521 HİSTON DEASETİLAZ İNHİBİTÖRÜ YÜKLÜ NİŞASTA NANOPARTİKÜLLERİN HAZIRLANMASI VE KARAKTERİZASYONU

ESMA ALP

ASSOC. PROF. DR. EYLEM GÜVEN
Supervisor

Submitted to
Graduate School of Science and Engineering of Hacettepe University
as a Partial Fulfillment to the Requirements
for the Award of the DOCTOR OF PHILOSOPHY in
Nanotechnology and Nanomedicine.

2021

ABSTRACT

PREPARATION AND CHARACTERIZATION OF STARCH NANOPARTICLES FOR DELIVERY OF HISTONE DEACETYLASE INHIBITOR CG-1521 IN BREAST CANCER TREATMENT

Esma ALP

Doctor of Philosophy, Department of Nanotechnology and Nanomedicine

Supervisor: Assoc.Prof. Dr. Eylem Güven
June 2021, 85 pages

Starch nanoparticles offer many possibilities in drug delivery systems due to their biocompatibility and appropriate physicochemical properties. Sufficient systems have not yet been designed to deliver histone deacetylase inhibitors due to their poor solubility. These inhibitors are the novel therapeutic agents used for the treatment of several cancer's types including breast cancer. The low solubility of the histone deacetylase inhibitors significantly reduces their bioavailability and therapeutic indices. In this study, biocompatible starch nanoparticles have been synthesized to improve the sub-optimal therapeutic index of the CG-1521. Physicochemical properties of nanoparticles (size, zeta potential, morphology, drug loading, and release) were optimized. The fabricated nanoparticles possess the required optimal average size (180 nm) and polydispersity index (0.138) for enhanced permeability and retention for

tumor targeting. Slightly negative zeta potential (-16.2 mV) of nanoparticles provides electro-kinetics stability and minimum aggregation. The scanning electron and atomic force microscopies analyses indicates that nanoparticles had spherical topographies and homogeneous distribution which is important for the fate of nanoparticles for cellular uptake. The spherical shape of nanoparticles provides faster internalization rates results in higher uptake. The physical characterization of nanoparticles followed by substantially high encapsulation efficiency (~69%) of drug. The encapsulation process reduces the rate of release of drug resulted in extended exposure to the drug. The faster drug release of encapsulated drug in acidic environment promotes more accumulation of drug in tumor site. In this study, the release of drug from nanoparticles in acidic environment exhibited additional release (16%) of encapsulated drug. The cytotoxic and apoptotic capacities of nanoparticles were investigated using MCF-7 breast cancer cells. The cytotoxic studies results demonstrated that at the equivalent concentration the encapsulated drug was more effective at inducing cell death. The apoptosis results confirmed that the encapsulated drug show significant apoptotic effect (60.45% apoptotic cells) in comparison free drug (28.45%) The cell cycles analysis demonstrated that treatment with the same concentration of encapsulaed drug significantly increase the cell proportion at the G1 phase (53.0%) compare to G1 population (49.5%) treated with free drug. G1/S arrest is most likely due the stabilization of acetylated isoform of p53 gene. To evalute the targeting potential of nanoparticles, the cytotoxic effects of Folic Acid–modified nanoparticles on MCF-7 and MDA-MB-231 breast cancer cell lines were investigated. The results showed that the response of triple negative cell line MDA-MB-231 was more sensitive to modified formulation than MCF-7 cell line. The higher sensitivity is due the more aggressiveness of MDA-MB-231 cells and higher expression level of folate receptors compared to MCF-7 cells. The biological mechanism of drug-loaded nanoparticles at the molecular level has been evaluated using real-time quantitative PCR. The transcripts level of several genes involves in cell death, apoptosis, cell cycle and spindle formation were measured after treatments with free and encapsulated for 48 hours. The expression levels of majority of the transcripts used in the study showed a similar trend of upregulation or downregulation after interaction with

the same dose of free and encapsulated drug. These results confirmed that the molecular activity of drug did not alter with the encapsulation process of drug. Within the scope of this study, the nanoencapsulation of CG-1521 significantly reduces the release of drug over time and increases its cytotoxic activity relative to the free drug at the same concentration. Moreover, CG-1521 encapsulated nanoparticles significantly induce cell cycle arrest and apoptosis in MCF-7 cells. This study demonstrates that starch nanoparticles may be a suitable and potential drug carrier candidate for histone deacetylase inhibitors in breast cancer treatment without interfering with the inhibitor's molecular activity.

KEYWORDS: Starch nanoparticles, drug delivery system, apoptosis, cell cycle arrest, histone deacetlylation, DNA fragmentation, breast cancer

ÖZET

MEME KANSERİ TEDAVİSİ İÇİN CG-1521 HİSTON DEASETİLAZ İNHİBİTÖRÜ YÜKLÜ NİŞASTA NANOPARTİKÜLLERİN HAZIRLANMASI VE KARAKTERİZASYONU

Esma ALP

Doktora, Nanoteknoloji ve Nanotıp Anabilim Dalı

Danışman: Doç.Dr. Eylem Güven
Haziran 2021, 85 sayfa

Nişasta nanopartiküller, ilaç taşınım sistemlerinde biyouyumlulukları ve uygun fizikokimyasal özelliklerinden ötürü birçok olanak sunmaktadır. Epigenetik ilaçların, özellikle meme kanseri dahil birçok kanserin tedavisinde kullanılmaya başlanan yeni nesil terapötik ajanlar olan histon deasetilaz inhibitörlerinin taşınımı için tasarlanan sistemler bu inhibitörlerin zayıf çözünürlüklerinden dolayı yeterli değildir. Histon deasetilaz inhibitörlerinin yetersiz çözünürlükleri, biyoyararlanımlarını ve terapötik indekslerini oldukça düşürmektedir. Histon deasetilaz inhibitörleri sınıfına ait CG-1521 ajanının standart altı terapötik indeksinin iyileştirilmesi amacıyla biyouyumlu nişasta nanopartiküller sentezlenmiştir. Nanopartiküllerin fizikokimyasal özellikleri (boyut, zeta potansiyel, morfoloji, ilaç yükleme ve salım) optimize edilmiştir. Sentezlenen

nanopartiküller, tümör hedeflemede artmış geçirgenlik ve tutulma için gerekli optimal ortalama boyuta (180 nm) ve polidispersite indeksine (0.138) sahiptir. Nanopartiküllerin sahip olduğu hafif negatif zeta potansiyeli (-16.2 mV), elektro-kinetik stabilite ve minimum agregasyonu sağlar. Taramalı elektron ve atomik kuvvet mikroskobu analizleri, nanopartiküllerin küresel topografyalara ve homojen dağılıma sahip olduğunu gösterir ki, bu nanopartiküllerin hücresel alımları için önemlidir. Nanopartiküllerin küresel yapıları internalizasyon hızlarını artırıp daha fazla hücresel alım sağlar. Nanopartiküllerin fiziksel karakterizasyonu, ilacın oldukça yüksek enkapsüle verimliliği (~%69) ile devam etmiştir. Enkapsülasyon ilacın salınım hızını azaltıp ilaca daha uzun süre maruziyet sağlar. Asidik ortamda enkapsüle ilacın nanopartiküllerden salınımı, tümör bölgesinde daha fazla ilaç birikimini sağlar. Bu çalışmada, nanopartiküllerden ilacın salınımı asidik ortamda % 16 lık ek salım yüzdesi sağlamıştır. İlaç yüklü nanopartiküllerin sitotoksik ve apoptotik kapasiteleri MCF-7 meme kanseri hücreleri kullanılarak incelenmiştir. Sitotoksik çalışmaların sonuçları, eşdeğer konsantrasyonda, enkapsüle ilacın hücre ölümünü indüklemede daha etkili olduğunu göstermiştir. Apoptoz sonuçları, aynı konsantrasyonda enkapsüle ilacın apoptotik etkisinin (%60,45) serbest ilacın etkisine (%28,45) oranla önemli derecede arttığı gözlemlenmiştir. Hücre döngüsü analizi, eşit konsantrasyonda ilaç içeren nanopartiküllerle etkileştirilen hücrelerin G1 fazındaki hücre popülasyonun (%53,0) serbest ilaçla etkileştirilen hücrelerin G1 fazı popülasyona (%49,5) göre önemli ölçüde artış göstermiştir. G1/S fazında durdurulma büyük olasılıkla p53 geninin asetilenmiş izoformunun stabilizasyonundan kaynaklanmaktadır. Nanopartiküllerin hedefleme potansiyellerin incelenmesi için Folik Asit ile modifiye edilen nanopartiküllerin sitotoksik etkileri farklı hücre hatları üzerinde (MCF-7 ve MDA-MB-231) incelenmiştir. MDA-MB-231 üçlü negatif hücre hattının ilaç yüklü modifiye formülasyona olan yanıtının MCF-7 hücre hattından daha duyarlı olduğunu göstermiştir. Daha yüksek hassasiyet, MDA-MB-231 hücrelerinin daha agresif olmasından ve MCF-7 hücrelerine kıyasla daha fazla folat reseptörleri eksprese etmelerinden kaynaklanmaktadır.

İlaç yüklü nanopartiküllerin moleküler düzeydeki biyolojik mekanizması gerçek zamanlı kantitatif PCR kullanılarak incelenmiştir. Hücre ölümü, apoptoz, hücre

döngüsü ve iğ iplikçilerinin oluşumunda yer alan çeşitli genlerin trankskript düzeyleri serbest ve enkapsüle ilaç ile 48 saatlik etkileşimlerden sonra ölçülmüştür. Çalışmada kullanılan transkriptlerin çoğunluğunun ekspresyon düzeyleri , aynı doz serbest ve enkapsüle ilaçla etkileşimlerinden sonra benzer bir yukarı regülasyon veya aşağı regülasyon eğilimi göstermiştir. Bu sonuçlar, ilacın moleküler aktivitesinin enkapsülasyon işlemi ile değişmediğini doğrulamıştır. Bu çalışma kapsamında CG-1521'in nano enkapsülasyonu, ilacın salım hızını önemli derecede azaltmış ve eşit dozdaki serbest ilaca göre sitotoksik aktivitesini arttırmıştır. Ayrıca ilaç yüklü nanopartiküller, hücrelerin apoptoz ve hücre döngüsünü durdurma yeteneğini önemli ölçüde indüklemiştir. Yapılan bu çalışma, meme kanseri tedavisinde nişasta nanopartiküllerinin, histon deasetilaz inhibitörlerin moleküler mekanizmasını değiştirmeksizin uygun ve potansiyel bir ilaç taşıyıcı adayı olabileceğini göstermektedir.

ANAHTAR KELİMELER: Nişasta nanopartiküller, ilaç taşıyıcı sistemler, apoptoz, hücre döngüsünün durdurulması, histon deasetilazasyon, DNA fragmantasyonu, meme kanseri.

ACKNOWLEDGEMENTS

I would like to acknowledge my supervisor, Dr. Eylem Güven, for providing valuable guidance, mentoring as well as encouragement through my graduate career. I specially thank her to supervise me from long distance for a while despite the diffucult time differences. I would like to also acknowledge Dr. Martin Tenniswood for giving me many opportunities to make research enjoyable. I am grateful for giving me opportunity to work in his laboratory in the USA. His guidance and support at every meeting were invaluable for my reseach. Without his help and support, I would not have had such precious research experience. I would like to also acknowledge my committee members, Dr. Necdet Sağlam and Dr. Mesut Şam. Their discussion and suggestions during my committee meetings allowed me to design my experiments better and to investigate vital aspect of my project. I also deeply appreciated Dr. Fehmi Damkacı's help and support. I would like to thank employees and my lab-mates of Hacettepe University for their constant support. Thank you to Drs. Tamer Çırak, Tayfun Vural, Öznur Akbal, Ebru Erdal and Zeynep Karahaliloğlu. I would like to thank employees of SUNY-Cancer Research Center for their support during my studies. I will always be thankful to Drs. JoEllen Welsh, Douglas Conklin, Jason Herschkowitz, Judy Narvaez, Sarah Beaudin, Leila Kokabee and Brenda Trevizo-Barresi. Lastly, I would like to thank my parents, Rahim and Ayse Alp, my brothers, Bilal, Adem, Zübeyir Alp and my sister Emine Dagli. I have been lucky enough to have their unconditional support and help.

TABLE OF CONTENTS

FIGURES

TABLES

SYMBOLS AND ABBREVIATIONS

Abbreviations

7-AAD	Aminoactinomycin D
AFM	Atomic Force Microscopy
Br-dUTP	5-Bromo-2'-Deoxyuridine 5'-Triphosphate
BSA	Bovine Serum Albumin
CDI	1,1-carbonyl diimidazole
CV-Assay	Crystal Violet Assay
DAPI	4',6-diamidino-2-phenylindole
DLS	Dynamic Light Scattering
EPR	The enhanced permeability and retention
EtOH	Ethanol
FBS	Fetal bovine serum
FDA	The Food and Drug Administration
FITC	Fluorescein Isothiocyanate
FT-IR	Fourier transform infrared spectroscopy
HAT	Histone acetylase transferase
HDAC	Histone deacetylase
HDACi	Histone deacetylase inhibitor
IC50	The half-maximal inhibition concentration
DEE	Drug encapsulation efficiency
mA	Milliamps
mi-RNA	Micro RNA
μM	Micromolar
mM	Millimolar
mL	Milliliter
μL	Microliter
NHS	N-hydroxysuccinimide
nm	Nanometer
NMR	Nuclear Magnetic Resonance
PBS	Phosphate-buffered saline
PDI	Polydispersity Index

PGA	Poly (glycolic acid)
PI	Propodium iodide
PLA	Polylactic acid
PLGA	Poly (lactic-co-glycolic acid)
PPM	Parts per million
PSMA	Prostate-specific membrane antigen
RES	Reticuloendothelial system
RNase	Ribonuclease
rpm	Revolutions per minute
SEM	Scanning Electron Microscopy
siRNA	Small interfering RNA
SPIONS	Superparamagnetic iron oxide nanoparticles
USPIONS	Ultrasmall SPIONS
TdT	Terminal deoxyuridine transferase
TUNEL	TdT-dUTP nick-end-labeling
VEGF	Vascular endothelial growth factor
XIST RNA	X-inactive specific transcript RNA

1. INTRODUCTION

Breast cancer is the second most common cause of death among all cancers in women in the United States with an estimated 43,600 deaths in 2021 [1]. The majority of breast cancer deaths are the result of metastasis to distant areas. While surgery and radiotherapy have been applied for localized breast cancer treatment, chemotherapy and immunotherapy are used to treat metastatic breast cancers systemically. Several techniques, including nanotechnology, have been investigated to enhance the efficacy of anticancer agents while reducing systemic toxicity. Nanotechnology offers various formulations to defeat many biological barriers and target the specific tumor tissues for the delivery of therapeutics.

In recent years, different nanotransporters have been studied for the delivery of cancer therapeutics such as liposomes [2], hydrogels [3], solid lipid nanoparticles [4] and polymeric nanoparticles [5,6]. Polymer-based nanoparticles, including starch nanoparticles, have potential to to treat many diseases, including cancer, due to their flexible structure, their suitability for modification, and their existence in various compositions. These nanoparticles increase the solubility of hydrophobic drugs, enhance the local concentration of therapeutics in tumor sites and extend the half-life of drugs in the body. The anatomical changes around the tumor microenvironment (e.g., the leaking vascular system, the poor drainage in the lymphatic system) allow the particles to be retained for a long time and pass through the vascular system more efficiently. This effect is known EPR enhanced permeability and retention) effect [7, 8].

The encapsulation of cytotoxic drugs into polymeric nanoparticles helps to reduce the toxicity of antitumor drugs while enhancing the therapeutic effects. Polymeric nanoparticles, promising subunits of the nanocarriers, have been investigated as drug delivery systems for many different types of cancer. [9]. Gryparis et al. investigated the activities of cisplatin-loaded polimeric nanoparticles on LNCaP prostate cancer cells. In this study, it was determined that drug loaded carriers were effectively taken up by cells and showed a higher

cytotoxic effect than free cisplatin [10]. In another study, Mobasseri et al. investigated the effects of lapatinib, the tyrosine kinase inhibitor, loaded chitosan nanoparticles in breast cancer. Lapatinib-loaded nanoparticles showed a more potent cytotoxic effect after 48 h treatment in BT474 breast cancer cells in the comparision of treatment with free inhibitor alone [11].

Nanoparticles enable the encapsulation of chemotherapeutics, proteins, nucleic acids, and contrast agents for biomedical applications by using synthetic and natural polymers [12]. Polymers obtained from natural sources are useful in terms of their similar biogical and chemical properties with the extracellular matrix (EMC), ease in modification chemically, and non-immunological reaction in the body after their enzymatic degradation.

Polysaccharides including starch have not been studied extensively as drug carriers, even though they possess many benefits, such as blocking of non-specific protein adsorption, the ability for low-energy neutral coating [13] and modification with various ligands. Starch has been investigated as a therapautic delivery system due to their biocompatibility and biodegradability properties [14]. Starch nanoparticles have been studied to deliver ciprofloxacin [15], curcumin [16], and diclofenac sodium [17] using oxidation, cross-linking, or hydroxypropylation modifications, respectively. However, there are limited nanoformulation studies have reported on synthesis starch nanoparticles without any chemical modification [18].

The acetylation and deacetylation processes of histones controlled by histone acetylase transferase (HAT) and histone deacetylase (HDAC) enzymes play an essential role in regulating chromatin structure and transcription. The alterations such as mutation, amplification, or translocation in the functions of these enzymes have been shown in multiple cancer types [19,20].

Histone deacetylation inhibitors (HDACi’s) represent a class of new-generation agents that have been used in clinical trials as monotherapies or combined therapies against multiple cancers [21]. These therapeutics induce cell proliferation inhibition, arresting cell cycle, differentiation and induce apoptosis

by maintaining histone acetylation [22]. CG-1521 is one of the HDACi at the preclinical stage. Various studies have shown that CG-1521 inhibits cell growth and stabilizes acetylation of the tumor suppressive gene p53. This leads to cell cycle arrest in both solid and hematological cancers [23,24,25]. However, many studies have shown that therapeutic potentials of many HDACi's, including CG-1521, are restricted by their limited solubility and rapid metabolism in vivo [26, 27].

Encapsulation of these therapeutic agents increases the solubility of the drug and systematically prevents them from being metabolized rapidly. The nanoparticles are selectively accumulated in tumor sites, as they benefit from both their small size and the EPR effect.

The anatomical changes in tumor microenvironment play a key role for the passive targeting of encapsulated drugs to reach the tumor site. The changes also affect the pharmacokinetics features of drugs [28,29]. Folic Acid, the active targeting agent, is a ligand with high affinity and is used to target nanotransporters to folate receptors that have been overexpressed on tumor cells. In this study, we selected Folic Acid which is satisfactory targeting moiety against different cancers including breast cancer to achive more selective accumulation into breast cancer cells.

This study aims to improve the efficiency of the CG-1521 by developing starch nanoparticles as a carrier for breast cancer treatment. The physicochemical properties of nanoparticles (size, charge, morphology, and drug release kinetics) were investigated, and optimum formulation was determined. The optimum characteristics of nanoparticles confimed the successful formulation. The biological response of breast cancer cells to free and encapsulated drug were compared in terms of cytotoxicity and apoptotic capacities. In addition, the cytotoxic effects of Folic Acid–bound nanoparticles were examined in breast cancer cell lines having different levels of folate receptors. Lastly, to determine the biological mechanism of drug-loaded nanoparticles, expression levels of specific transcripts involved in apoptosis, cell cycle and spindle formation were measured by quantitative polymerase chain reaction (q-PCR). The data obtained show that starch nanoparticles enhance the *in vitro* half-life of

encapsulated CG-1521, increase therapeutic effect significantly without alter the molecular mechanism of drug.

2. GENERAL INFORMATION

2.1. Nanotechnology in Drug Delivery Systems

The use of nanotechnology in medicine offers innovative methods and advantages for the treatment of many diseases. Nanomedicine generally involves the design, development, and transport of diagnostic and therapeutic agents for various applications in biological systems [30,31]. Some biomedical applications of nanotherapeutics are shown in Figure 2.1 [32].

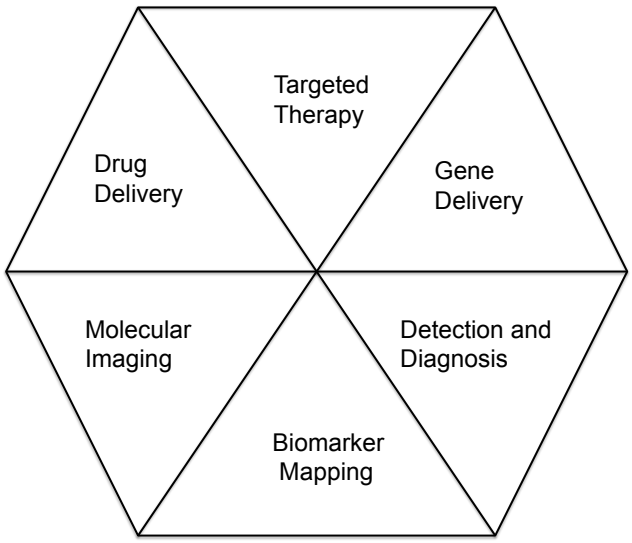

Figure 2.1. Biomedical applications of nanotherapeutics [32].

Nanocarriers must overcome biological barriers such as skin, mucosa, blood, intercellular matrix, and cell membrane to reach sub-cell areas. Successful transportation depends on physical and chemical characteristics of nanoparticles such as size, shape, and surface charge. Modification with targeting moieties that recognize and bind to biological receptors can increase its changes of successful transportation. The appealing features of nanoparticles in medicine are their high surface area over volume ratio, unique quantum effects, and different absorbing properties. They have capacity to deliver different therapeutics and diagnostics simultaneously.

Nanoparticles can be designed from biological based products such as phospholipids, lactic acid, dextran, or chitosan, as well as chemically modified polymers, carbon, silica or metals. The materials used in drug delivery systems

are desired to biodegradable to minimize side effect of therapeutics in the biological environment and be eliminated.

Some of the main objectives in systems designed for drug delivery within nanobiotechnology are [34]:

- More specificity in drug targeting and transportation,
- Reduction of toxicity while maintaining the therapeutic effect of the drug,
- Optimized release kinetics of drugs in body's circulation
- Increased stability of therapeutics
- More biocompatibility,
- Rapid development for safer production of new materials.

2.2. Nanoparticle Design in Drug Delivery Systems

Many natural and synthetic materials have been formulated as drug delivery vehicles, especially for threranostics purposes in cancer. As shown in Table 2.1, nanoparticles as a drug delivery system generally consist of liposomes, polymeric structures such as micelles, dendrimers, nanoshells, or protein derived particles [30,35,36,37,41]. Among nanoparticles, the majority of approved nanoformulations for clinical use are either liposomal or polymeric formulations [38, 39,40].

Table 2.1 Classification of nanoparticles and their application areas [41]

Particle Class	Materials	Application Area
Natural Polymeric Material and Derivatives	Chitosan Dextran Gelatin Alginate Starch	Gene/drug delivery
Liposomes	Phospholipids	Drug/gene delivery
Dendrimers	Branched polymers	Drug delivery
Fullerenes	Carbon based materials	Photodynamic/drug delivery
Synthetic Polymeric Carriers	Polylactic acid Polycyanoacrylate Polyethyleneamine Block copolymers Polycaprolactone	Drug delivery
Ferrofluids	SPIONS USPIONS	Imaging (MRI)
Quantum Dots	Cd/Zn Selenides	Imaging/*in vitro* diagnosis

2.3. Polymeric Nanoparticles

Despite the progress made by liposome-based nano carriers in clinic, many factors limit their ability to be the primary platform for drug delivery systems. These restrictive factors include difficulties in modulating drug release during *in vivo* applications, the limited therapeutics loading efficiency, the possibility of oxidation of phospholipids, and the inability to maintain constant shelf life. Conversely, polymeric nanoparticles are more stable in their *in vivo* applications, have higher drug loading capacities and allow more controllable drug release kinetic. Thus, polymeric-based nanostructures have the potential for greater contributions to cancer treatment [42,43].

Polymeric nanoparticles can be obtained as nanospheres or nanocapsules. Nanospheres are particles usually obtained by dispersing drugs in a polymeric matrix, while nanocapsules are reservoir-based systems, obtained by the

encapsulation of a drug into an oily or aqueous core surrounded by a polymeric membrane. The schematic figures of nanoshpere and nanocapsule are shown in Figure 2.2 [44].

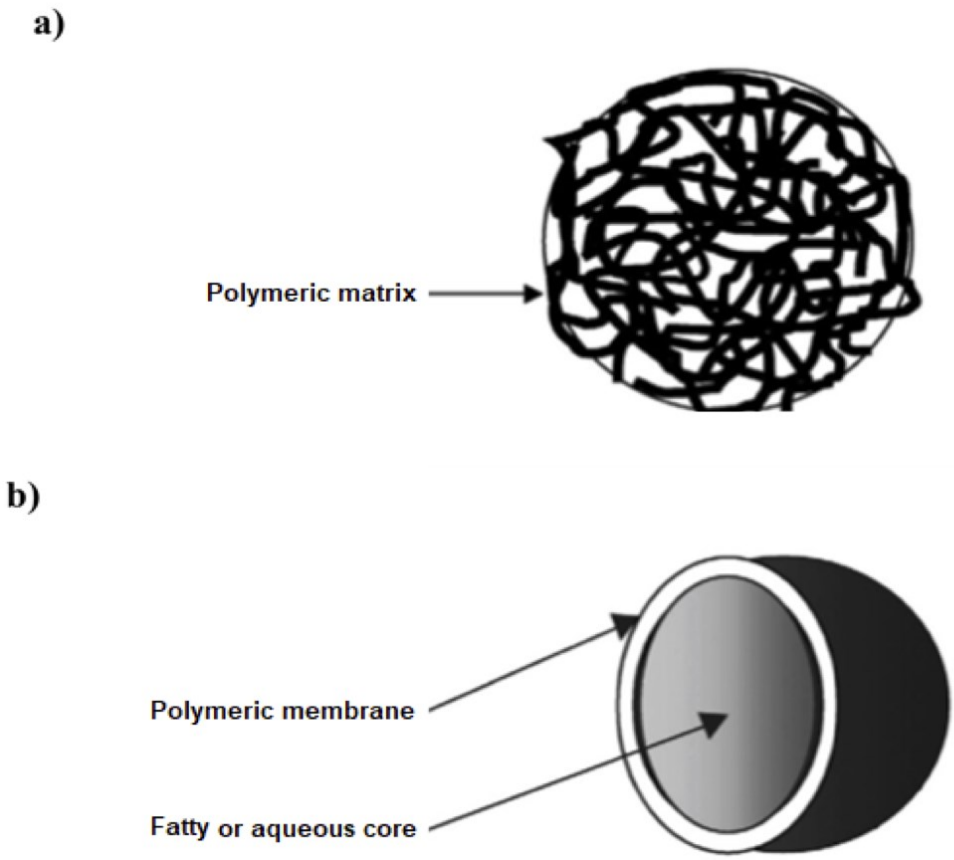

Figure 2.2. Nanoparticles: a) Nanosphere b) Nanocapsule [44]

2.3.1. Preparation Techniques of Polymeric Nanoparticles

Polymeric nanoparticles can be fabricated from pre-formed polymers or by starting from the direct polymerization of monomers, as shown in Figure 2.3 [46]. They can be constructed from pre-formed polymers using techniques solvent evaporation, dialysis, or supercritical fluid technology techniques. They can also be synthesized using monomers applying techniques such as micelle polymerization or interfacial polymerization.

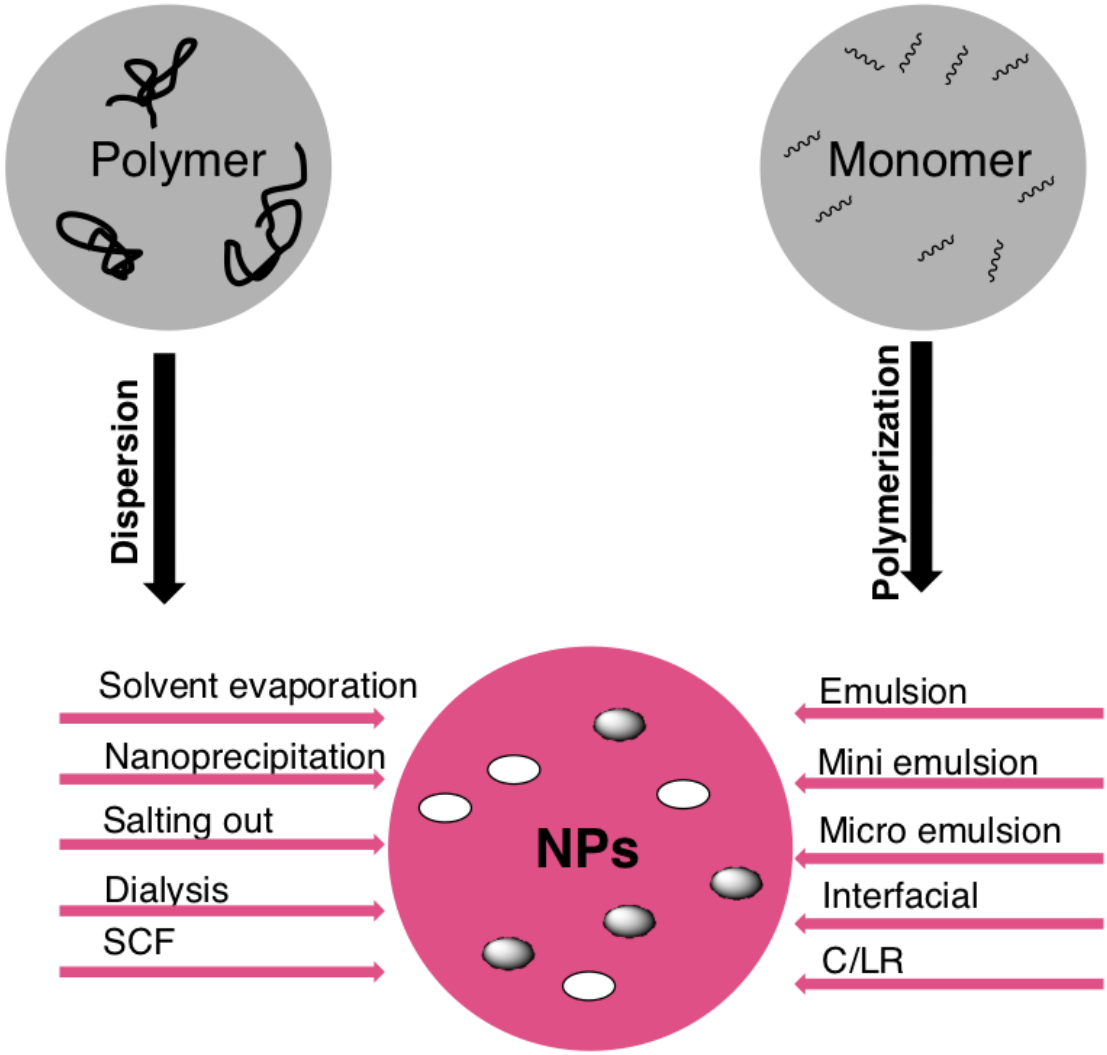

Figure 2.3. Polymeric nanoparticle preparation techniques [46]
(SCF: supercritical fluid technology and C/LR: Controlled/Living radical polymerization)

The solvent evaporation technique is one of the most common techniques used for the preparation of nanoparticles. In this technique, single or multiple emulsions are disintegrated into nanodroplets by using external force using ultra-homogenization or ultrasonication. The nanodroplets form solidified nanoparticles upon evaporation of highly volatile solvents used in formulation using a magnetic stirrer for several hours. Afterward, the solidified nanoparticles are recovered from the suspension using ultracentrifugation and lyophilizes [46].

2.3.2. Polymers Used in the Preparation of Polymeric Nanoparticles

Polymers used in controlled drug delivery are generally classified as natural or synthetic polymers as shown in Figure 2.4 [47].

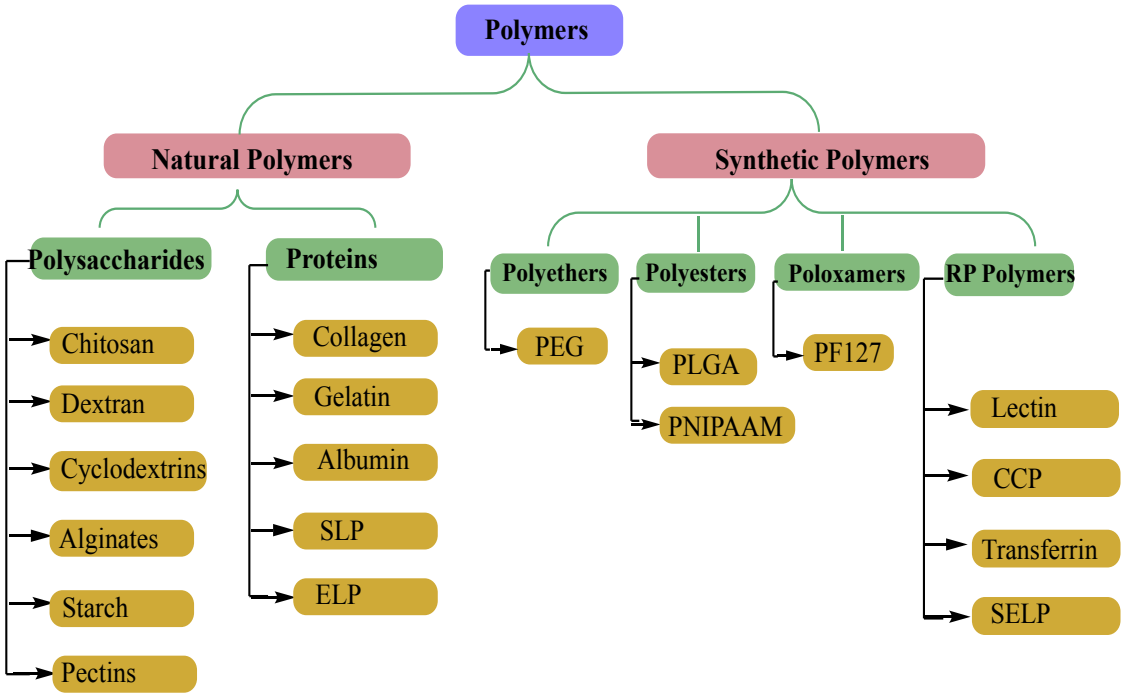

Figure 2.4. Synthetic and natural polymers used in drug delivery systems [48] (SLPs: Silk-like proteins, ELPs: Elastin-like proteins, PEG: Polyethylene glycol, PLGA: Poly (lactic-co-glycolic acid), PNIPAAM: Poly(N-isopropylacrylamide), PF127: Pluronic F127, CPP: Cell Penetrating Proteins, SELPs: Silk-elastin–like proteins.)

PLGA, PGA and PLA are commonly used polymers as shown in Figure 2.5 [49] have multiple applications in controlled release systems due to their biocompatibility and biodegradability. For example, Zoladex is a formulation of the drug goserelin acetate encapsulated with PLGA. It was approved for clinical use by the FDA in 1998 and is used to slow down the drug's release and increase its therapeutic efficacy in breast and prostate cancers treatments. [50].

In another study, PLGA microparticles encapsulating leuprolide acetate were approved by the FDA to treat prostate cancer [51].

In 2000, another FDA-approved PLGA microparticle system was used clinically to transport a drug called Trelstar Depot in prostate cancer treatment [52]. Clinical achievements of this formulation include the sustainable and controlled release of drug from the polymer. With the increase of nanotechnology applications in nanomedicine, the transition of microscale products to nanoscale products of polymers as drug delivery agents has been facilitated.

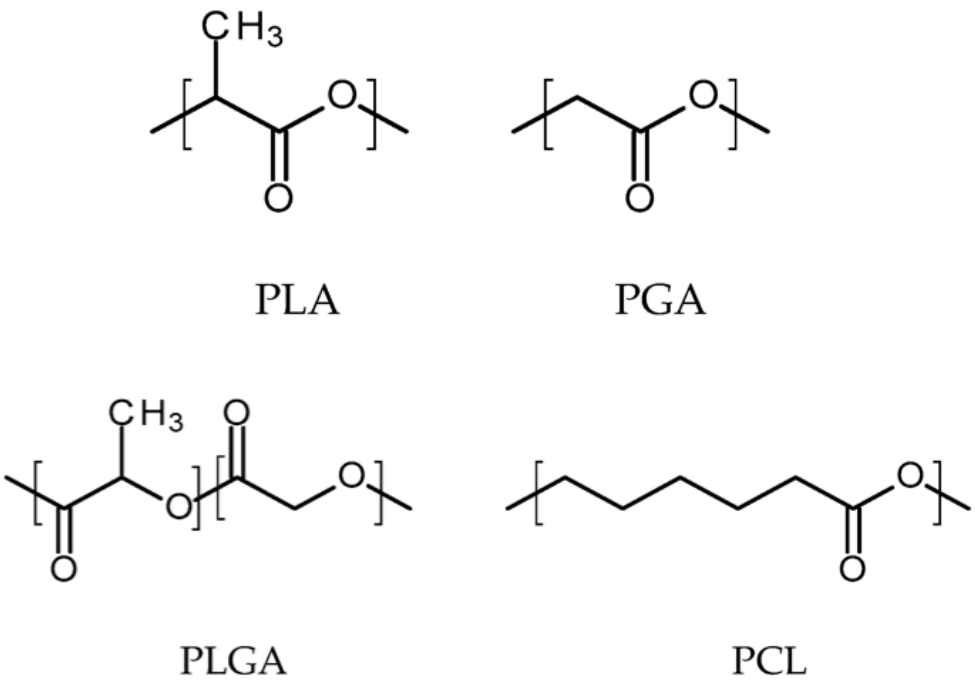

Figure 2.5. Commonly used biodegradable polymers in controlled drug systems [49]

2.4. Polysaccharide-Based Polymeric Nanoparticles and Their Applications

Polysaccharides are complex carbohydrates formed by repeating units of monomers called monosaccharides. The benefits of their usage as drug delivery vehicles are listed [53];

- They are biocompatible and not toxic

- Their reactive functional groups increase the retention times of drug delivery systems and the absorption of more drugs due to the establishment of non-covalent bonds with the epithelial cells in the target tissues.
- They increases the specifity of targeting due to their receptor recognition properties.
- They prevent non-specific protein binding by a neutral coating
- They can be bound to multiple ligands due to their excess hydroxyl groups

2.4.1. Starch as Drug Delivery System

Starch is a natural polymer that has been used as drug delivery vehicle due the its nontoxic nature. The structure of starch as shown in Figure 2.6 consist two types of polymer called amylose (linear) and amylopectin (branched). The different types of starch with different amylose to amylopectin ratio can play a vital role on the physicochemical proporties of nanocarriers.

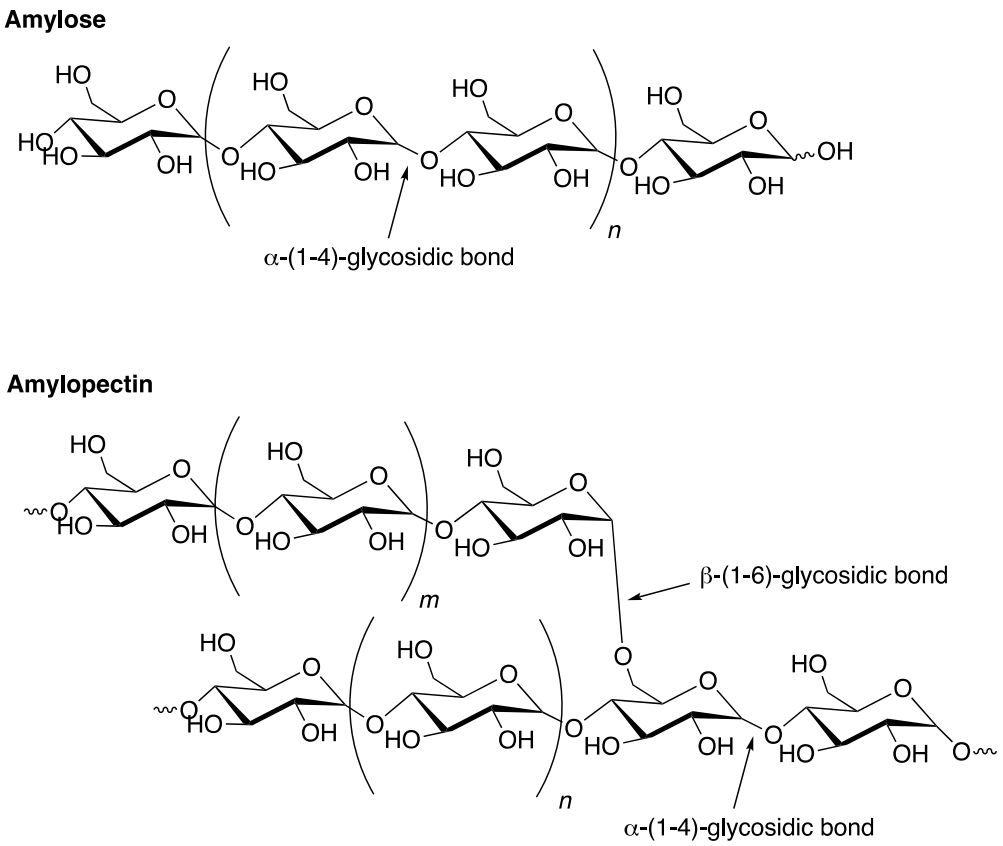

Figure 2.6. Chemical structure of amylose and amylopectin [54]

Pharmaceutical applications of starch have become very popular as copolymers or excipients [54,55,56] in controlled drug systems. They have also been used in the fabrication of tissue scaffolds [57], hydrogels [58] and solubility enhancers [59].

In 2010, Santander and his group investigated [60] starch nanoparticles in the context of transdermal drug delivery systems. In transdermal applications, in which skin is generally a deeply effective barrier, active ingredient–loaded starch nanoparticles provide a clear passage to the skin without any adverse effect on the integrity of the deep skin structure.

In another study conducted in 2010, carboxymethyl starch hydrogels, in which chitosan was used as a cross-linker, were used for oral delivery of insulin [61]. *In vitro* studies have shown that insulin retained in polymer delayed the release of non-enzymatic simulated gastric and intestinal fluids.

In another study in 2015, two insoluble drugs encapsulated in cross-linked starch nanoparticles were examined *in vitro* and drugs retained in the polymeric matrix showed a controlled and sustained release profile [62].

2.5. Target-Oriented Cancer Therapy

Nearly 1.9 million new cases of cancer (except basal cell and squamous cell skin cancers) are expected to be reported in 2021 [63]. Cancer is still the second-leading cause of death, despite the superior effort and developments in therapy against cancer. The main reason for negative clinical outcomes in cancer treatment is the disease's heterogeneous and complex structure. While surgery and radiotherapy are conventionally employed for localized tumors, systematic treatment uses hormone therapy, immunotherapy, chemotherapy, and other targeted therapies [64, 65]. Chemotherapy has been the standard therapy for many primary and metastatic cancers for many years. Since its clinical advantages are quite limited, especially in case of the use of a single drug called monotherapy. Disadvantages encountered in monotherapy can be summarized as particular drug resistance at the cellular level, low drug efficacy,

more tumor heterogeneity, and dose toxicity. To minimize these drawbacks, combination therapies (those in which two or more chemotherapeutic agents are used at the same time) have begun to be used. However, clinical outcomes still have not been improved to the desired level. A better understanding of the tumor microenvironment has led to the development of new-generation combination therapies, particularly with the elucidation of molecular pathways and tumor-drug interactions: a chemotherapy-immunotherapy combination, a chemotherapy-oriented therapy combination, and a chemotherapy-gene therapy combination or epigenetic therapy (DNA and RNA based) [66, 67, 68].

The new-generation cancer drugs interact with a specific molecular target (usually a protein), is critically important in tumor progression. Determination of appropriate targets is possible by understanding the mechanisms of genetic and molecular changes underlying cancer progress. These changes also play an enormous role in the development of drug delivery systems designed for oriented cancer therapy [69].

The main mechanisms that regulate gene expression are listed below [70].

- Regulation of the activities of proteins activating and repressing of transcription
- Covalent modifications and alterations to DNA and chromatin (epigenetic control) structures

2.5.1. Epigenetic Mechanisms

2.5.1.1. DNA Methylation

DNA methylation is one prominent epigenetic mechanism that suppresses gene expression in general and affects transcription, chromatin structure, and chromatin stability. DNA methylation is catalyzed by DNA methyltransferase enzymes, and addition of a metyl group occurs usually in the cytosine within CpG (5'-C-phosphate-G-3') dinucleotides region. It has been known that hypermetylation causes inactivation of tumor suppressive genes and resulting in genomic instability and cell transformation. Tumor suppressor genes which involved in DNA repair, the cell cycle, and apoptosis, are mostly hypermethylated in the promoter region, which suppresses these genes, causing cancer cells to grow and increase and accelerating metastasis [71, 72].

2.5.1.2. Histone Modifications

Histone modification is another key epigenetic mechanism that affects the chromatin structure. The relaxation of packing between the histone proteins and DNA alters the nucleosome structure that plays a vital role in expressing of genes [73].

Although there are different posttranslational modifications, the most-studied histone modification is the acetylation-deacetylation mechanism. As shown in Figure. 2.7, in the acetylation mechanism regulated by the histone acetylase transferase (HAT) and histone deacetylase (HDAC) enzyme groups, a positively charged lysine amino acid loses a part of its charge by attaching the negatively charged acetyl group to the amino terminal of the histone protein. The chromatin structure starts loosening and transcription factors attach to promotor regions of the genes, resulting in successful transcription [74].

In deacetylation, a reversible mechanism, the acetyl group is removed from the lysine amino acid, which results in condensed chromatin and suppressed transcription. While certein histone proteins remain acetylated in spesific regions of chromatin and resulting in activation of those regions with greater level of gene transcription, deacetylated histone causes suppression of transcription [75].

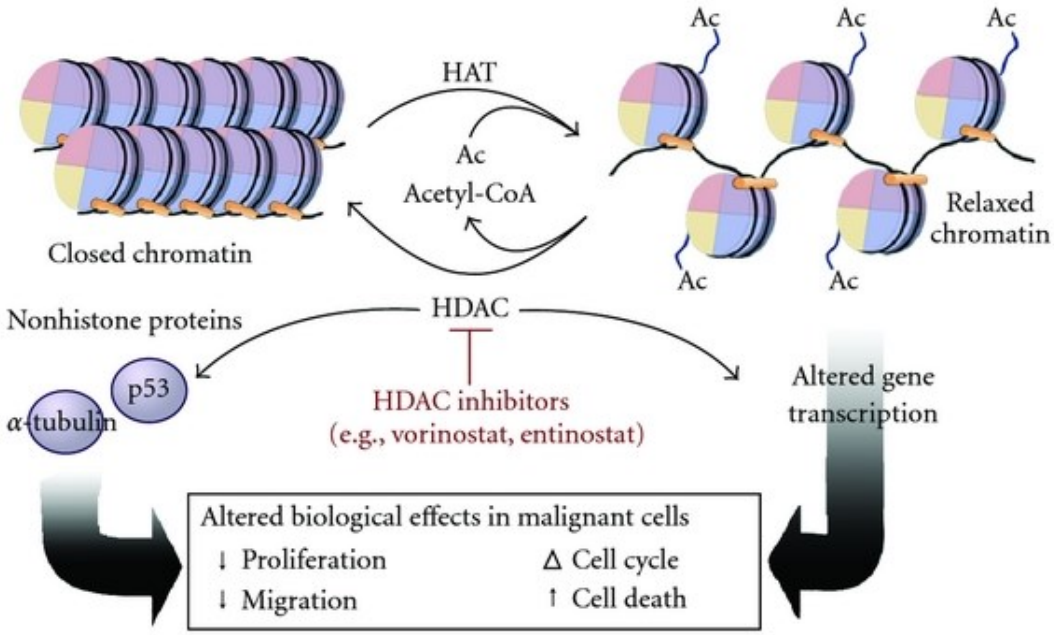

Figure 2.7. Histone acetylation-deacetylation mechanism [76]

2.5.1.3. RNA-Induced Silencing

It has been reported thath someRNA molecules are defined as driving force to initiate DNA methylation mechanism or affect histone modifications. They perform a hereditary silencing process by contributing to the construction of the heterochromatin site Some small non-coding RNA molecules called RNAs, such as mi-RNAs (micro-RNA), siRNAs (small interfering RNA), and XIST (RNA that plays a role in X chromosome inactivation) act by interfering in posttranscriptional and posttranslational silences [71,72].

2.6. Anticancer Mechanism of HDAC Inhibitors

Histone deacetylase inhibitors, as epigenetic agents, act as modifiers in expressing genes without disturbing DNA sequencing. Epigenetic changes caused by HDAC inhibitors have been studied extensively to treat several diseases including cancers. [77]. Expression levels of isoforms of HDACs are higher in some types of cancer cells than normal cells due to the abnormal transcriptional gene silencing. For example, studies have shown that

expression levels of HDAC2 along with HDAC3 proteins increase in colon cancer, and levels of HDAC1 protein elevate in gastric cancer [78].

The inhibition of HDACs repairs the expression of certain specific genes induced by acetylation mechanism of histone or non-histone proteins. Reacetylation of the histones increases the expression level of tumor suppressor genes including p21 and p27, and downregulate he expression of genes responsible for cell growth such as Cyclin D.

Acetylation of proteins such as non-histone p53 and STAT3 is an important contributor to improving the function of these proteins and inhibiting cancer cell growth cells [79, 80].

HDAC inhibitors may also allow for acetylation of some non-histone proteins results in activation of apoptotic pathways and free radicals which prompt the neoplastic cell death. For example, the level of the Vascular Endothelial Growth Factor is reduced because of HIF-1 alpha protein (non-histone) acetylation. This reduces angiogenesis and invasion of tumor cells.

2.6.1. HDAC Inhibitors

As shown in Figure 2.8, HDAC inhibitors (HDACi's), which are used in cancer therapy, are generally classified into six main groups [81]. These inhibitors can be attached to different catalytic domains of histone deacetylase enzymes.

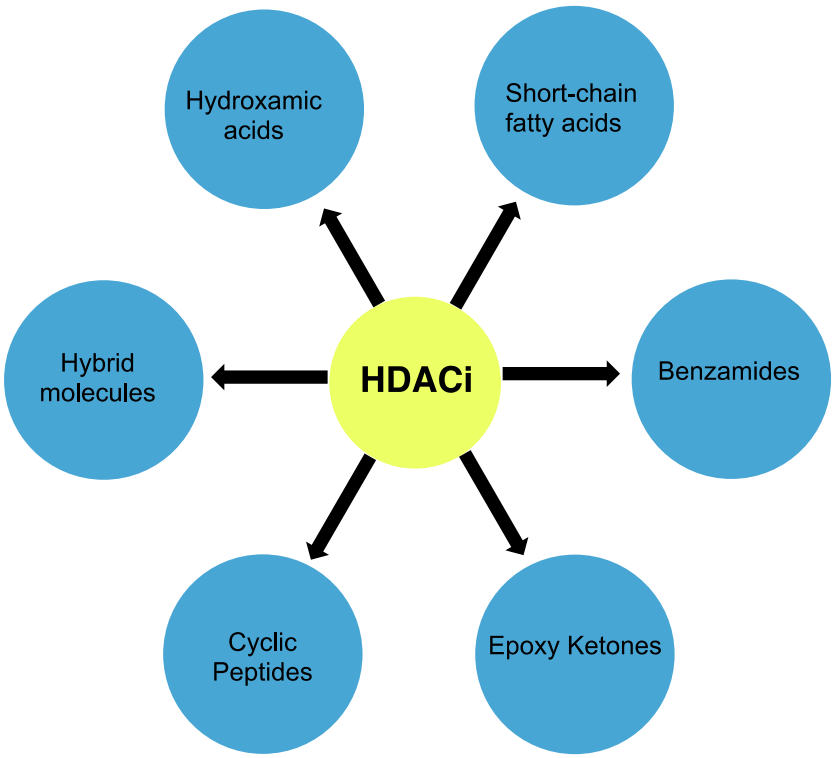

Figure 2.8. HDAC inhibitors [82]

2.6.2. Hydroxamic Acids

The most potent inhibitors are hydroxamate-containing compounds. They usually consist of a metal-binding functional group, a hydrocarbon-binding group, and a protective group that is responsible for surface recognition. The most common examples of these inhibitors are shown in Figure 2.9.

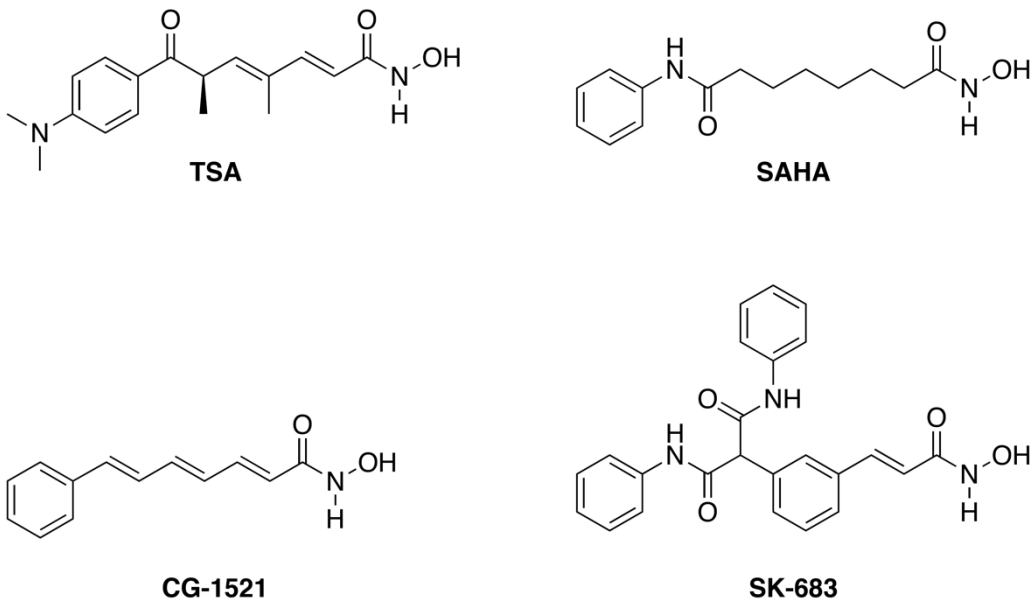

Figure 2.9. Hydroxamic acid-based inhibitors [82]

2.6.3. CG-1521 (7-Phenyl-2,4,6-hepta-trienoyl hydroxamic acid) HDAC Inhibitor

Hydroxamic acid–based CG-1521 is one histone deacetylase inhibitor in the last phase of the preclinical stage. This compound has been shown to inhibit cell proliferation in both tissue and hematological cancer types. It has been shown that CG-1521, which interacts with LNCap prostate cancer cells, promotes p21 protein (which regulates cell cycle expression), stabilizes acetylation of the p53 gene, and induces apoptosis at a significant level [83]. CG-1521, responsible for stabilizing the Ac-Ly 373 isoform of the p53 gene, arrests the cell cycle especially in the G2-M phase.

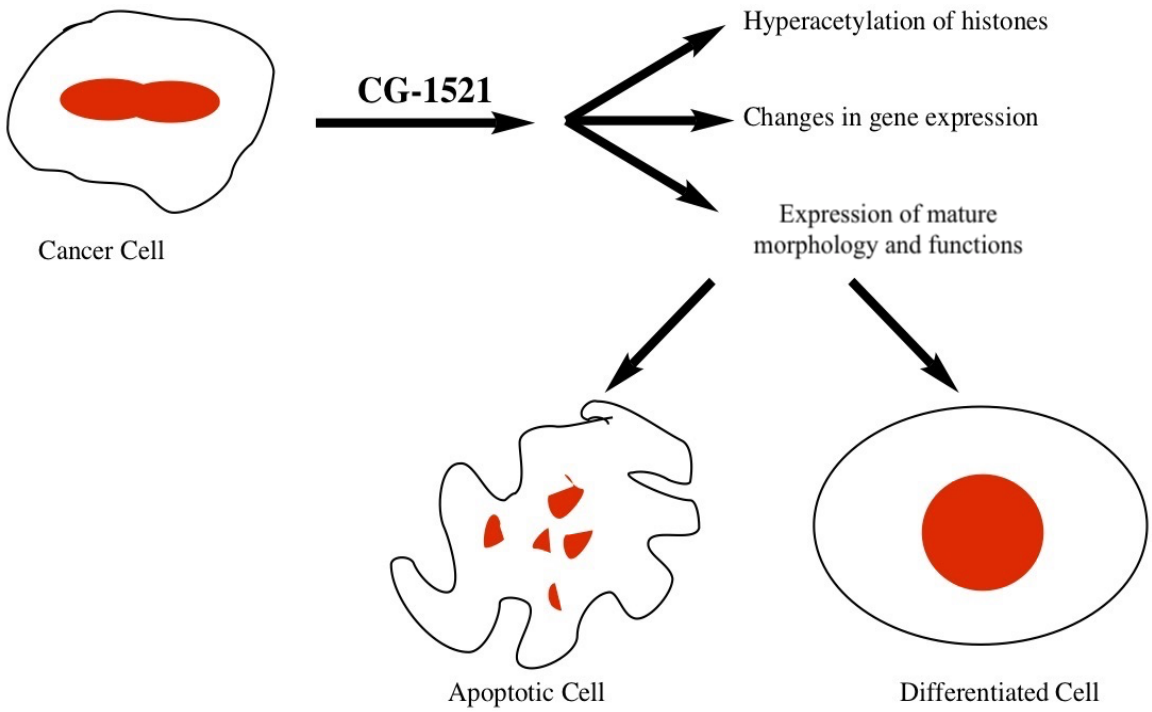

Figure 2.10. Biological mechanism of CG-1521 [83,84]

The use of CG-1521 as an active ingredient in nanoformulated drug delivery systems is limited. In a study by Urbinati et al. (2010) [84], three different histone deacetylase inhibitors, including CG-1521, were loaded into liposomes, and their cytotoxic capacities for breast cancer treatment were investigated. Natural polymeric nanoparticles may be utilized to enhance the activity of CG-1521, which exhibits a weak cytotoxic effect relative to other inhibitors. Polymeric nanoparticles increase the solubility of drugs with limited solubility and provide selective delivery of the compounds to the tumor zone, thereby reducing systemic toxicity. Figure 2.11 shows the proposed mechanism of CG-1521, the p53 protein domains, and posttranslational modifications. The three vital acetylation areas in the carboxyl group continue to acetylation by the inhibition of the HDAC enzyme and allow the p53 gene to remain more stable.

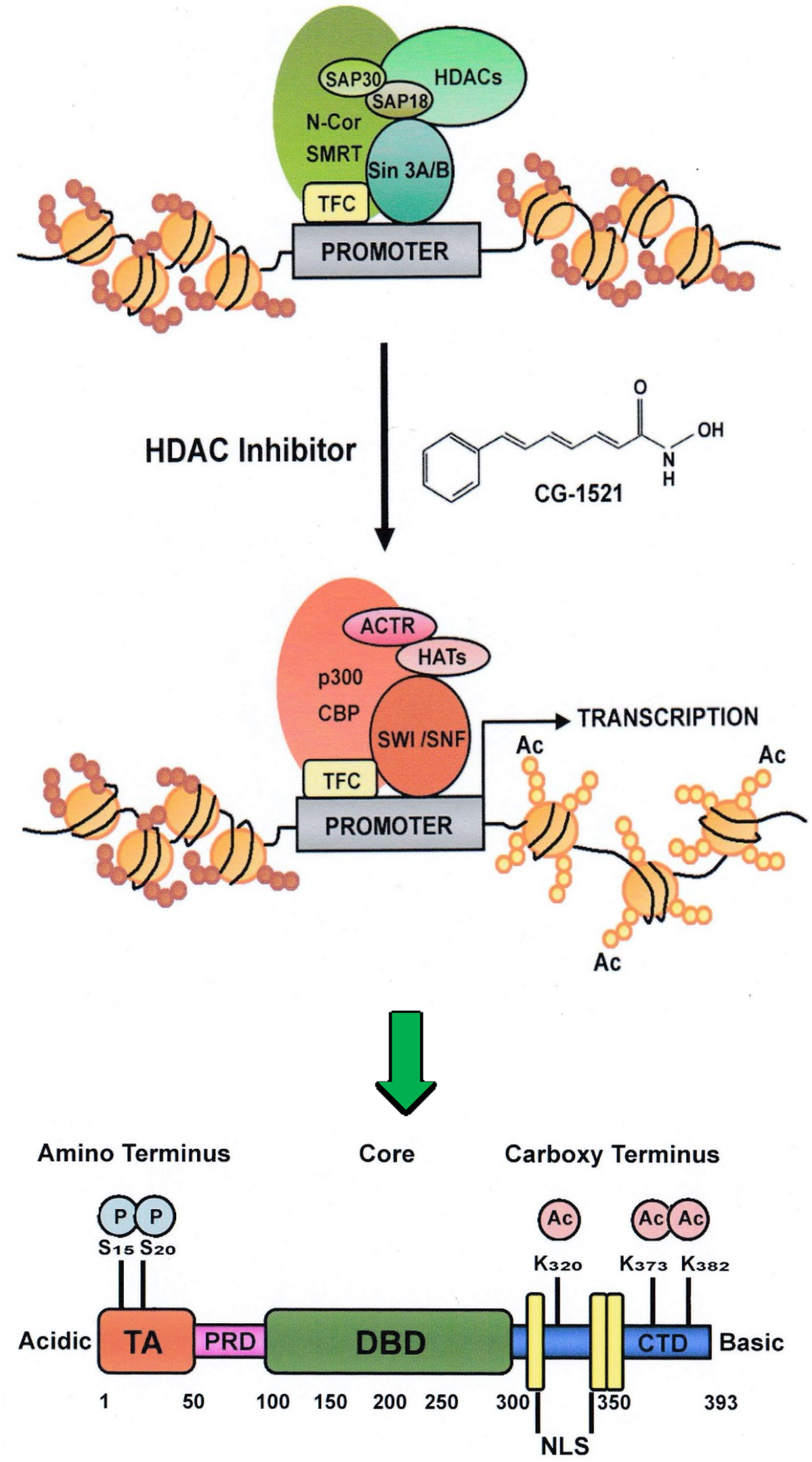

Figure 2.11. p53 protein domains and the posttranslational modification of p53 [85]

Stabilization results in the transcription of the p53 gene and activates downstream targets (e.g., p21 gene) associated with the p53 gene.

Figure 2.12 shows the ontology of genes modulated by CG-1521 as determined by Knutson et al. Downregulation and upregulation of the expression of various genes related to apoptotic and cell death pathway as well as the cell cycle arrest and spindle formation are classified.

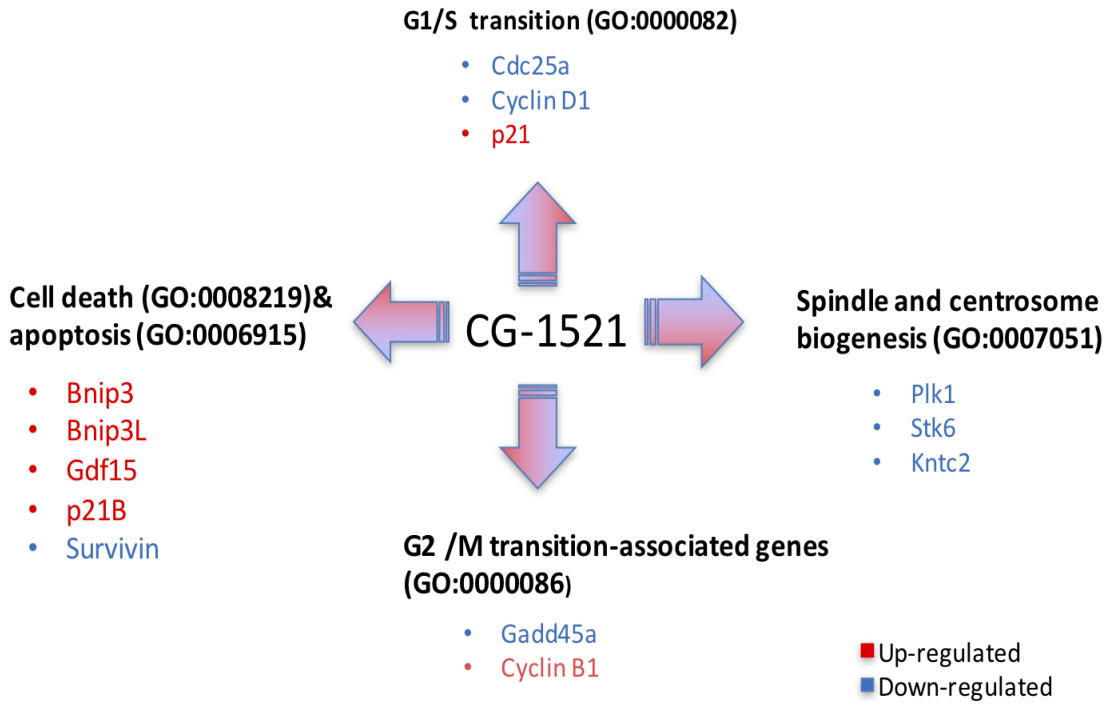

Figure 2.12. Gene ontologies modulated by CG-1521 [85]

2.7. Nanoparticle Targeting Strategies

2.7.1. Passive Targeting

Most nanoparticle systems that approved for clinical use in diagnosis and treatment are passively targeted formulations [86]. Most of these nanoparticle systems have been shown to have a more extended period of circulation *in vivo*. Due to the hemodynamic and diffuse mechanism of the blood, the nanoparticles can accumulate in a particular site.

Passive targeting which channeling the nanocarriers in tumor regions with EPR effect has become a common strategy in oncological applications.

In the 1980s, Maade and his group examined colloidal particle targeting to tumors, marking a turning point in the understanding of the principles of passive targeting. In the study, the cytotoxic effect of polymer drug conjugation was found to be higher than that of the free application. This study, in which the term “EPR effect” was used for the first time, emphasized that the different tumor vascular structure promotes increased permeability [87].

Tumor tissue is unusual in that it is highly heterogeneous and has a leaky structure. The tumor microenvironment is generally characterized by a hyperbranched irregular structure, increased endothelial cavities formed by loosening tight junctions, and disintagrate basal membrane [88]. The gaps between endothelial cells let particles to leak out of the veins near tumor site [89]. In standard vascular structure, tight junction prevents the crossing of particles (>2nm) between the endothelial cells. However, deteriorated basal membranes in the tumor vascular system and loose junctions allow structures between 10 and 500 nm to leak and accumulate in tumor interstitium. Poor and deteriorated lymphatic drainage allow particles to be retained longer before clearance. As shown in Figure 2.13, the pathophysiological properties of tumors site allowing nanoparticles to accumulate and retain more in tumor tissues than in normal tissues which knowns as passive targeting. Nanocarriers are also can be incorparated with active targeting ligands for enhanced cellular uptake. [90].

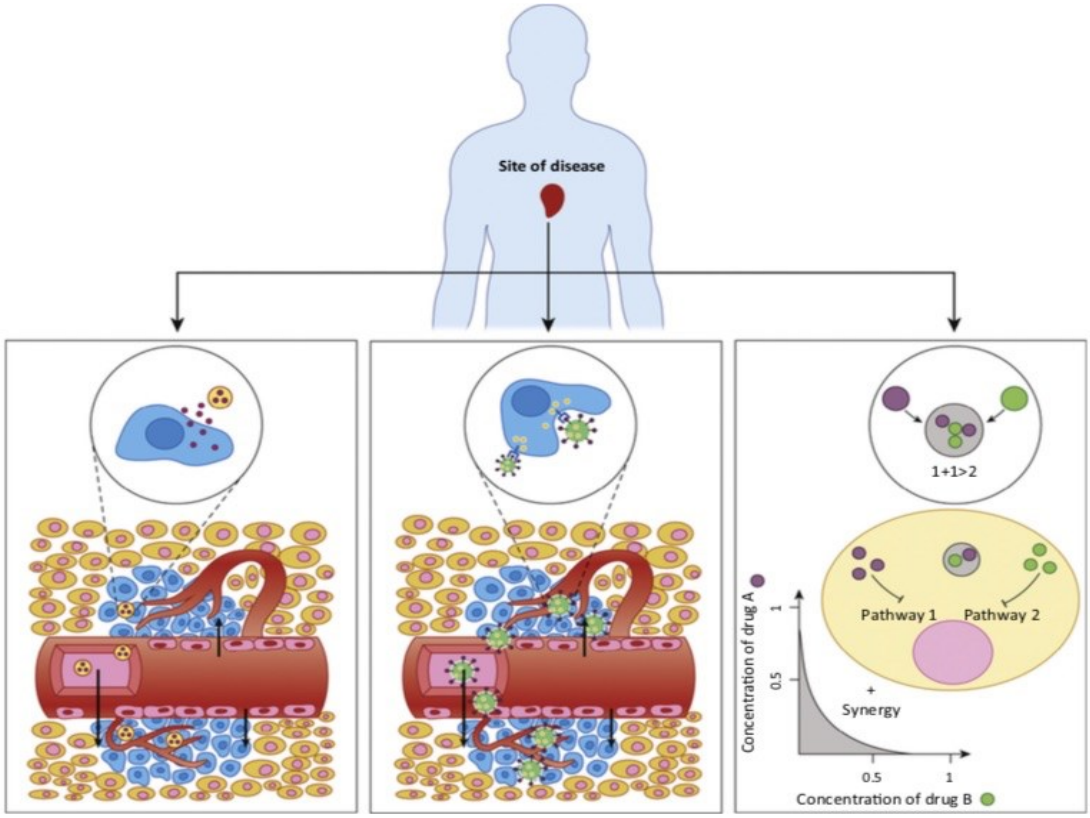

Figure 2.13. Passive targeting, active targeting, and combinational transport in drug delivery systems [41]

Stealth modification (such as PEGylation) or reticuloendothelial system (RES) protected nanoparticles might have extended circulation time compared to unmodified nanoparticles [91].

By mimicking the natural structure of the body, the circulation time for nanoparticles in the body can be increased. In one clinical study, it was found that the longest circulation time in the body for synthetic particles was about 300 hours, while the average circulation time of red blood cells ranges from 100 to 120 days [92]. The CD47 membrane protein on cell membranes stimulates the phagocyte receptor CD172a prevents cells from phagocytosis. In a study based on this mechanism, *in vivo* studies of nanoparticles modified with a synthetic peptide showed an extended half-life in the body [92].

In yet another study, erythrocyte membranes were extracted and used as coating agents on PLGA nanoparticles. With this method, the nanoparticles retain and circulate for longer period with PEGylation process [93].

Passive targeting, however, has several disadvantages. RES elements such as the liver and spleen retain nanoparticles, thus restricting their biodistrubution. Furthermore, the level of the EPR effect varies between tumors, and the heterogeneity of the tumor periphery negatively affects the efficacy of passive targeting [94,95].

2.7.2. Active Targeting

Despite the EPR effect and the positive contribution of PEGylation to the bioutilization of nanoparticles, the retention of nanoparticles by RES elements at a certain level is inevitable [96]. The active targeting method allows nanotransporters to be directed to the desired area while avoiding the nonspecific targeting. Active targeting allows the surface of nanoparticles to be modified with a particular ligand that attaches to the over-expressed receptors in the targeted cells. This dynamic binding method thus induces the uptake of nanoparticles by receptor-mediated endocytosis into the cells described as in Figure 2.13 schematically.

Table 2.2. Examples of passively and actively targeted nanotherapeutics in clinical testing [90]

Formulation	Targeting Ligand	Therapeutic Agent	Indication	Clinical Phase
Liposomes				
ALN-TTR02	Passive	siRNA	TTR amyloidosis	II
CALAA-01	Transferrin	siRNA	Solid tumors	I
CPX-351	Passive	Cytarabine/Daunorubicin	Acute myeloid leukemia	III
SGT53-01	Transferrin	Oxaliplatin	Gastroesophageal adenocarcinoma	II
TKM-PLK1	Antibody Fragment	p53 gene	Solid tumors	I
MBP-426	Transferrin	siRNA	Solid tumors	II
Polymeric Nanoparticles				
BIND-014	Small Molecule	Docetaxel	Solid tumors	II
Atu027	Protein Kinase N3	siRNA	Solid tumors	II
CRLX-101	Passive	CPT	Non-small cell lung cancer/ rectal cancer/ renal carcinoma	II

There are few actively targeted nanocarrier formulations at the clinical test stage. Several examples of these formulations are shown in Table 2.2 [90], including MBP-426, with siRNA as the active agent encapsulated in a cyclodextrin-based structure that is modified by a transferrin ligand. This nanoformulation, given intravenously to patients who are diagnosed with melanoma, is directed to the transfer receptors that overexpress on the surface of melanoma cells [97,98].

Excessive increasing of the expression levels of specific receptors in cancer cells leads to more effective delivery of nanotransporters. For instance, prostate-specific surface antigen (PSMA) is a specific receptor for prostate tissue, and nanotransporters modified with PSMA have been used in clinical

trials. The formulation called BIND-014, which is at Phase 2, was investigated the encapsulated docetaxel into polymeric nanoparticle carrier modified with PSMA. The modified nanoparticles were targeted to prostate and some metastatic tumors. A promising study of PSMA-targeted nanostructures showing a significant effect in reducing tumor size was published in 2012 by Hrkach et al. [99].

2.7.2.1. Ligands Used in Active Targeting

2.7.2.1.a. Monoclonal Antibodies and Fragments

Monoclonal antibodies, leading ligands used in targeting nanoparticles, are antibodies that only react against an epitope. In different studies, Trastuzumab, and Ritukzimab monoclonal antibodies were conjugated with PLA nanoparticles, and the effect of modification on cellular uptake was investigated. The results show that the cellular uptake of monoclonal antibody-modified particles by cells is higher than unmodified particles [100,101].

Nanoantibodies, which are single-domain variable fragments of special type of antibodies, have been used as a new-generation targeting agent. These small antibodies have full antigen binding capacity and are very stable compared to classical monoclonal antibodies. [102]. A recent study showed that nanoantibodies can minimize the immunologic response compared to monoclonal antibodies [103].

2.7.2.1.b. Proteins

In targeting by receptor-mediated endocytosis, many endogenous proteins are specifically taken into cells the receptors on the cell membrane. For example, the transferrin protein involved in iron transport has been used to decorate nanoparticles to target transferrin receptors on various cell surfaces specifically. In a study by Choi et al., the ligand-bound nanoparticles targeted to the transferrin receptors were found to be more abundantly taken up by cancer cells [104]. In addition, epidermal growth factor (EGF) [105] and neural growth factors (NGF) [106] are alternative proteins used in protein-targeted nanoparticles.

2.7.2.1.c. Peptides

Peptide agents have shown promise as targeting agents in recent years. Their smaller size, lower immunological response, higher stability, and ease of conjugation make them advantageous as ligands [107]. The development of peptide phage libraries and advances in new imaging techniques make it possible to synthesize peptide ligands for a variety of targets [108,109]. The RGD (Arg-Gly-Asp) peptide sequence binds to upregulated αvβ.3 integrin receptors in tumor cells as well as angiogenic endothelial cells to provide targeted transport of nanostructures [110].

2.7.2.1.d. Aptamers

Aptamers belongs to the nucleic acid ligands and oligonucleotides family that can bind to specific target molecules. They might be DNA oligonucleotides, RNA oligonucleotides, or modified version of oligonucleotides. Their ability not to be affected by nuclease degradation makes them attractive ligand [111]. Aptamers are produced using randomly selected indices from the pool containing single-chain DNA and RNA by a technique called Systemic Evolution of Ligands by Exponential Enrichment (SELEX) [112]. In a study by Guo et. al, PLA-PEG nanoparticles modified with AS1411 aptamer were designed to bypass the blood–brain barrier. Using aptamer-mediated targeting resulted in higher cellular uptake by glaucoma cells, which express higher level of nucleolin protein than normal cells. [113].

2.7.2.1.e. Small Molecules

The small molecules have been studied to modify nanoparticles in nanomedicine field. The advantages of using these molecules as ligands can be summarized as follows [114,115];

- They are less prone to degradation than biomolecular ligands.
- There are multiple chemical methods for their conjugation.
- They have higher density of molecules on nanoparticles' surfaces.
- They interact with many different functional groups.
- They cause less immunogenic response *in vivo* studies.
- They allow for reproducibility.

The most common targeting ligands is the Folic Acid (folate) molecule, as its molecular structure is shown in Figure 2.14. This high-affinity vitamin is modified with nanotransporters and is used to selectively target over folate receptors on a variety of tumor cells.

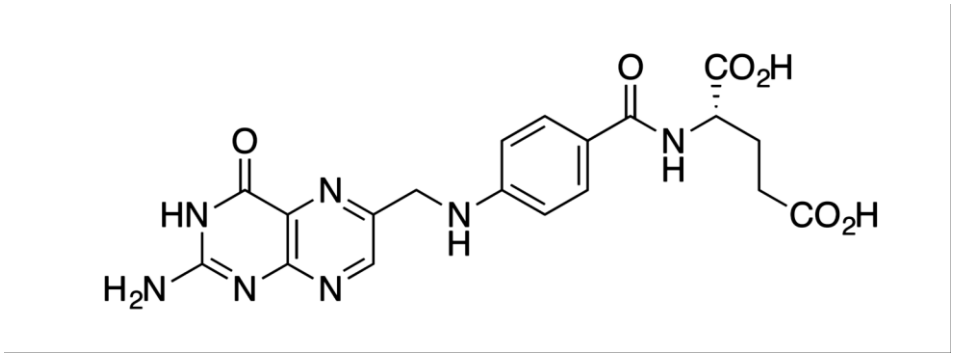

Figure 2.14. Chemical structure of Folic Acid

Besides its combinations with drugs, Folic Acid can be modified with polymeric or liposomal carriers for targeted therapy. Folic Acid receptors are not only expressed in tumorous tissues but are also present at a certain level in the placenta, intestine, and kidney tissues [116]. Therefore, nanoparticles need to have an optimal density of receptors on the surface to reach the target cell population [117].

The use of carbohydrates as targeting ligands is also remarkable due to its easy production process and their low molecular weight. The carbohydrate ligands generally target cell membrane protein lectins on the surface of the cells. Ligand activities have been tested in various studies on mannose [118], glucose [119], galactose [120] and their derivatives in nanoparticle systems designed for drug-based nucleic acid delivery.

2.7.3. Combinational Transport and Multiple Targeting

Cancer is a complex disease where many sequential mutations occur in genes, within different pathways and progressions in different tumors. Treatment with a single therapeutic may sometimes be ineffective in reducing the tumor growth. In conventional chemotherapy, drugs have been combined to utilize their synergistic effects. However, the optimal dosage of different drugs in the same

formulation may be complicated due to their different pharmacological properties [121]. It is possible to minimize this complication by applying multiple therapeutic agents into the nanoformulation with different physicochemical properties and pharmacological behavior. Nanotransporters ensure that the different drugs can be retained in the targeted region, maintaining therapeutic effects until they reach to the cells. The liposomal nanoparticle system CPX-351, which is still in the preclinical study phase, was tested for use in the treatment of myeloid leukemia by confining two different anticancer drugs in the same formulation but in different proportions [122].

Within the scope of multi-targeting, nanoparticle surfaces with multiple ligands provide the various interactions with receptors on different cell targeted sites. The effectiveness of the method named “two- or three-punch” was studied by Kluza and his group [123]. In the study, RGD (integrin receptor targeted) and anginex ligands were modified with liposomes containing paramagnetic and fluorescent agents and their cellular uptake was examined. Interestingly, the combined use of these ligands significantly increased the cellular uptake of nano formulations by HUVEC cells.

2.8. Real-Time PCR (qPCR)

Polymerase chain reaction (PCR) is one of the most common and reliable techniques used in molecular biology. In the PCR technique, specific sequences belonging to DNA or cDNA (complemantary DNA) are amplified (copy, replication) by using oligonucleotides specific to the sequences, heat-resistant polymerases, and a heat cycle. In traditional (endpoint) PCR technique, at the end of the reaction (after the last cycle), the detection and measurement of amplified sequences require a method such as gel electrophoresis and imaging analysis. However, in real-time quantitative PCR technique, PCR products are measured after each cycle. The exponential amplification phases of the reaction as shown in schematic Figure 2.15 can be monitored throughout the reaction, and the starting amounts of target sequences are determined. Theoretically, PCR allows the DNA to replicate exponentially, that is, to double each target molecule. The product efficiency

after the reaction is measured by the detection of the fluorescent signal amplification proportionally to the number of products (amplicons) formed by using fluorescent dyes (e.g., SYBR Green).

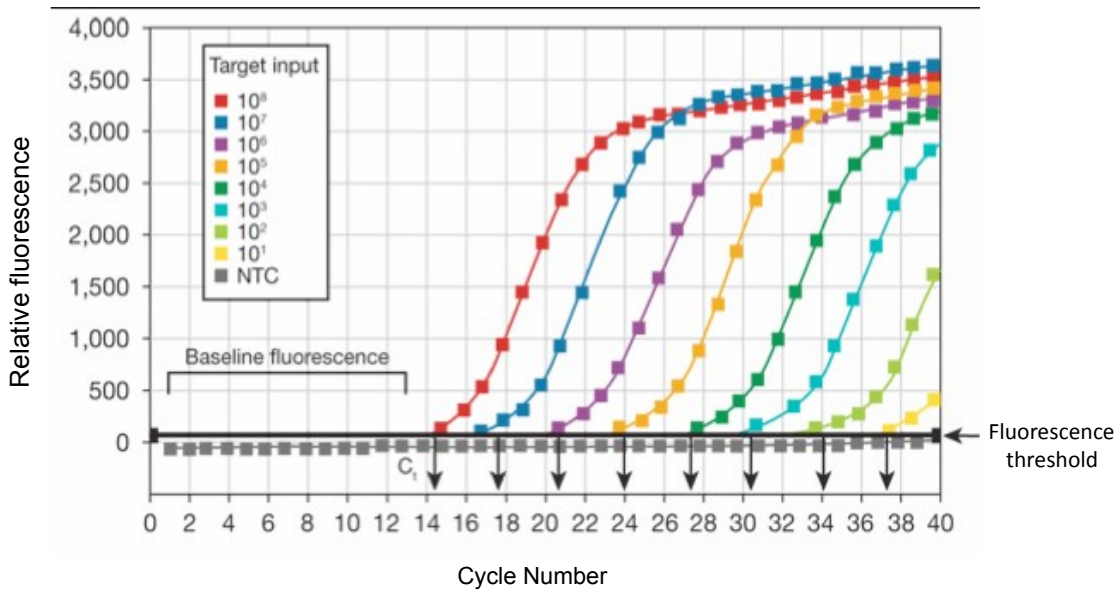

Figure 2.15. Amplification curves during qPCR [124]

In the real-time PCR reaction, there are three fundamental steps of each cycle.

1. Denaturation: The double-stranded structure of DNA is separated into single chains by incubation at high temperature (usually 95 ºC).
2. Annealing: During the annealing (usually at 50–70 ºC), the primers bind to the specific sequences with hydrogen bonds at the ends of the region to be amplified.
3. Polymerization: DNA molecules are synthesized by adding the enzyme molecules bound to the primers to the nucleotides appropriate for the template DNA at 70–72 ºC (the optimum temperature for DNA polymerase activity).

These three steps constitute a single cycle, and the reactions are usually carried out to complete at least 40 cycles. In real-time PCR, the amount of product obtained after amplification can be determined by various methods. The most common of these methods is to use SYBR Green dye, that binds double-

strand DNA molecules. During the polymerization, the amount of dye attached to the double helix of the target DNA increases, with an accompanying increase in fluorescence. The obtained fluorescence vs. the specific amplification product is analyzed by melting curve analysis.

3. MATERIALS AND METHODS

3.1. Chemicals

Alfa-MEM cell culture medium, glutamax, glutaraldehyde and trypsin-ETDA were obtained from Thermo-Fisher Scientific (Life Technologies Corporation, Waltham, MA). Fetal bovine serum (FBS) was purchased from Atlanta Biologicals (Norcross, GA). Formaldehyde was obtained from Polysciences Inc. (Warrington, PA). Starch (unmodified-73% amylopectin/27% amylose, CAS Number: 9005-25-8), Bromodeoxyuridine triphosphate (Br-dUTP) was obtained from Phoenix Flow Systems (San Diego, CA). Triton X-100, dimethyl sulfoxide (DMSO), polyvinyl alcohol (PVA), bovine serum albumin (BSA), Rhodamine 6G and propidium iodide, were purchased from Sigma-Aldrich (Saint Louis, MO). Hexadeuterodimethylsulfoxide (DMSO-d_6) was obtained from Cambridge Isotope Laboratories, Inc. (Andover, MA). Terminal transferase, RNase and cobalt chloride products were obtained from Roche Applied Science (Indianapolis, IN).

Crystal violet dye was obtained from Acros Organics (Morris Plains, NJ). ProLong Gold Reagent-DAPI nucleus dye purchased from Invitrogen (Carlsbad, CA). Muse kit analysis products from EMD Millipore (Billerica, MA). CG-1521 was provided by Errant Gene Therapeutics, LLC (Chicago, IL) as a present.

3.2. Synthesis of Folic Acid–Bound Starch Polymer

Starch solution (5% w/v) was prepared using 20 mL of anhydrous DMSO in a nitrogen gas atmosphere. 1 mL of 1% 1-carbonyl diimidazole (CDI) solution (w/v, DMSO) was added in a nitrogen gas atmosphere. The resulting CDI-starch solution was kept reacting for 15 min at 50 ºC in the presence of nitrogen gas. Ethylenediamine (1 mL) was then added, and the polymer solution was stirred for 24 hours in a nitrogen atmosphere at 50 ºC. The solution was placed on the dialysis membrane (Molecular Weight Cut-off,12–14 kD) and purified by dialysis for 24 hours in a glass container with a volume of 9 liters of continuous inflow and outflow of water. After that, the polymer solution, which was further purified for 2 hours more under distilled water flowing using the same system, was first dried by rotary vacuum evaporator followed by high vacuum. 0.75 g of

the transparent, opaque solid polymer obtained was used in the next reaction without further modification.

In the next step, 1% Folic Acid and 1.5% N-hydroxysuccinimide (NHS) solutions (w/v) were prepared in 10 mL anhydrous DMSO in nitrogen gas and stirred for 5 minutes for the activation of carboxyl groups corresponding to Folic Acid. Then 1.4% 1-Ethyl-3-(3-dimethylaminopropyl) carbodiimide (EDC) was dissolved in 5 mL DMSO (w/v) and mixed the Folic Acid /NHS solution and stirred at 50 °C for 10 minutes under a nitrogen gas atmosphere. This mixture was then mixed with 2.5% aminated starch solution in 20 mL DMSO and stirred at 50 ° C for 3 hours under nitrogen atmosphere. The resulting solution was again purified using a dialysis membrane for 24 hours under flowing water and 2 hours under distilled water. The Folic Acid–bound starch polymer dried with using a rotary evaporator under high vacuum. The modified polymer was obtained in the solid form in orange color. This modified starch polymer was stored in a dark and dry place at room temperature for further steps. The synthesis method of the Folic Acid–bound starch polymer is shown in Figure 3.1.

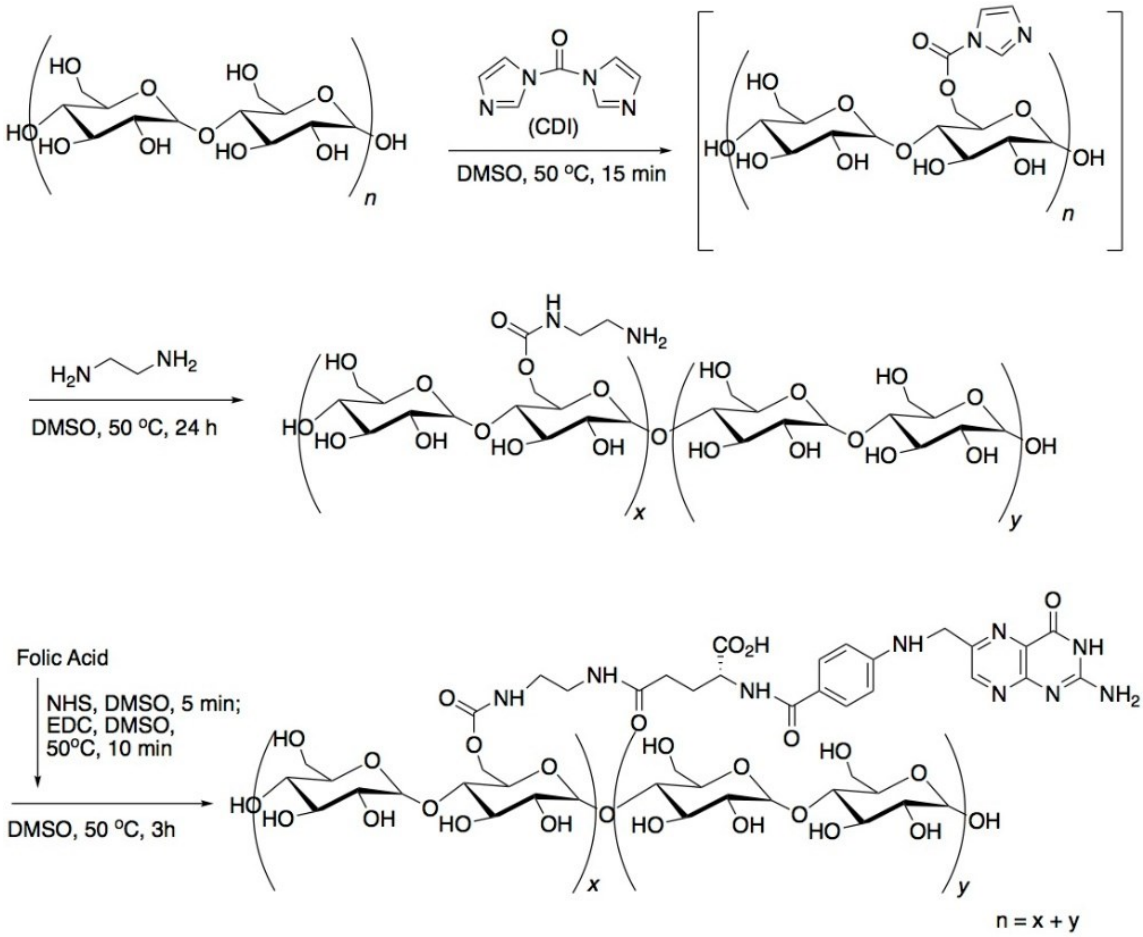

Figure 3.1. The synthesis of Folic Acid conjugated starch

3.3. Chemical Characterization of Folic Acid–Bound Starch Polymer

^{1}H-NMR and IR were used to confirm the covalent bonding of the Folic Acid to the polymer. 2–3 mg of starch, lyophilized modified starch, and free Folic Acid were dissolved in deuterated solvent (DMSO-d_6), 1 mL) and characterized by NMR spectroscopy (Bruker AVANCE III, 300 MHz).

The characteristic features of the same samples were investigated with FT-IR spectroscopy (Thermo Scientific Nicolet iS5). For this analysis, 2–3 mg of solid sample was placed onto a diamond compression cell and then analyzed in the spectral range of 600–4,000 cm^{-1} to chemically characterize the drug-loaded NPs.

3.4. Preparation of Folic Acid–bound Starch Nanoparticles

Starch nanoparticles were synthesized based on the emulsification-solvent evaporation method as shown in a schematic workflow in Figure 3.2.

- First, the organic phase (w/v, DMSO) of 1%, 10 mL starch polymer was prepared.
- The prepared organic phase was injected into a 2% PVA aqueous phase by spraying with nitrogen gas with an Ultra-Turrax homogenizer (24,000 rpm, IKA T-18 Ultra-Turrax, Wilmington, NC).
- Then 30 mL more distilled water was added to the mixture and stirred at 24,000 rpm for 5 min in the homogenizer to accelerate the diffusion of DMSO to the aqueous phase.
- The emulsion was mechanically stirred for 2 hours to allow for hardening of the formed nanoparticles and organic phase evaporation at room temperature.
- Finally, nanoparticles were precipitated in an ultracentrifuge (12000 rpm, 30 min, Eppendorf-5810R), and washed three times with distilled water using ultracentrifuge at the same rate and time.
- Washed nanoparticles were dried using a lyophilizer.

Void nanoparticles were prepared using unmodified starch polymer with same technique. Drug-loaded nanoparticles were prepared using the same protocol after the drug and polymer were dissolved in DMSO. For cellular uptake studies, Rhodamine 6G fluorescent dye loaded nanoparticles were also prepared using the same protocol.

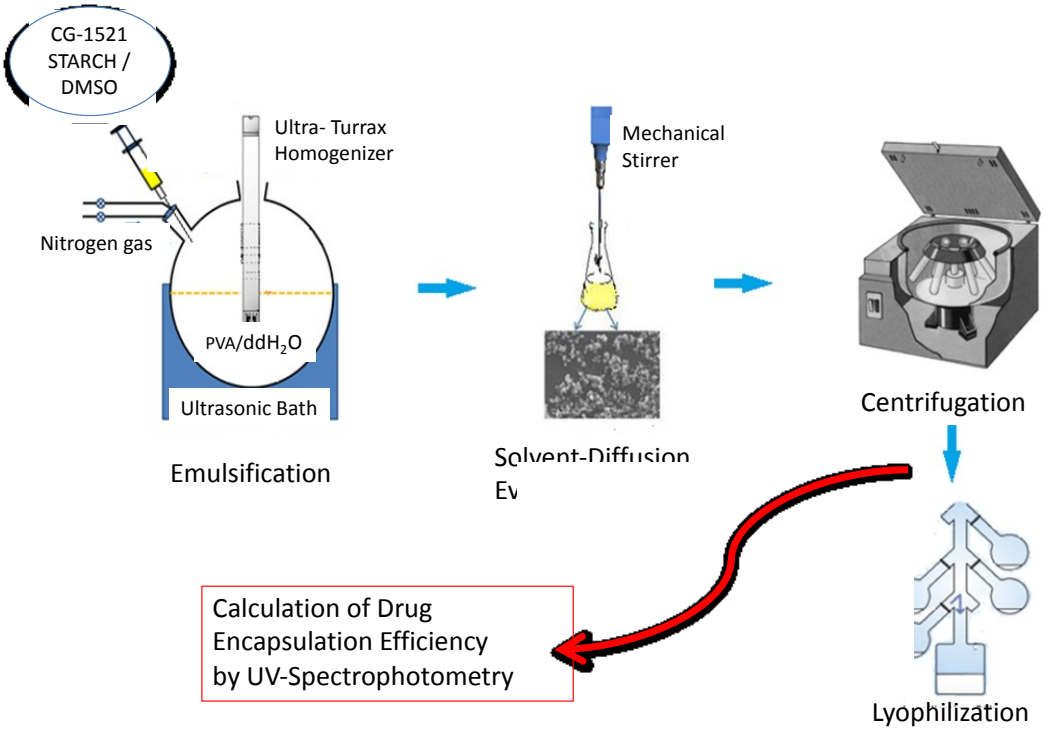

Figure 3.2. Preparation steps of starch nanoparticles

3.5. SIze and Morphological Analysis of Starch Nanoparticles

The average hydrodynamic diameter of starch nanoparticles, zeta potential and polydispersity index (PDI) and were analyzed by dynamic light scattering (Zetasizer, 3000 HSA, Malvern, UK) at 25 ºC.

Scanning electron microscopy (SEM, JEOL 6100LV, MA) was used for morphological characterization of the nanoparticles. For SEM analysis, a 3 µL sample from the diluted nanoparticle aqueous dispersion was dropped onto an aluminum holder and allowed to dry for 15 hours. Then, nanoparticles were coated with gold (35 mA, 60 sec) and examined by SEM.

For analysis by atomic force microscopy (NanoMagnetics EzAFM Oxford, UK), one drop of nanoparticle suspension was dropped onto a silicon plate and dried. Samples were scanned at a resonant frequency of 310 kHz in tapping mode with a standard silicon cantilever.

3.6. Effect of Formulation Parameters on Nanoparticle Size

The effects of different parameters on the properties of nanoparticles have been examined. The parameters examined, one parameter varied at a time, are as listed.

- Polymer concentration (2%, 3%, 4%)
- Surfactant concentration (0.5%, 1%, 2%)
- Homogenization speed (rpm), (6000, 12000, 24000)

3.7. Determination of Drug (CG-1521) Encapsulation Efficiency

The entrapment efficiency of CG-1521 in starch nanoparticles was determined by NanoDrop 2000 (Thermo Fisher Scientific, NY, USA) spectrophotometer. Nanoparticles were recovered from dispersion using ultracentifuge running at 12,000 rpm and washed three times. The supernatants were collected and analyzed to determine the amount of released drug measured by Nanodrop at 335 nm. The calibration curve of CG-1521 (Suppl Fig. 1) was used to calculate percentage of encapsulated drug. As shown in Equation 1, the encapsulation efficiency determined by substacting total drug present in supernatants from the starting amount of drug used in formulation.

$$\text{Encapsulation efficiency (EE \%)} = \frac{\text{Weight of drug entrapped within nanoparticles}}{\text{Total drug added}} \times 100$$

(Equation 1)

The drug encapsulation capacity of the polymer was investigated using different drug/polymer ratios.

3.8. Determination of Drug Release Profiles

Drug release profiles were determined by using a dialysis method according to the following protocol:

- 3 mg of CG-1521 loaded starch nanoparticles were dispersed in 3 ml PBS and placed in dialysis membranes.
- Dialysis membranes were placed in 50 mL of PBS release media of different pH values (6 and 7.4) and mixed at 300 rpm and 37 °C.

- 0.5 mL samples were taken from the release media at predetermined time intervals for over 120 hours.
- After sample withdrawals, 0.5 mL PBS buffered solution was added to keep PBS volume same.
- Drug concentrations in the samples were determined by UV spectrometer, and cumulative drug releases were calculated according to Equation 2 below.

The effects of different pH values on drug release profiles were examined. Under the same conditions, the free drug was used as the control group.

$$\text{Cumulative release of CG-1521 (\%)} = \frac{C_n V_t + V_0 \sum_1^{n-1} Ci}{W_{CG\text{-}1521}} \times 100$$

(Equation 2)

where $W_{CG\text{-}1521}$ is the total amount of drug loaded in NPs, V_0 is the replaced volume of medium (0.5 ml), V_t is the total volume of PBS (50 ml), and C_i and C_n are the concentrations of drug at different times ($mgmL^{-1}$).

3.9. *In Vitro* Cytotoxicity

3.9.1. Crystal Violet Test

In cell culture, cells adhering to surface are detached from the surface after cell death. This characteristic allows the determination of the difference in proliferation of cells that are activated by agents inducing cell death, thereby allowing quantitative measurement of cell death. The crystal violet dye, its chemical structure is shown in Figure 3.3 as organic chloride salt, attached to the proteins and DNA of the cells provides a detection of the remaining cells adhering to the surface. Crystal violet has (deep purple) blue-violet color in aqueous solution with maximum absorbance at 590 nm.

The live cell population interact with therapeutic agents cause a decrease in the crystal violet dye in the culture. Thus, cytotoxic agents can be examined for cell viability and growth inhibition effects [125, 126].

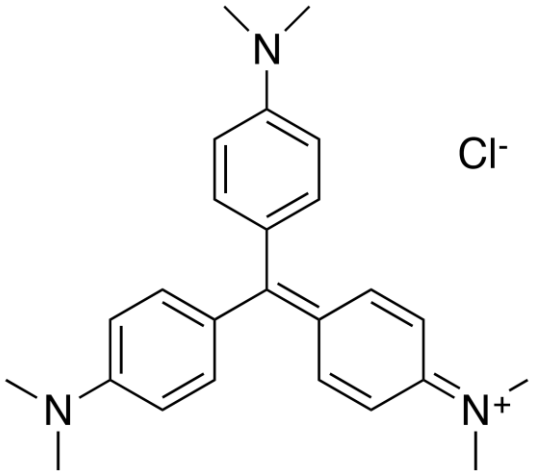

Figure 3.3. Chemical structure of crystal violet

To determine the half-maximal inhibition concentration (IC_{50}), MCF-7 breast cancer cells were interacted with free drug at different doses (0–10 μM). The optical densities were measured using a plate reader by applying the crystal violet test as detailed below. The cytotoxic drug loaded into the nanoparticles was compared with the cytotoxic effect of the free CG1521 by applying the same protocol.

The protocol applied to the crystal violet test includes the following steps which is summarized in a schematic flow-chart in Figure 3.4, respectively.

- The MCF-7 breast cancer cells used in the study were obtained from American Type Culture Collection (Rockville, MD).
- The cells were grown in a 150 cm^2 culture container in alpha-MEM (pH 7.1) medium cell medium 5% FBS and 1% GlutaMax.
- Cells are routinely passaged every 4-5 days.
- MCF-7 cells (1300 cells/well) were plated in a 96-well for 48 hours and treated with free CG-1521 (0-7.5 μM dose interval), CG-NPs and FA-CG-NPs at equivalent drug concentration.
- DMSO, VD-NPs and drug-loaded unmodified nanoparticles (CG-NPs) for were used as control groups.

- The culture medium in each plate was discarded at predetermined time intervals (24, 48 and 72 hours) and 200 µL glutaraldehyde (2% / PBS) was added to each of the plates, for fixation.
- The plates were agitated for 20 min at 50 rpm on a mechanical shaker. Then the glutaraldehyde was discarded, and 150 µL crystal violet (0.1%/distilled water) dye was added to each well and the plates were shaken on a mechanical shaker for 30 minutes.
- The plates are then placed and washed with distilled water flowing continuously until the water becomes clear.
- Plates were left to dry at room temperature and then the dye was solubilized by adding 200 µL Triton X-100 to the wells.
- The optical density (absorbance at 590 nm) of plates shaken for 30 min was then measured using a plate reader (Viktor Plate reader-Perkin Elmer).
- MDA-MB-231 cells (800 cells/well) were allowed to interact with nanoparticles using the same protocol and doses.

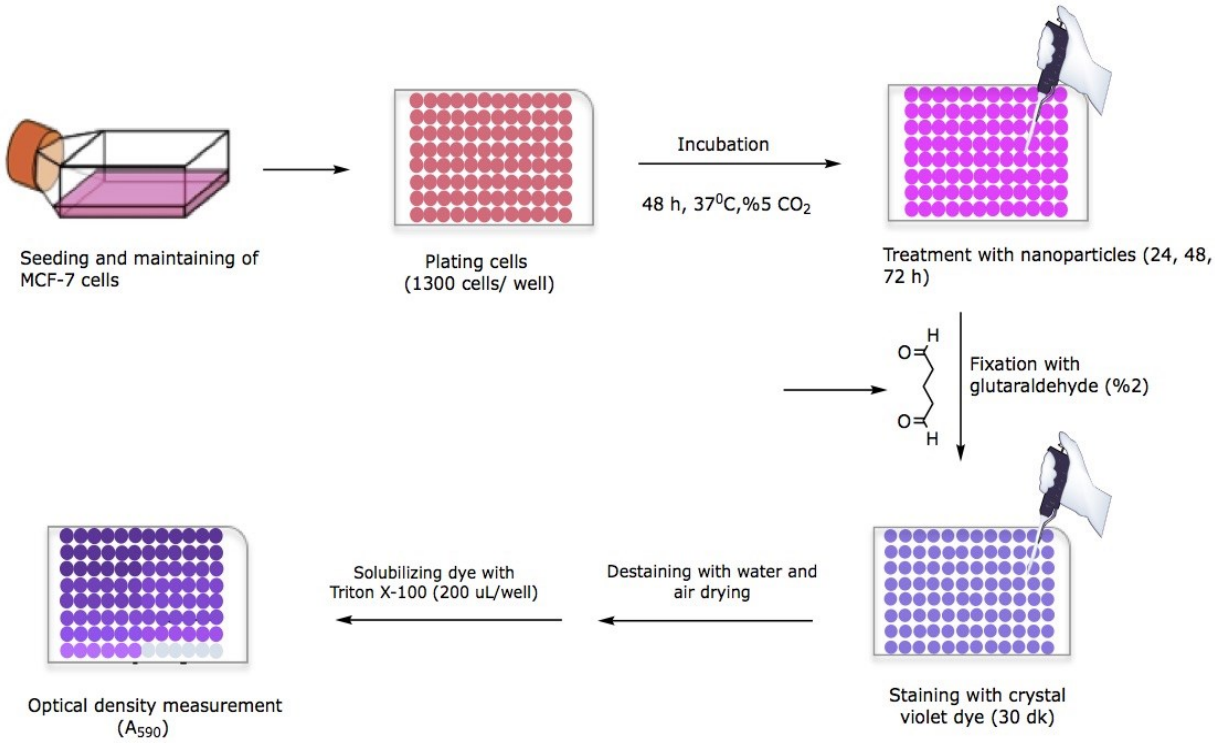

Figure 3.4. Workflow chart of crystal violet assay

3.9.2. Muse Cell Analysis System

The Muse cell analysis system is a compact and new-generation analysis system that allows for determination of cell concentration, cell viability, apoptosis, and the cell cycle with high accuracy and precision. The system facilitates vital multidimensional analysis of cells in a single platform. This system is based on microcapillary flow technology and detects fluorescence of cells as well as analyzes vital cellular parameters by using cell counts at a minimal level [127, 128].

3.9.2.1. Examination of Viability Profiles with Muse Cell Analysis System

In the studies conducted with this system, the viability profiles of MCF-7 cells after treatments with free CG-1521 and CG-NPs were analyzed. The Muse Count Life Kit contains two different dyes that link to DNA and stain live and dead cells according to the permeability of cell membranes. One of the dyes attaches to DNA to dye the nuclei of dead or dying cells whose membrane integrity is deteriorated. This parameter shows the viability profile and

distinguishes dead cells from live cells. The other dye stains all the cells with a nucleus and distinguishes the nucleated cells from the residues or cells without a nucleus. Figure 3.5 represents the cell viability profile of cell population analyzed with Cell muse analyzer.

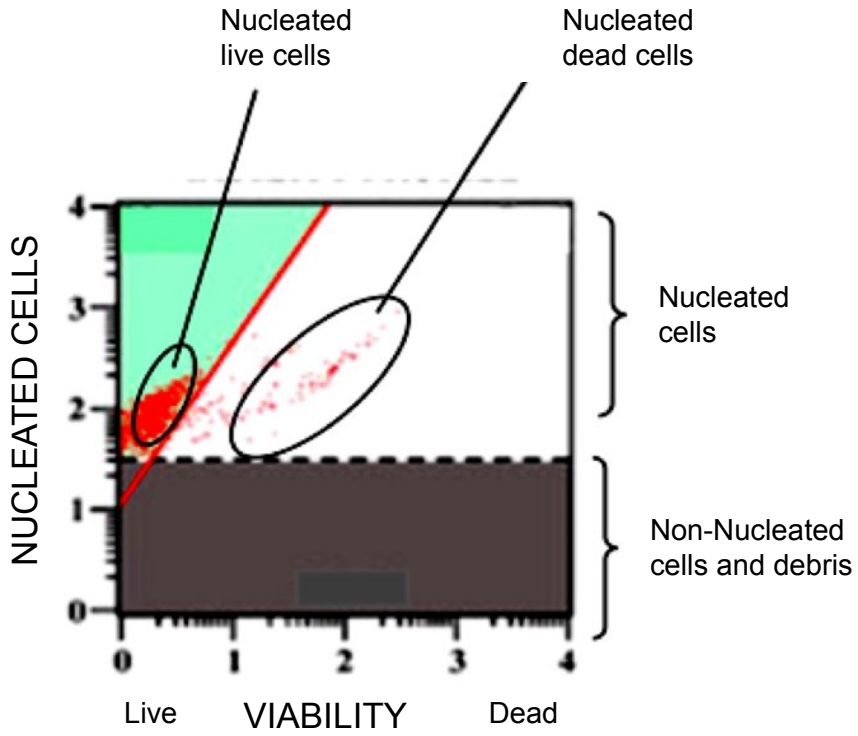

Figure 3.5. Schematic representation of the cell viability profile [129]

The protocol used for the examination of the viability profiles is as follows

- Cells were plated in 4 different 100x15 mm petri dishes ($3x10^5$ cells/dish).
- After 48 hours, the cells were treated with the free drug (3 μM CG-1521) and CG-NPs at the same concentration. DMSO and VD-NPs were used as control groups.
- Cell media were collected in 50 mL tubes after 72 hours of treatment.
- The cell plates were washed two times with PBS, and the washing water was added to the collected cell media.
- The cell suspension/washing water collection was added to the incubated petri dishes for 5 min with the Trypsin-EDTA solution and the cell suspensions were transferred to the centrifuge tube.

- During the transfer process, the cell suspensions are kept in a container containing ice. After transfer, the cells were pelleted for 3 min at 1500 rpm and 4 ºC using centrifuge. Supernatants were discarded and the cell pellets were dispersed in PBS containing 1% FBS. The volume of FBS/PBS solution added is noted for the calculation of the cell density for further steps.
- For analysis of viability profiles, 25 µL of each cell suspension dispersed in FBS/PBS was added to 225 µL (1:10) MUSE VIA reagent solution.
- Samples were incubated in the dark for 5 minutes room temperature and analyzed by Muse cell analyzer.

(The remaining cell suspensions were used for subsequent Annexin V, cell cycle, and DNA fragmentation experiments.)

3.9.2.2. Examination of Apoptotic Populations with Muse Cell Analysis System

Apoptosis, also known as programmed death, regulates the cell growth and proliferation. The cells can respond to signals initiated by some intercellular processes and cause characteristic physiological changes. These physiological changes include translocation of phosphatidylserine to exterior of cell membrane, degradation of some specific cell proteins, DNA fragmentation in nuclear chromatin, and the loss of cell membrane integrity [130,131].

Annexin V, a calcium-dependent protein, has a high affinity to phosphatidylserine. Usually, phosphatidylserines localized inside the cell membrane begin to transfer to the outside of the cell membrane during the early stages of apoptosis. Annexin-V binds to these phosphatidylserines translocated to the outer part of the cell [132].

Annexin-V and the Dead Cell Muse kit provide the detection of PS transferred to the outer surface of apoptotic cells. The 7-AAD (Aminoactinomycin D) in the kit is a fluorescent-based chemical compound that is used as a biomarker for dead cells. Figure 3.6 represents the cell populations that are distinguished from each other using Cell muse analyzer.

Non-apoptotic cells pepresents Annexin V and 7-AAD negative. The cells in early phase are Annexin V positive but 7-AAD negative. The dead cells and

apoptotic cells are both Annexin V and 7-AAD positive. Nuclear debris is Annexin V negative while it is 7-AAD positive.

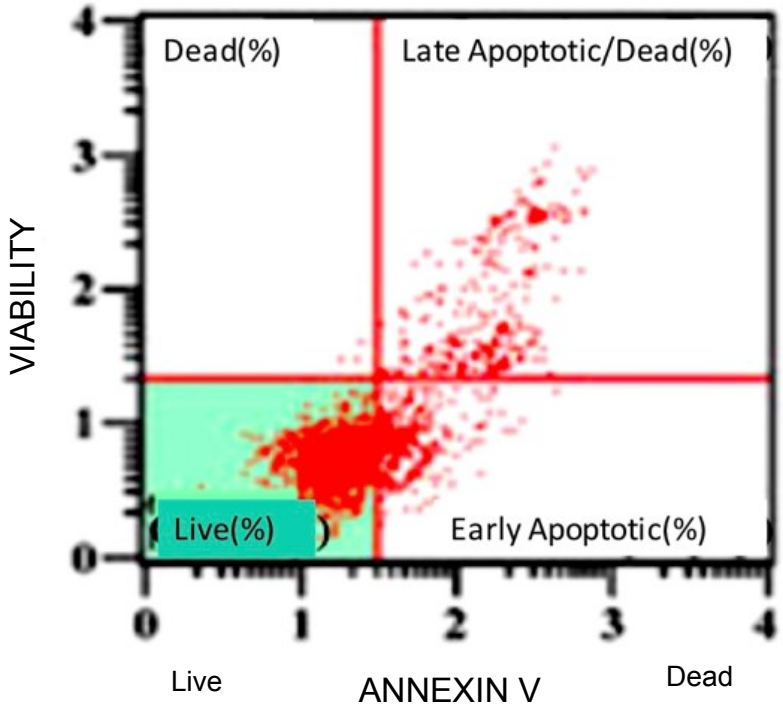

Figure 3.6. Schematic representation of cell populations in different stages of apoptosis [133]

Apoptotic cell populations were examined according to the following procedure:

- Cell suspension (100 µL) was taken from each of the samples used for the viability test and diluted in an appropriate proportion to 1% FBS/FBS (dilution factor noted).
- MUSE ANX reagent solution (100 µL) was added to a 100–µL aliquot of each diluted cell samples.
- The samples were incubated for 20 minutes in the dark at room temperature and analyzed by Muse Cell Analyzer.

3.9.2.3. Examination of Cell Cycle by Muse Cell Analysis System

The cell cycle is one the fundamental mechanisms involved in cell growth and division in eukaryotic cells. The mechanism also involves in genetic disorders repairment and uncontrolled cell growth. Disorders in the cell cycle and

mutations in the genes involved in the cell cycle are characteristic features of many cancer types. Cell cycle analysis is an important contribution to understanding the molecular mechanisms of many anti-cancer compounds [134].

The Muse Cell Cycle reagent solution consists of a mixture of propidium iodide (PI), DNA intercalator dye, and RNase A enzyme. PI dye provides the quantification of DNA contant in each phase in the presence of the RNase enzyme. During resting phase (G0/G1), the cells have two copies of each chromosome. After that DNA start to replicate during S phase. The intensity of PI continues to increase until the chromosomal DNA doubles at the G2/M phase. At this point, the G2/M phase cells emit fluorescence intensity two times higher than the cells in the G0/G1 population. The G2/M phase cells are eventually divided into two separate cells. Figure 3.7 represents the phases of the cell cycle.

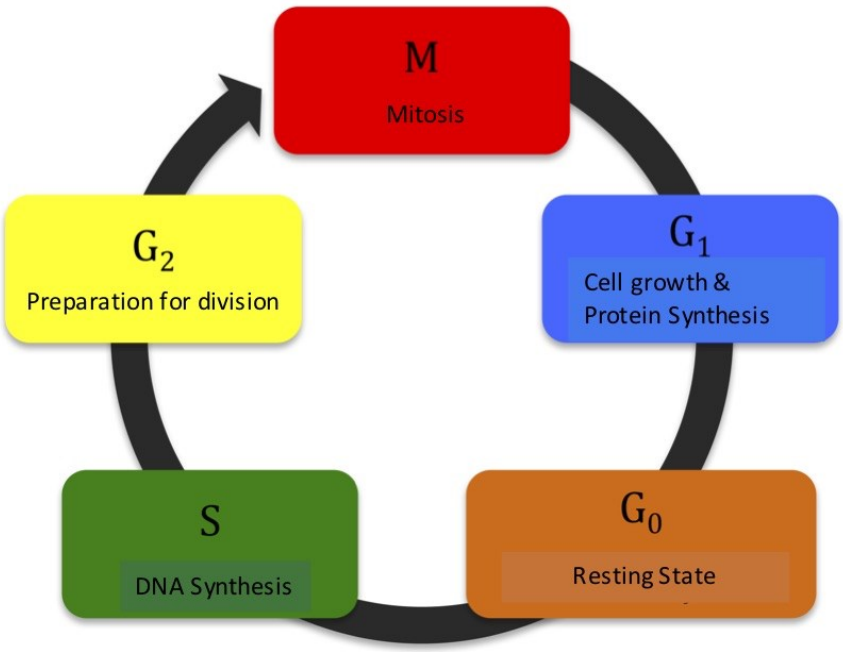

Figure 3.7. Phases of the cell cycle [135]

The following protocol was followed to examine the cell cycle.

- The cell suspensions used for viability assay were centrifuged again (1500 rpm/4 ºC/3dk), and the cell pellets were dispersed in 500 µL PBS.

- Samples (100 µL portions) were added to microcentrifuge tubes containing 400 µL of cold EtOH (90%). The samples were incubated for 18 hours at –20 ºC.
- The total number of cells in the petri dish was calculated and approximately 300,000 cells were transferred to the microcentrifuge tube.
- 600 µL of PBS (0.2% BSA) was added and centrifuged at 1200 rpm at 4 ºC for 3 min. 200 µL of the Muse cell cycling solution was added, which was then incubated for 30 min in the dark and analyzed by the Muse cell analyzer.

3.9.2.4. Determination of DNA Fragmentation by Flow Cytometry (TUNEL Test)

Flow cytometry is a cell analysis method to determine the physical and chemical characteristics of cell population or particles containing nuclei, microorganisms, or chromosomes. Fluorescent dyes can bind to DNA or RNA directly, or they can bind to any part of DNA and RNA as an intercalator. The labeled cells are allowed to flow past from a source emitting laser light. The signals from the cells or particles are collected and analyzed. The cell's physical properties such as its size, its granularity, and the fluorochromes bound to the cells constitute specific signals. These signals can give information about the immune phenotype of the cells, enzyme activities, DNA contents, membrane potentials, and viability. Figure 3.8 shows the components of the flow cytometer and the working principle.

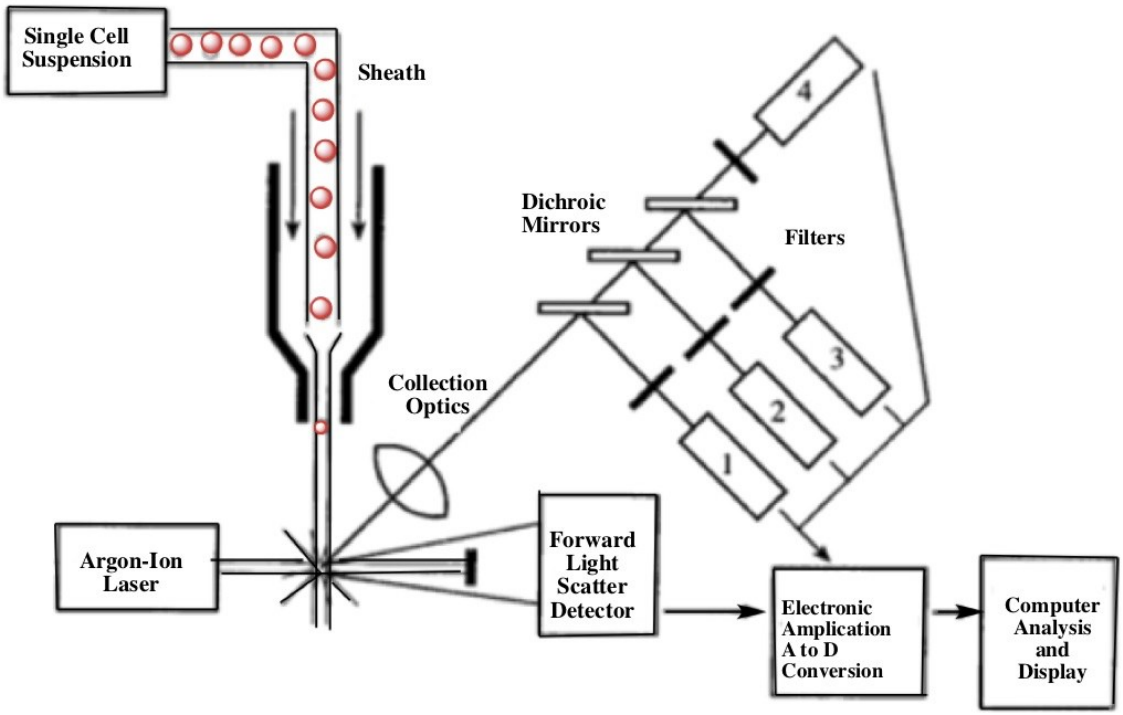

Figure 3.8. Schematic representation of the flow cytometer [136]

The TUNEL (TdT-dUTP nick-end-labeling) assay provides the detection of DNA fragments during apoptosis. Binding of the FITC-labeled anti-BrdU monoclonal antibody to the free 3'-OH ends of DNA breaks that are emerging during apoptosis ensured by adding terminal deoxyuridine transferase (TdT) enzyme. At the same time, counter-dying is performed for total DNA by adding PI/RNAnase to the medium. Figure 3.9 represents the mechanism of the TUNEL assay.

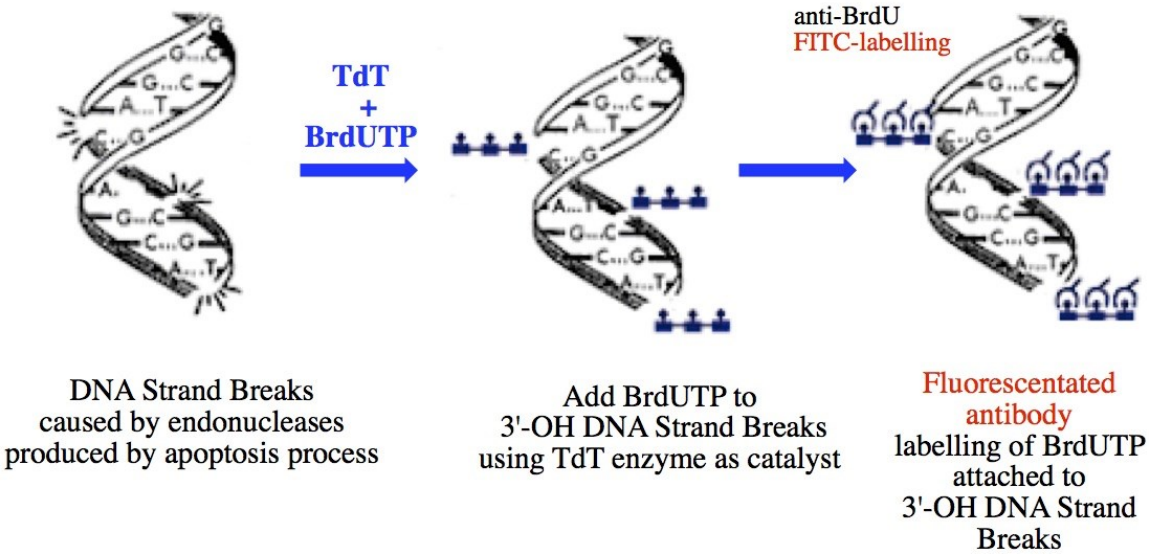

Figure 3.9. Mechanism of the TUNEL assay [137]

The TUNEL test was performed according to the following protocol:

- A sample of $1x10^6$ cells (Free CG-1521, CG-NPs and control groups treated) remaining from the Muse viability test were transferred to 1.5 mL microcentrifuge tubes for the TUNEL test.
- PBS/0.2% BSA solution (600 µL) was added to samples and the tubes were centrifuged (1200 rpm/ 4 ºC/ 3 min).
- The washing process was repeated once again under the same conditions.
- 50 µL DNA labeling solution added to cell pellets after supernatants were discarded. Table 3.1 shows the content of the DNA labeling solution for one assay.

Table 3.1. Content of the DNA labeling solution

DNA labeling solution	1 Assay
TdT reaction buffer	10.00 µL
Br-dUTP	8.00 µL
Cobalt chloride	5.00 µL
dH2O	25.75 µL
TdT enzyme	1.25 µL

- The samples were incubated for at 37 ºC for 1 hour.
- At the end of incubation, each tube was centrifuged (1200 rpm / 4 ºC / 3 min) after 600 µL PBS/0.2% BSA solution was added.
- 600 µL wash buffer solution (PBS/ 0.1% Triton X-100/1% BSA) was added to pellets and centrifuged under the same conditions and washed.
- 100 µL of anti-BrdU monoclonal antibody solution (1:5, FITC-labeled) diluted in washing buffer solution was added to the pellets.
- Samples were transferred to 12x75 mm tubes used for flow cytometry analysis.
- The samples were incubated for 30 minutes in a dark environment.
- PI dye (500 µL of 5 µg/mL) containing RNase (1: 1000) was then added into the samples and incubated for an additional 30 min in the dark.
- After incubation (less than 1 hour), samples were analyzed by flow cytometry.

3.10. Cellular Uptake Study

The cellular uptake of Rhodamine 6C–labeled starch nanoparticles by the MCF-7 cells was examined. The following protocol was followed for the cellular uptake study.

- First, 20000 cells/well were seeded in a four wells-glass chamber slide.
- After 48 hours, cell media was discarded, and cells were treated with Rhodamine 6G fluorescent dye–labeled and drug-loaded (300 µg/mL) nanoparticles. Unlabeled void nanoparticles were used as the control group.
- After 12 hours of exposure, the media was removed and 500 µL paraformaldehyde (4%/PBS) was added to chambers for fixation at room temperature and incubated for 20 min.
- The paraformaldehyde was discarded, and slides were washed two times with PBS.
- 200 µL Triton X-100/PBS (0.2%) was added to chambers for 5 min.
- Each cell was then incubated in the dark for 20 min with the addition of cell nuclei dye, Hoechst dye (1:1000).

- The plates were washed with PBS, instilled with a mounting media containing DAPI (4', 6-diamidino-2-phenylindole) dye (25 µL/well) and fixed with glass covers.
- Plates were examined for cellular uptake using a confocal microscope (LEICA TCS SP5, USA) after 24 hours.

3.11. Determination of Biological Mechanism of Drug-Loaded Nanoparticles by RT-qPCR

The cellular response of MCF-7 cells to CG-1521 and CG-NPs was determined by examining the mRNA levels of different genes associated with p-53 target gene. The following protocol was followed for gene expression studies.

- MCF-7 cells were plated in petri dishes (100x25 mm in diameter) at $3x10^5$ cells/dish density.
- The cells incubated for 48h and followed by treatment with 3 µM CG-1521 and CG-NPs at the same drug concentration.
- After 48-h treatment, RNA was extracted using the RNeasy mini kit (Qiagen, Valencia, CA). In brief, cell mediums were transferred to the tubes. The cell pellets were washed with PBS and the washing waters were collected into the tubes.
- Trypsin (1 mL) was added to each cell pellet, which was incubated at 37 ºC for 5 min. The collected media and the washing media (5ml/dish) were added to the dishes.
- The collected cells suspension was then pelleted by centrifugation (1200 rpm/ 4 ºC/3 min) and the supernatant was discarded. 350 µL of RLT Plus Buffer solution containing 10 µL of beta-mercaptoethanol was added to the pellets for cell lysis and transferred to RNAse-free tubes.
- Samples were vortexed, transferred to a QIAshreder spin column and centrifuged (10000 rpm /2 min) for homogenization.
- Homogenized cell lysates were stored at –80 ºC for the next step.
- Homogenized cell lysates were transferred to the gDNA eliminator spin column and centrifuged, and the column was thrown away.
- 350 µL of 70% ethanol was added to the centrifuge-separated suspension and transferred it to the RNeasy spin column. 700 µL RW1 Buffer solution

was added to the re-centrifuged (10000 rpm, 30 sec) samples and the membrane was washed again.

- At the next stage, 500 µL RPE Buffer solution was added to the RNeasy spin column and centrifuged (8000 rpm, 2 min). The same process was repeated.
- The RNeasy spin column then placed in a collection tube. RNase-free water (50 µL) was added to tubes. For disassociation of the RNA content, the sample was centrifuged (10000 rpm, 1 min) and the RNA concentrations of the samples were measured by NanoDrop.
- 1.5 µg of total RNA was used to convert the RNA to cDNA. RT reagents and MultiScribe reverse transcriptase (Applied Biosystem) was used for cDNA synthesis. The appropriate reaction mixture was prepared for RNA patterns containing certain amounts of reverse transcriptase buffer, MultiScribe reverse transcriptase enzyme, random hexamer primer, dNTP, $MgCl_2$ and water.
- The reaction mixture was incubated in a Mastercycler (Eppendorf) for 10 min at 25 ºC, 1 h at 37 ºC and 5 min at 95 ºC and stored at –20 ºC. Each cDNA was synthesized from 3 independent biological RNA extraction replicates.
- 384-well plates were used for the measurement of gene expressions. SYBR Green PCR Master mix (Applied Biosystems, TX, USA) and water-free RNase were added to the diluted mixture of each specific forward and reverse primers (12 µM).
- Primer mixture (7 µL) was added to the wells.
- A 3 µL sample of cDNA was added to each well. The plate was covered, and the plate is centrifuged.
- SYBR Green PCR Master mix (Applied Biosystems, TX, USA) was used to determine transcript levels by a QuantStudio 12K Flex Real-Time PCR system (Fisher Scientific) running for 40 cycles (15 sec, 95 ºC and 1 min, 60 ºC). After 40 cycles were completed, the melting curve analyses were conducted. The results are obtained as the Ct value (threshold cycle value), which is known as the value at which the fluorescence of a PCR product can be detected above the threshold value. GAPDH was used as an endogenous group (housekeeping gene). The mRNA level of each

transcript was normalized to GAPDH. The data obtained were analyzed using the $2^{-\Delta\Delta Ct}$ method to calculate the expression fold change for each gene.

- The primer sequences used in qPCR (Integrated DNA Technologies, USA) are shown in Table 3.2 below.

Table 3.2. Forward and reverse sequences of primers

Primers	**Forward**
KNTC2	5'- AAA AGT CTC GCT ATT TGG CAA AA-3'
GADD45A	5'- GGA TGC CCT GGA GGA AGT G-3'
GDF15	5'- CCA TGG TGC TCA TTC AAA AGA C-3'
BNIP3	5'- CAC AAG ATA CCA ACA GGG CTT CT- 3'
BNIP3L	5- TGA TGA AAA CTG GCT CAA GAT GTT T-3
P21	5' CCT AAT CCG CCC A CA GGA A-3'
P21B	5' CCA GGA TAC AGC CTT TCA TTC AG-3'
CYCLIN B1	5'- TTT CTG CTG GGT GTA GGT CCT T-3'
CYCLIN D1	5'- ACT CCA AAT CTC AAT GAA GCC AG-3'
STK6	5'- ACA CCC CTG GAT CAC AGC AA-3'
SURVIVIN	5' CTG TGG GCC CCT TAG CAA T- 3'
PLK1	5' CTC AAC ACG ACG CCT CAT CCT C -3'
CDC25A	5' AAG AAG CCC ATT GTA CCT GAT G
	Reverse
KNTC2	5'- GCT TGT AGA GAT TTC ATG GAC ACA TT-3'
GADD45A	5'- GGA TCA GGG TGA AGT GGA TCT G-3'
GDF15	5'- CCC AAG AAG GTC ACC CCA AT -3'
BNIP3	5'- TGC GCT TCG GGT GTT TAA AG- 3'
BNIP3L	5 TTA TCT GAC TGG CTA AGT CTT CAA TTC T-3
P21	5' ACC TCC GGG AGA GAG GAA AAG-3'
P21B	5' CAG TTC CTC CAG CCT CCT AAG TC-3'
CYCLIN B1	5' -GCC ATG TTG ATC TTC GCC TTA-3'
CYCLIN D1	5'-CTT TTG GTT CGG CAG CTT G- 3'
STK6	5'-GAT TGA GGG CAG CAG TCA ATG -3'
SURVIVIN	5' TAA GCC CGG GAA TCA AAA CA-3'
PLK1	5' GTG CTC GCT CAT GTA ATT GC-3'
CDC25A	5' ATA CAG CTC AGG GTA GTA GTG GAG TTT G

- Statistical analyses were performed by GraphPad Prism Software using one-way ANOVA (Tukey's test). Significance was defined as a p-value of $p< 0.05$. The data represents the mean ($\pm$ SD) of three replicates.

4. RESULTS AND DISCUSSION

4.1. Characterization of Folic Acid–Bound Starch Nanoparticles

4.1.1. Chemical Characterization of Folic Acid–Bound Starch Polymer

Proton NMR characteristic peaks of C-H2, C-H3, C-H4, C-H5 and C-H6 of starch are seen at δ 3.5, and 3.9 ppm interval as shown in Figure 4.1.A. CH1 proton peak is seen at δ 5.1 ppm. The peaks in the vicinity of δ 4.50 and 5.40 ppm are attributed to the OH protons of starch. The characteristic proton H-7 and H-8 NMR peaks of Folic Acid are in the range of δ 2.0-2.3 shown in Figure 4.1.B, and the peaks of H-2 and H-6 are the in the range of δ 4.2-4.5, aromatic proton (H-1, H-3, H-4) and NH peaks are in the range of δ 6.5 to 8.5. Proton peaks around δ 11.3 belong to the carboxylic acid protons (H-5, H-9).

The proton NMR of Folic Acid modified starch was examined. Characteristic peaks of both Folic Acid and starch were observed near δ= 2.0. The peaks in the interval of 6.5-8.5 belong to Folic Acid. The peaks in the range of δ= 3.5-3.9 and in the vicinity of δ=4.5, 5.1 and 5.40 proton peaks also correspond to starch. The proton NMR peaks of the ethylenediamine protons, which are the binding group between Folic Acid and starch, were not observed in the spectrum because the expected broader H2-H6 proton peaks of starch in the same region overlapped as shown in Figure 4.2.

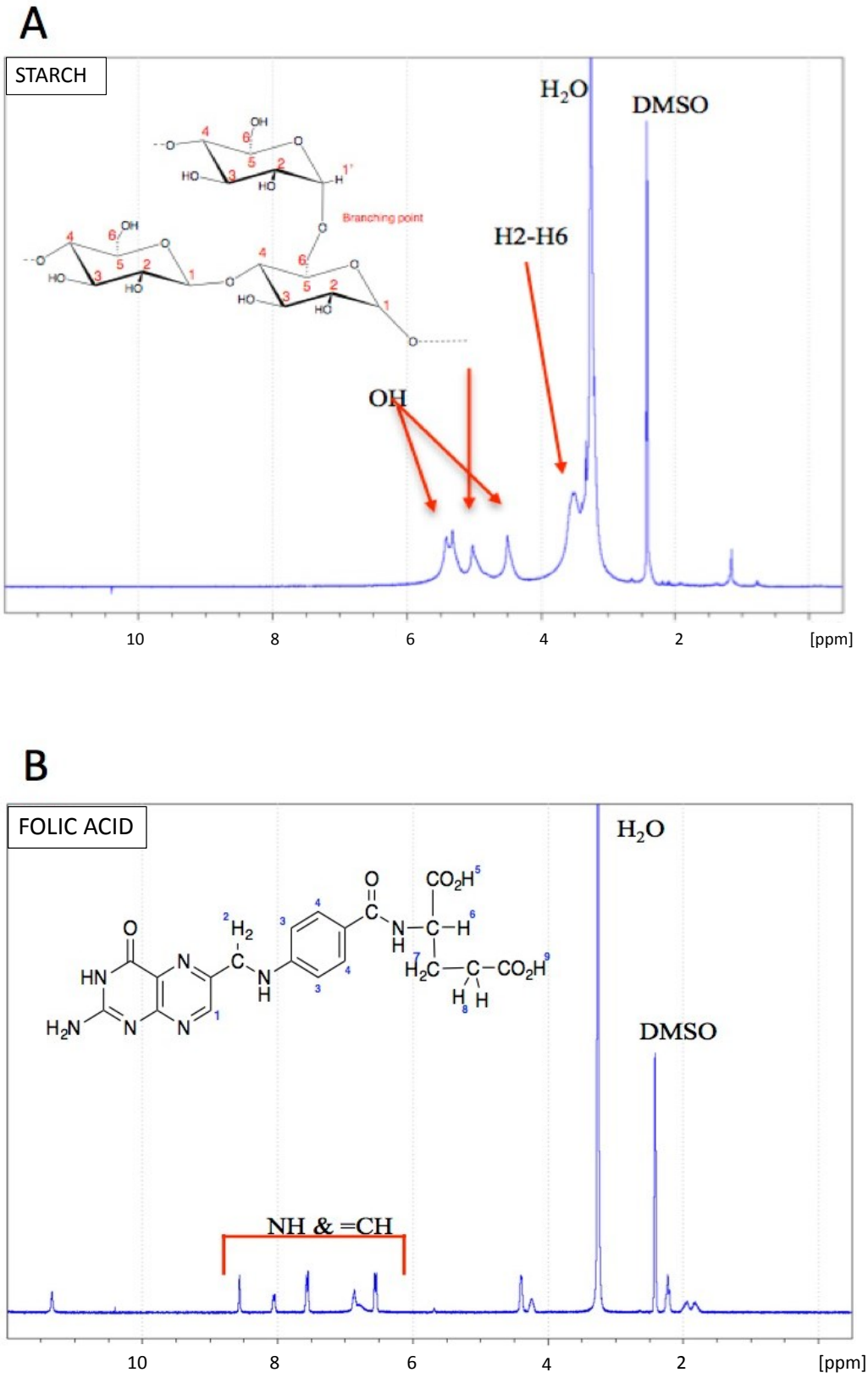

Figure 4.1. NMR spectrum of starch (A) and Folic Acid (B)

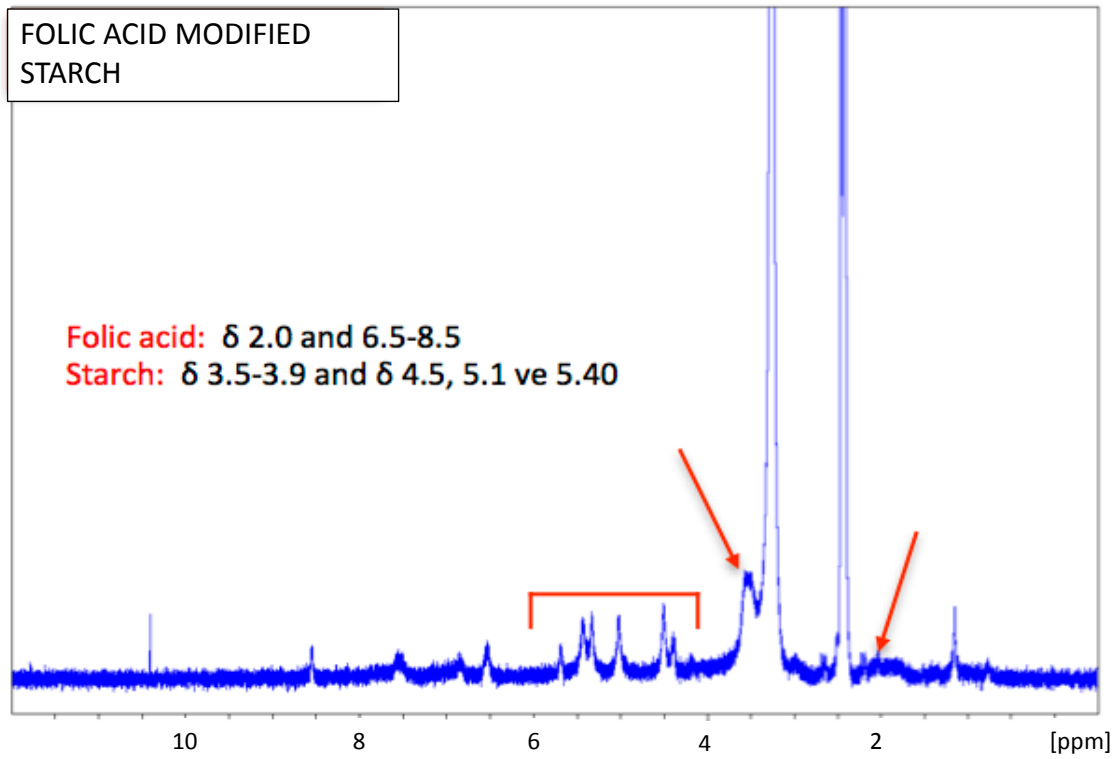

Figure 4.2. NMR spectrum of Folic Acid conjugated starch

4.1.2. Size Distribution, Zeta Potential and Morphological Properties of Nanoparticles

The average size and zeta potential of the nanoparticles were analyzed by a Zeta-Sizer Nano-ZS (Malvern Instruments). As shown in Figure 4.3 A, the average diameter of void nanoparticles is 180.0 nm and have the polydispersity index of 0.138. One of the most crucial parameters can affect the transportation of nanoparticles and their uptake by the cells is particle size [31]. The small size of nanoparticles we synthesized can provide higher uptake efficiency resulting in more intracellular delivery of our drug.

The slim polydispersity index (<0.4) confirmed that the nanoparticles are in a narrow size range, which can play a vital role in the accumulation of nanoparticles in tissues and the mechanism of renal clearance. The drug encapsulation does not cause a significant increase in the size of nanoparticles (Figure 4.3.B).

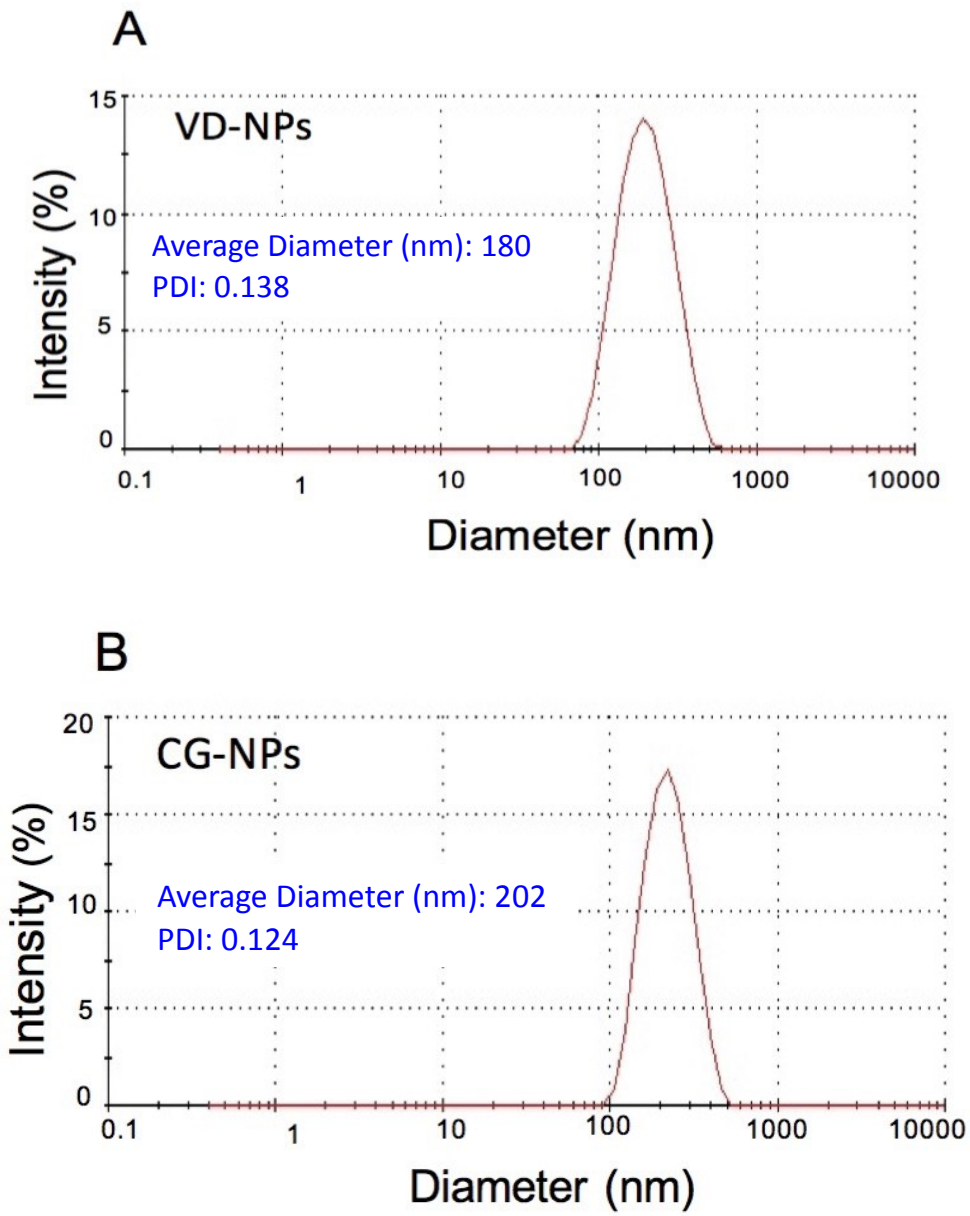

Figure 4.3. Size distribution of void (A) and drug-loaded (B) nanoparticles

Another critical physical parameter that can affect the stability of the nanoparticles in a specific region in the circulation is the zeta potential (net surface charge) [144]. While the zeta potentials of void nanoparticles were measured as –16.1 mV, drug-loaded nanoparticles had zeta potential of –10.2 mV as shown in Figure 4.4. The parameters we obtained can provide satisfactory stability of our nanoparticles in the circulation and can lead to more specific drug delivery in the targeting site. The zeta potential of a slightly negatively charged nanoparticle originates from hydroxyl groups which are localized on the surface of the starch.

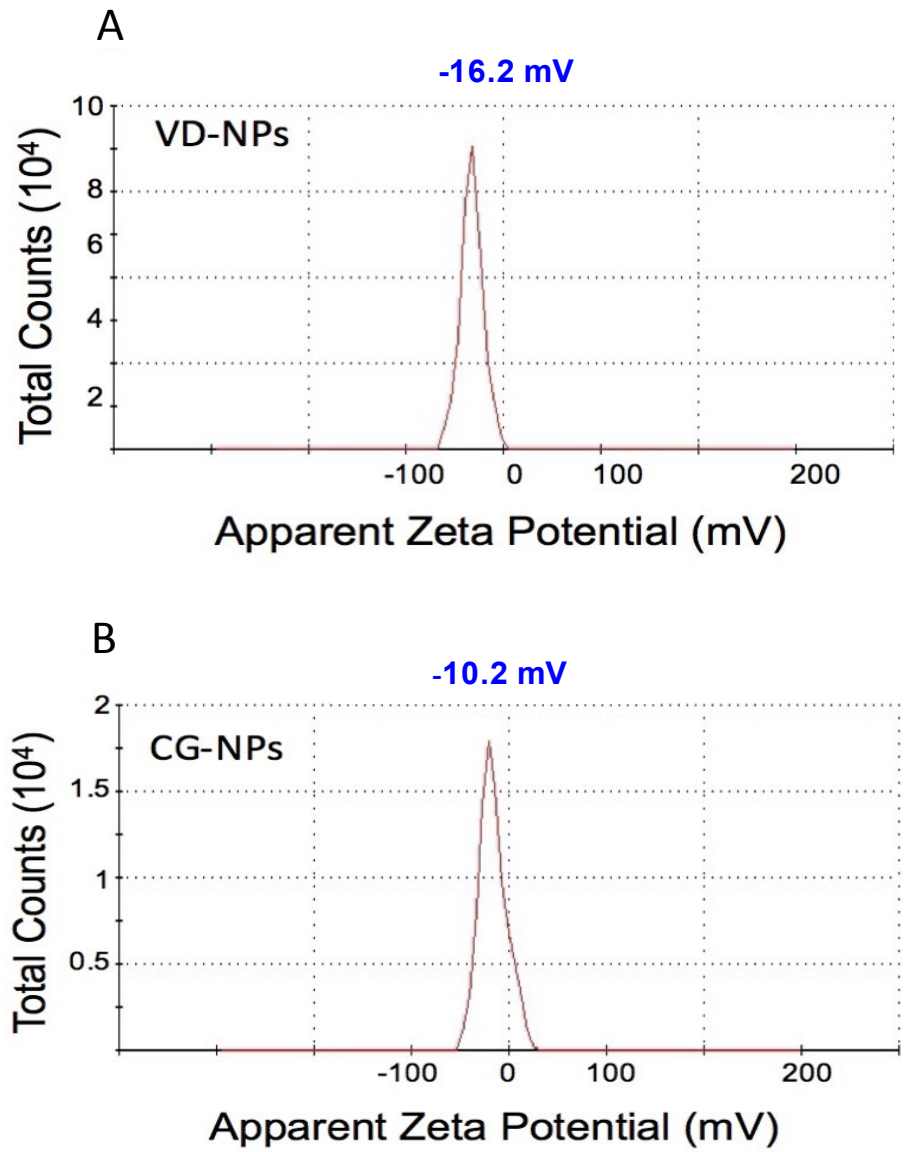

Figure 4.4. The zeta potential distribution of void (A) and drug-loaded (B) nanoparticles

Morphological characteristics of void nanoparticles were investigated using SEM and AFM. From both SEM (Figure 4.5.A) and AFM (Figure 4.5.B) images, it is observed that the boundaries of the nanoparticles are well-defined in the spherical structure. The size of the nanoparticles is consistent with the size distribution obtained from the Zeta-sizer.

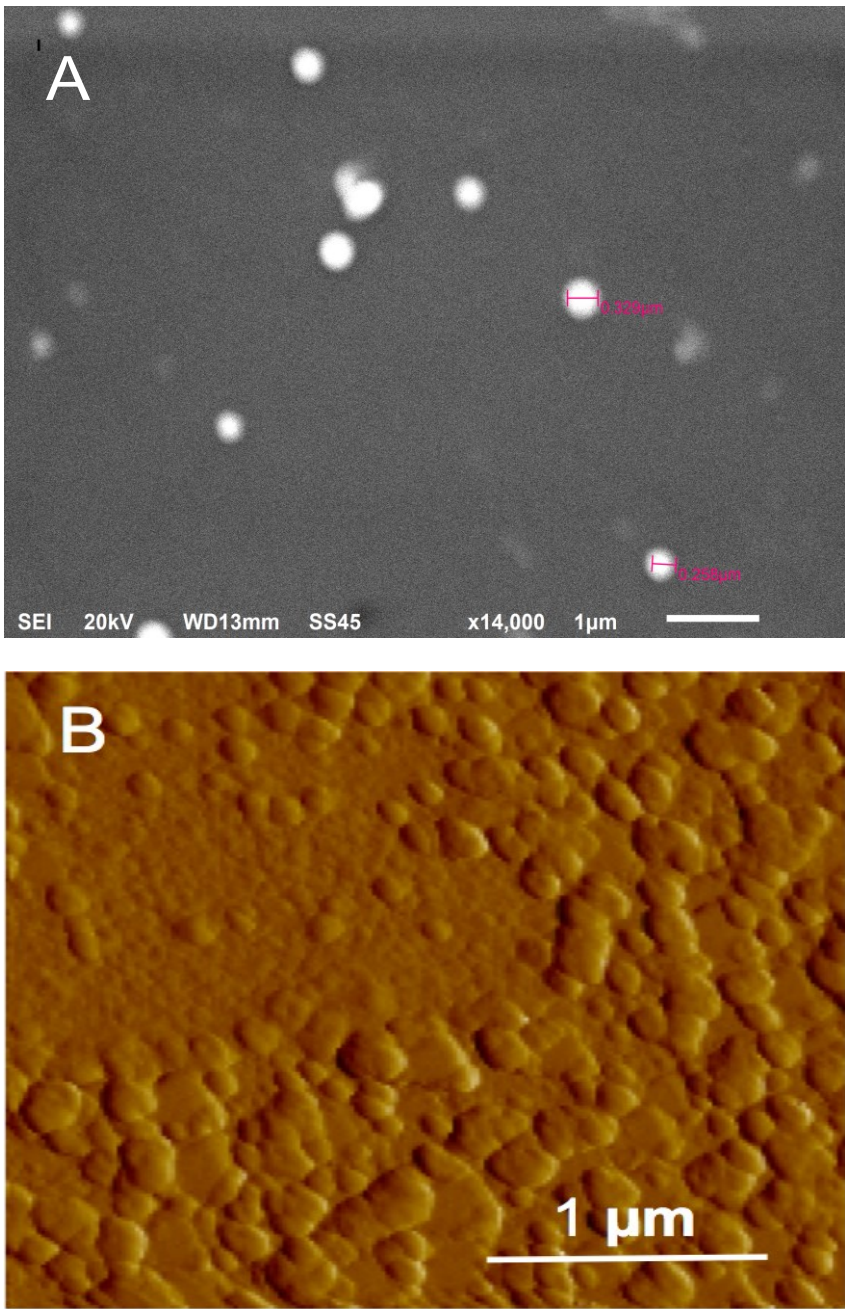

Figure 4.5. SEM (A) and AFM (B) images of nanoparticles

4.1.3. Effects of Formulation Parameters on Nanoparticle Size

The effects of nanoparticle formulation variables (polymer concentration, surfactant concentration, and homogenization rate) on nanoparticle size were investigated. The size distributions of the nanoparticles prepared using different polymer concentrations (2%, 3%, and 4%) were compared. It was found that an increase in polymer concentration resulted in larger particle size (Figure 4.6).

An increase in polymer viscosity contributes to the formation of larger size emulsion droplets [138].

Surfactant concentration is a parameter that can affect the formation and stabilization of emulsion globules dramatically. Surfactant molecules inhibit coalescence and reduce the free energy between two intermediate phases. More surfactant is needed to stabilize nanodroplets with a larger surface area [138]. From the data we obtained, it is inferred that the size range of the particles decreases with an increase in concentration of the PVA (0.5%–2%) as surfactant (Figure 4.6).

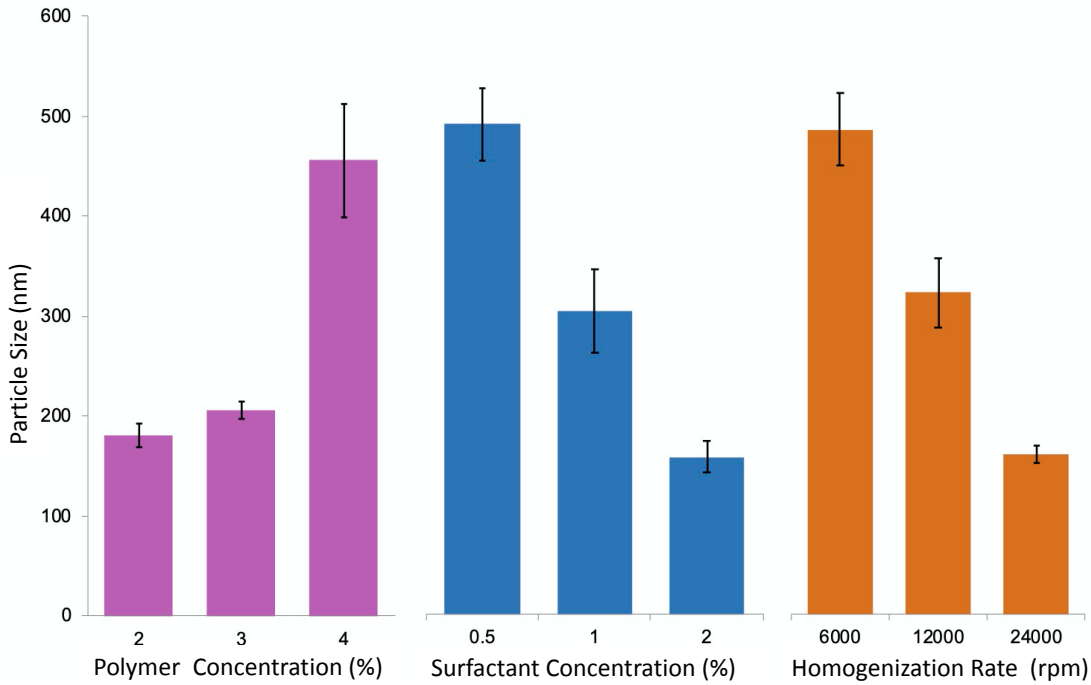

Figure 4.6. Effect of formulation parameters on size distributions of nanoparticles. Data are shows as mean± SD. (n=3).

Finally, the effect of the homogenization rate on the particle size distribution was investigated. The energy density applied during the emulsion affects the particle size [139]. Nanoparticles prepared at lower homogenization speeds (6000, 12000, 24000 rpm) were found to have larger nanoparticle sizes (512 nm, 363 nm, and 180 nm, respectively). As the energy density transferred to the

media during the homogenization process increased, the polymeric-based organic phase passed through the aqueous phase faster.

Under the scope of optimization studies, we synthesized the smallest particle size of nanoparticles using 2% polymer and surfactant concentration, and 24000 rpm homogenization rate [Suppl. Table 1]. We used the same formulation criterions for the further studies.

4.1.4. Effect of Polymer-Drug Ratio on Encapsulation Efficiency

To evaluate the maximum encapsulation efficiency of a nanoparticle, various amounts of drug (drug/polymer ratios of 0.1; 0.15; 0.25; 0.4) were added to organic phase (100 mg) containing a fixed concentration of polymers. The encapsulation efficiency results showed an upward trend for the drug/polymer ratio in the range of 0.1-0.25. There was a slight decrease in efficiency in the 0.4 drug/polymer formulation (Figure 4.7). The surfactant concentration (2%) and homogenization rate (24000 rpm) were kept constant for all experiment. Most polymers, including starch, have limited encapsulation capacity [140]. The formulation has 1/4 drug/polymer ratio (maximum drug encapsulation, 69%) used for all cell studies.

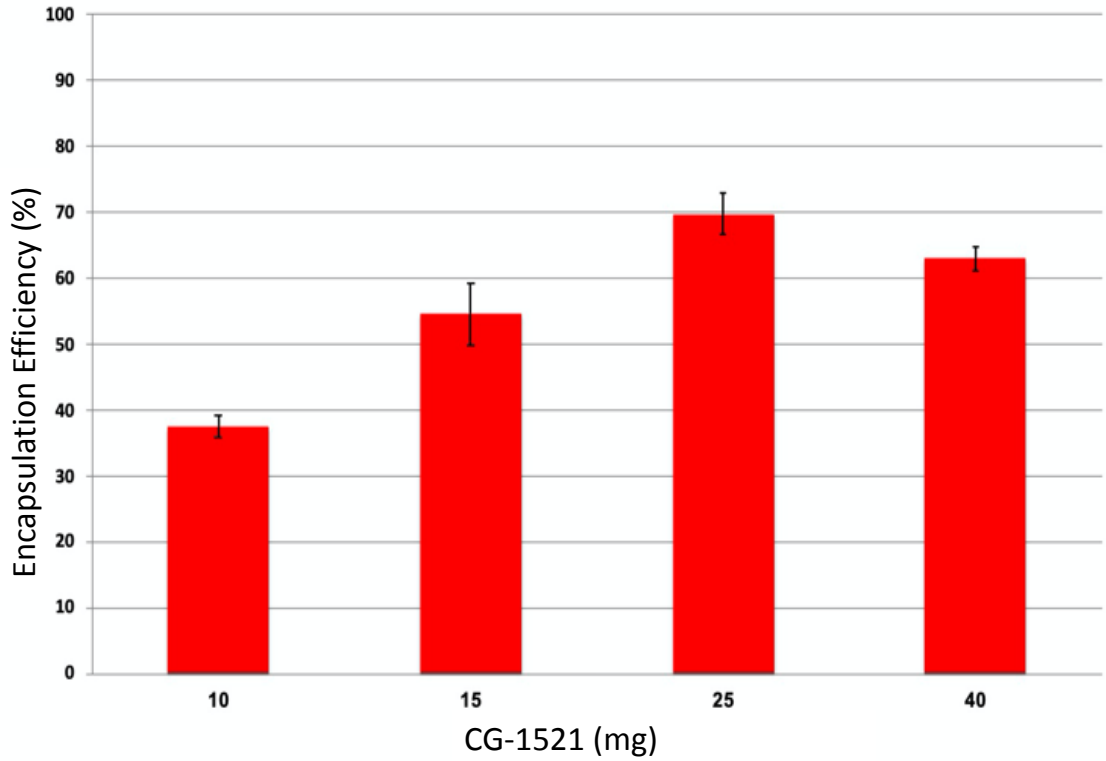

Figure 4.7. Drug encapsulation activity of nanoparticles. Data represents mean± SD. (n=3).

4.1.5. FT-IR and ^{1}H-NMR Analysis of Starch Nanoparticles

Chemical characterization of drug-loaded nanoparticles was investigated using FT-IR. The characteristic absorption frequency of CG-1521 showed its presence in the spectrum of drug-loaded nanoparticles (Figure 4.8). 1632 cm^{-1} IR absorption peak of CG-1521 belongs to =CO functional group and stretching peak in the range of 1580-1600 cm^{-1} belongs to C=C stretching peak. The peak appearing at 3011 cm^{-1} wavelength belongs to the C-H (aromatic) characteristic group of the CG-1521.

It has also been found that there is no chemical interaction between the drug molecules and the polymer matrix. In the next step, to investigate the chemical characterization of Folic Acid–bound and drug-loaded starch nanoparticles as final products, both FT-IR and proton NMR were used.

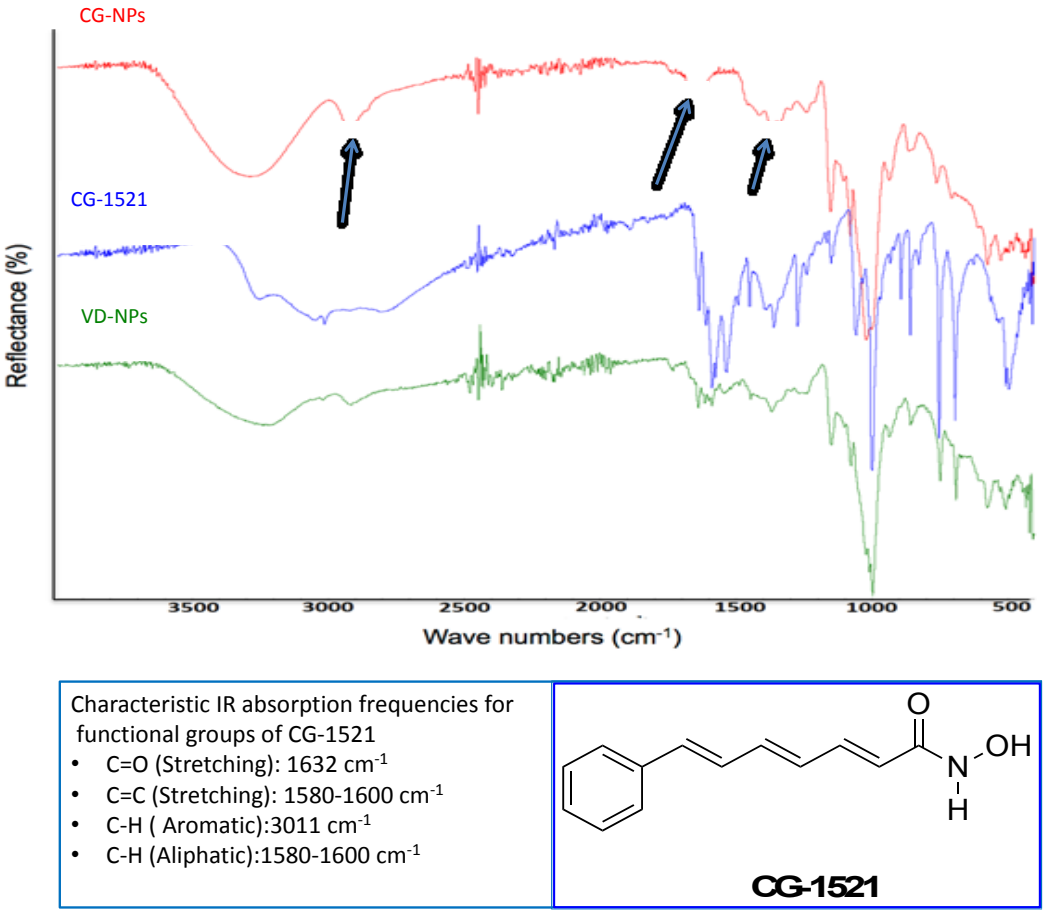

Figure 4.8. FT-IR spectra of the free drug and void and drug-loaded nanoparticles

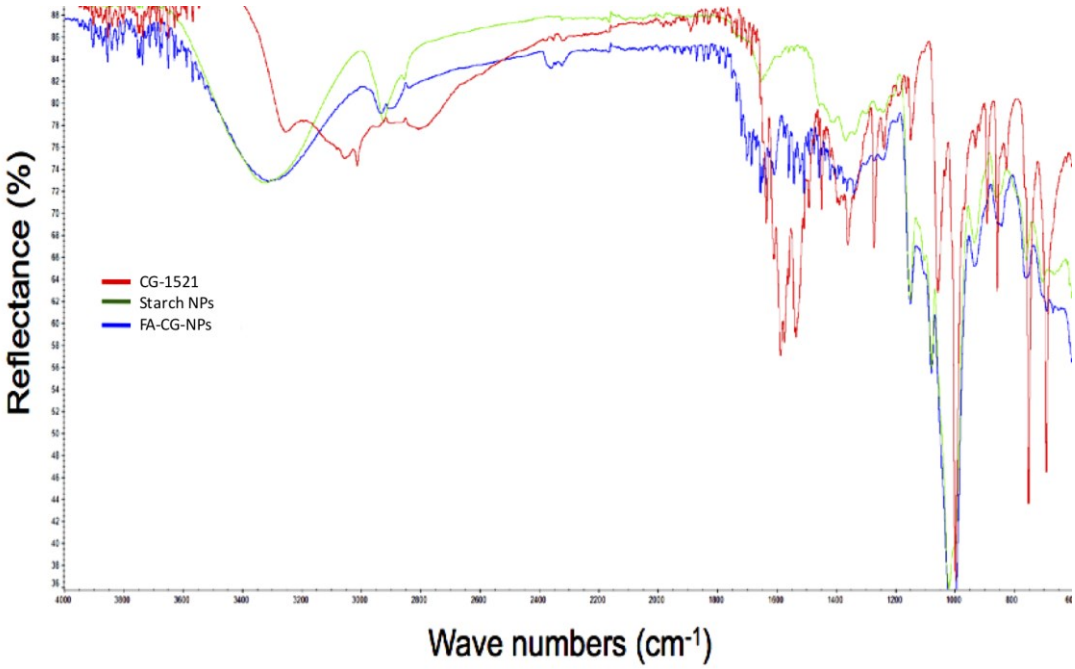

Figure 4.9. FT-IR spectrum of the free drug and drug-loaded and Folic Acid–conjugated nanoparticles

The FT-IR spectrum of Folic Acid and Folic Acid–modified nanoparticles are shown in Figure 4.9. Many characteristic peaks belonging to the free Folic Acid were observed at 3540 cm^{-1}, 3400 cm^{-1}, 3300 cm^{-1}, 3300 cm^{-1}, 2900 cm^{-1}, 2800 cm^{-1}, 1690 cm^{-1}, 1600 cm^{-1}, 1480 cm^{-1}, 1410 cm^{-1} inter-band [141]. The peaks at the area of 3600 and 3000 represent vibrations from hydroxyl (OH) and NH-stretching. The peaks at 1650-1690 belong to the C=O group and indicate the amide group both in the Folic Acid and in the CG-1521 molecule. It is difficult to distinguish between the peak belonging to the C=O group in the new amide bond formed between starch and Folic Acid, since overlapped with the peak of the C=O group of the CG-1251 molecule. Due to the overlapping absorption frequencies of the drug and Folic Acid in the fingerprint region of the spectrum, some peaks could not be detected.

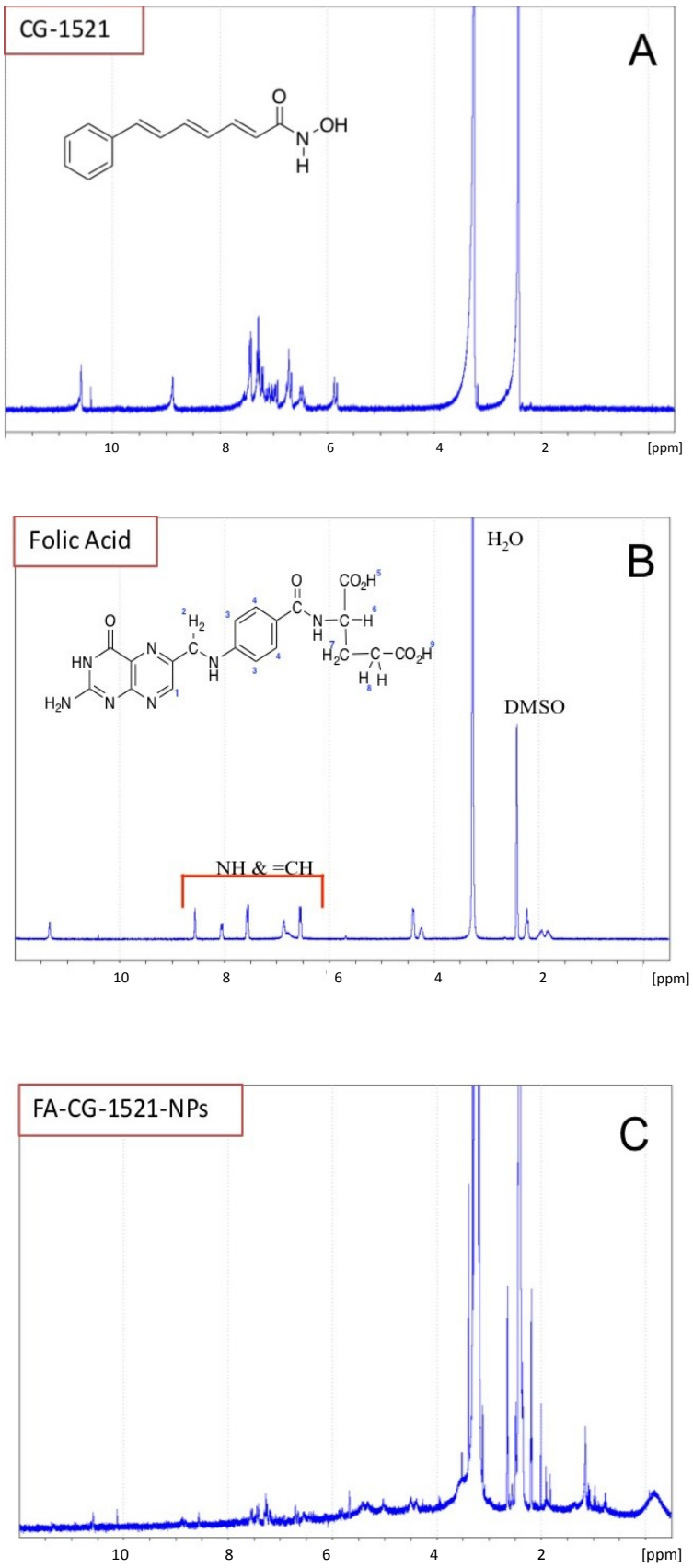

Figure 4.10. NMR spectra of the free drug (A), Folic Acid (B) and drug loaded Folic Acid–conjugated nanoparticles (C)

In the NMR spectra of drug-loaded and Folic Acid–bound NPs, specific =CH protons belonging to CG-1521 were found in the range of δ 6-7.5 ppm (Figure. 4.10C). Folic Acid peaks in the range of δ 2.0 and 6.5-8.5 were also observed in the spectrum of ligand-conjugated nanoparticles.

4.1.6. Drug Release Study of Nanoparticles

In vitro drug relase studies showed that nearly 95% of the free drug was released in a 4-hours period as control group. In contrast, the release of encapsulated drug showed an initial burst release within 10 hours. After that point, a slower but continuously release was observed over 120 hours. The release kinetics of CG-1521 was also determined in PBS at pH 6.0 and pH 7.4. The release profiles of CG-1521 from the nanoparticles at pH 6.0 or at pH 7.4 are not distinct in the first 10 hours. The release of CG-1521 from the nanoparticles at pH 7.4 does not rise further after 24 hours. However, the drug release continues to increase at pH 6.0 from ~48% to 64% between 24 hours and 120 hours period. The additional release of ~16% of drug confirming that CG-1521 is released from nanoformulation in sustainable manner.

Studies have suggested that the human cancer tumor environment has a pH range of 5.7-6.9 so that a nanotransporter will release its active ingredient slightly more quickly in a more acidic environment, reducing the toxicity of the drug and increasing the local concentration of the drug in tumor site [147].

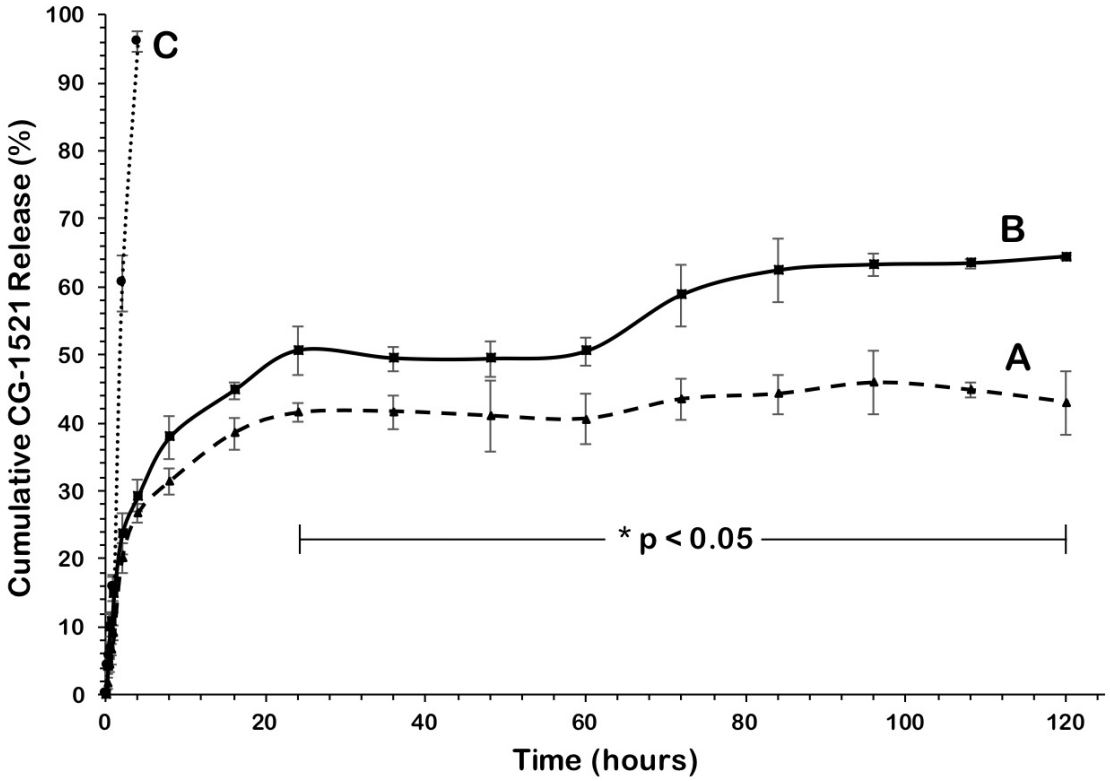

Figure 4.11. *In vitro* release profiles of encapsulated drug nanoparticles at different pH conditions (pH 7.4 (Curve A), pH 6.0 (Curve B) and pH 7.4 free drug (Curve C)).
Data are shown as mean ± SD. (n=3). ANOVA (One-way analysis of variance, Tukey's test) was performed for statistical analyses. Difference between each time points corresponding to curves A and B were significant at p-value < 0.05 after 24h.

4.1.7. The Half-Maximal Inhibition Concentration of the Drug

The half-maximal inhibition (IC50) of the free drug calculated for incorporation into nanoparticles was found to be 3–3.5 μM as shown in Figure 4.12. The dose range that had been selected for the cell studies was determined based on IC50 value.

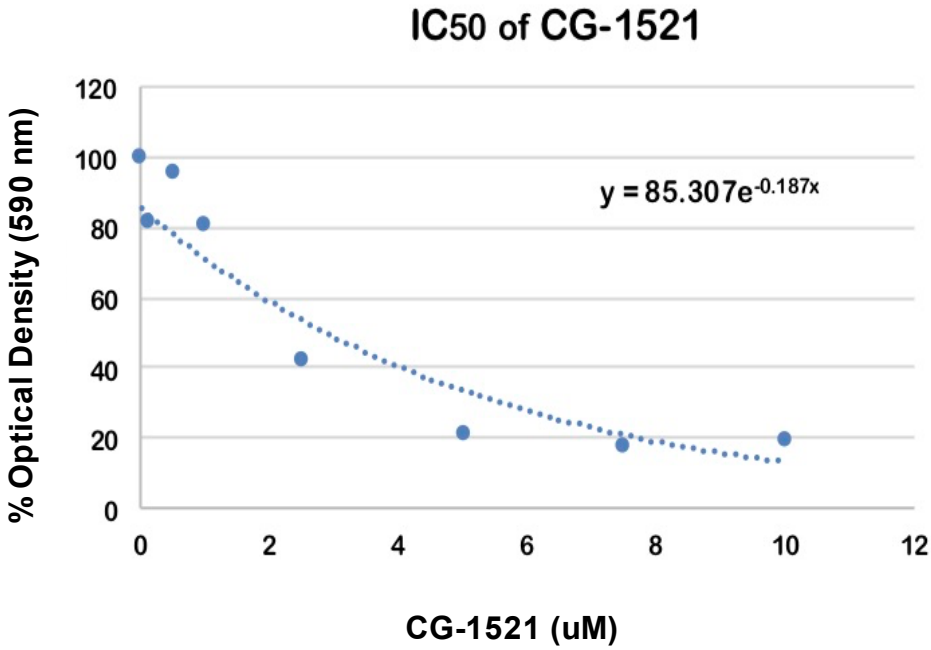

Figure 4.12. The half-maximal inhibition concentration of free drug

4.2. *In Vitro* Cytotoxicity Studies

The crystal violet assay was used to determine the effect of free CG-1521 and CG-NPs at different concentrations on MCF-7 cells growth for 24, 48, 72 hours. The obtained results show that at same drug concentrations, drug loaded nanoparticles are more effective to inhibit cell growth than free drug in a concentration- and time-dependent manner (Figure 4.13).

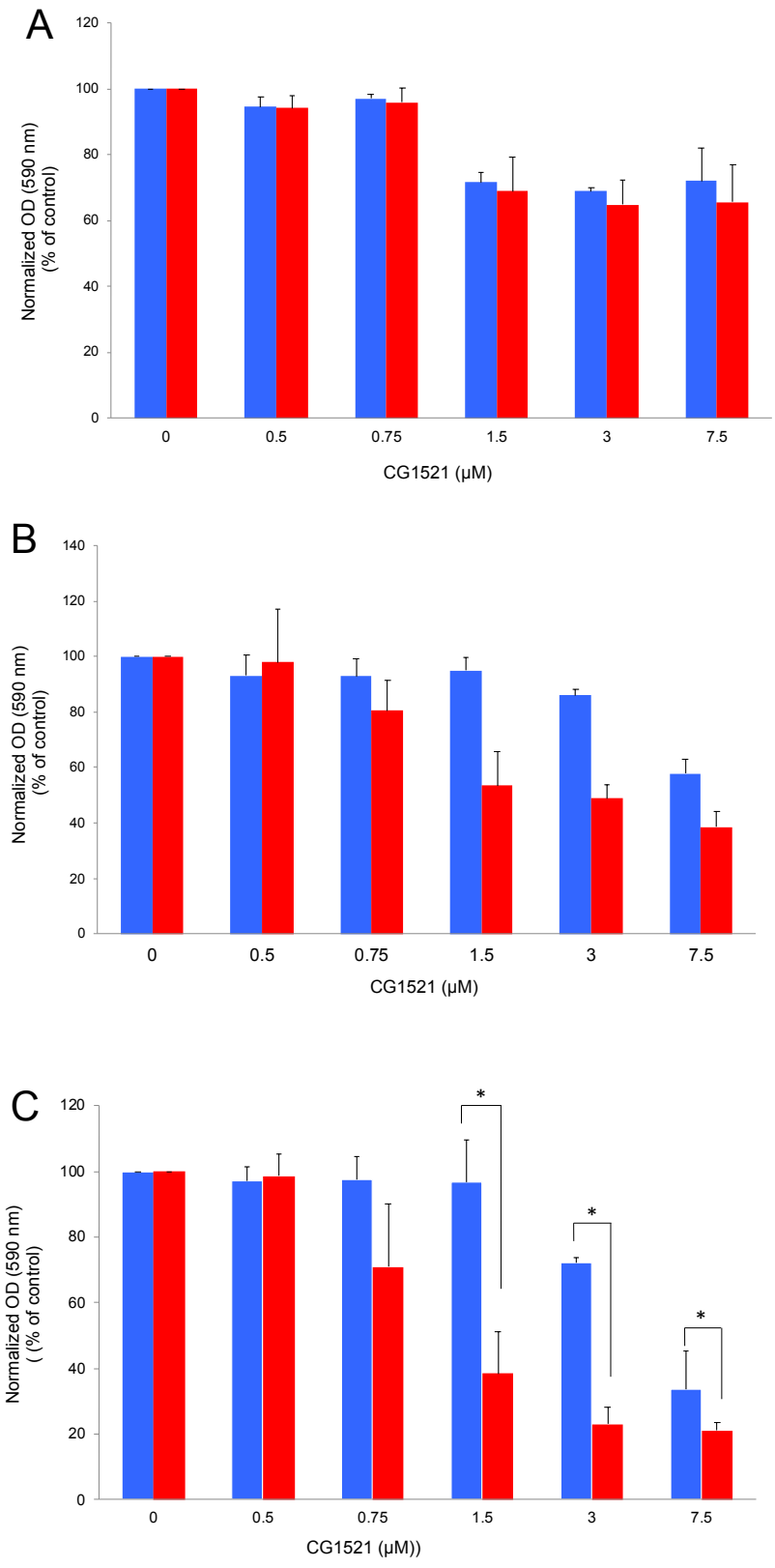

Figure 4.13. Cytotoxicity of the free drug (blue bars) and drug-loaded nanoparticles (red bars) on MCF-7 cells over A) 24 h, B) 48h C) 72h.

The data represent the mean ± SD from three independent experiments. One-way analysis of variance ANOVA (Tukey's test) was performed for statistical analyses of the treatment 72h treatment. The differences were statistically significant at p-value < 0.05.

4.2.1. Assessment of Viability Profiles with Muse Cell Analysis System

The viability profiles of cells interacted with free drug and drug loaded nanoparticles examined with a flow cytometry-based Muse device are consistent with the results of crystal violet. The dead population of cells exposed to the encapsulated drug was observed to be approximately three times that of the dead population of those treated with the free drug alone. This data confirmed that drug loaded nanoparticles are more effective to increase the cell death capacity compared to free drug alone.

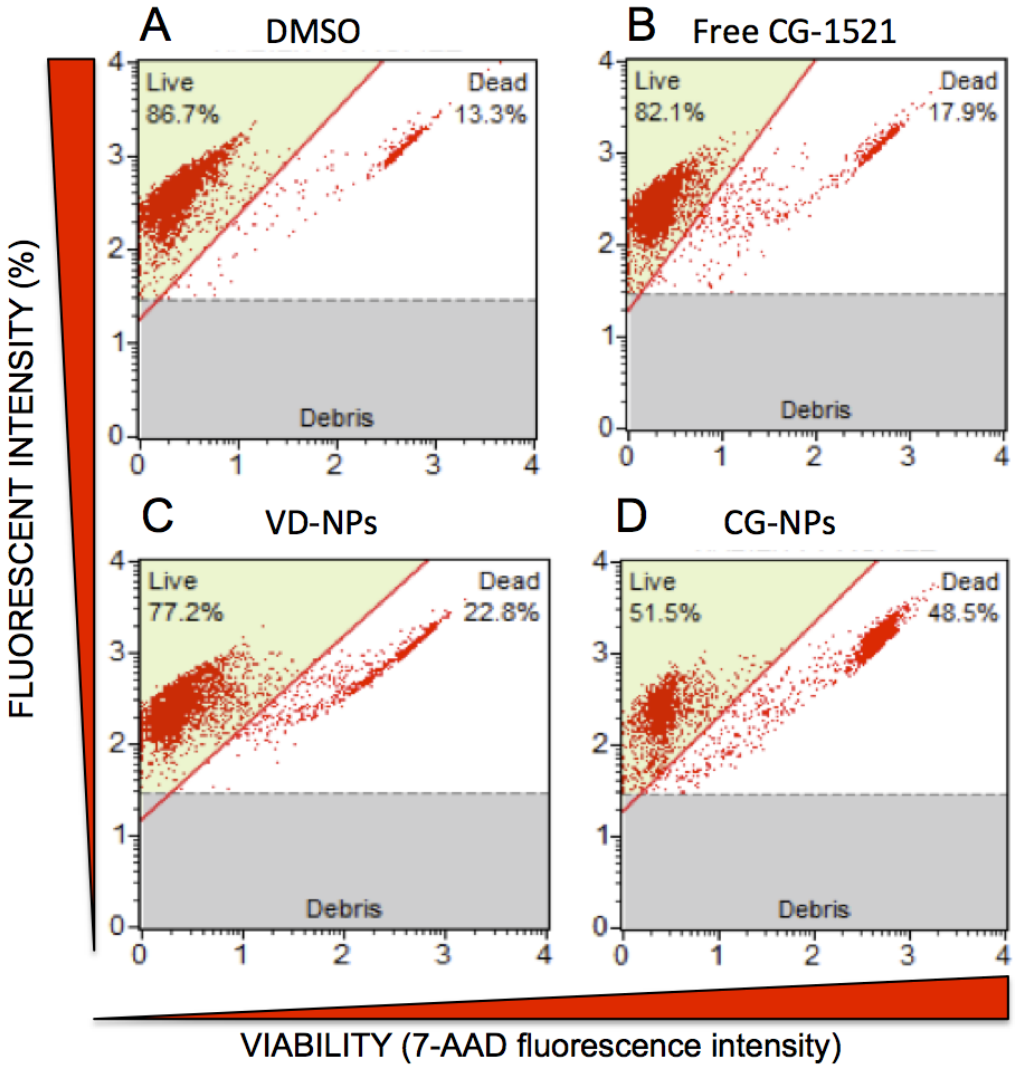

Figure 4.14. Viability profiles of MCF-7 cells exposed to free and encapsulated drug -72h

4.2.2. Evaluation of Apoptotic Populations by Muse Cell Analysis System

The evaluation of apoptotic MCF-7 cell population indicated that treatment with encapsulated CG-1521 increases the percentage of the cells undergoing apoptotic cell death in comparion of cell population treated with free drug. As shown in Figure. 4.15, the proportion of dead cells in the cell population treated with CG-NPs is nearly 2.5-fold higher than cells treated with CG-1521.

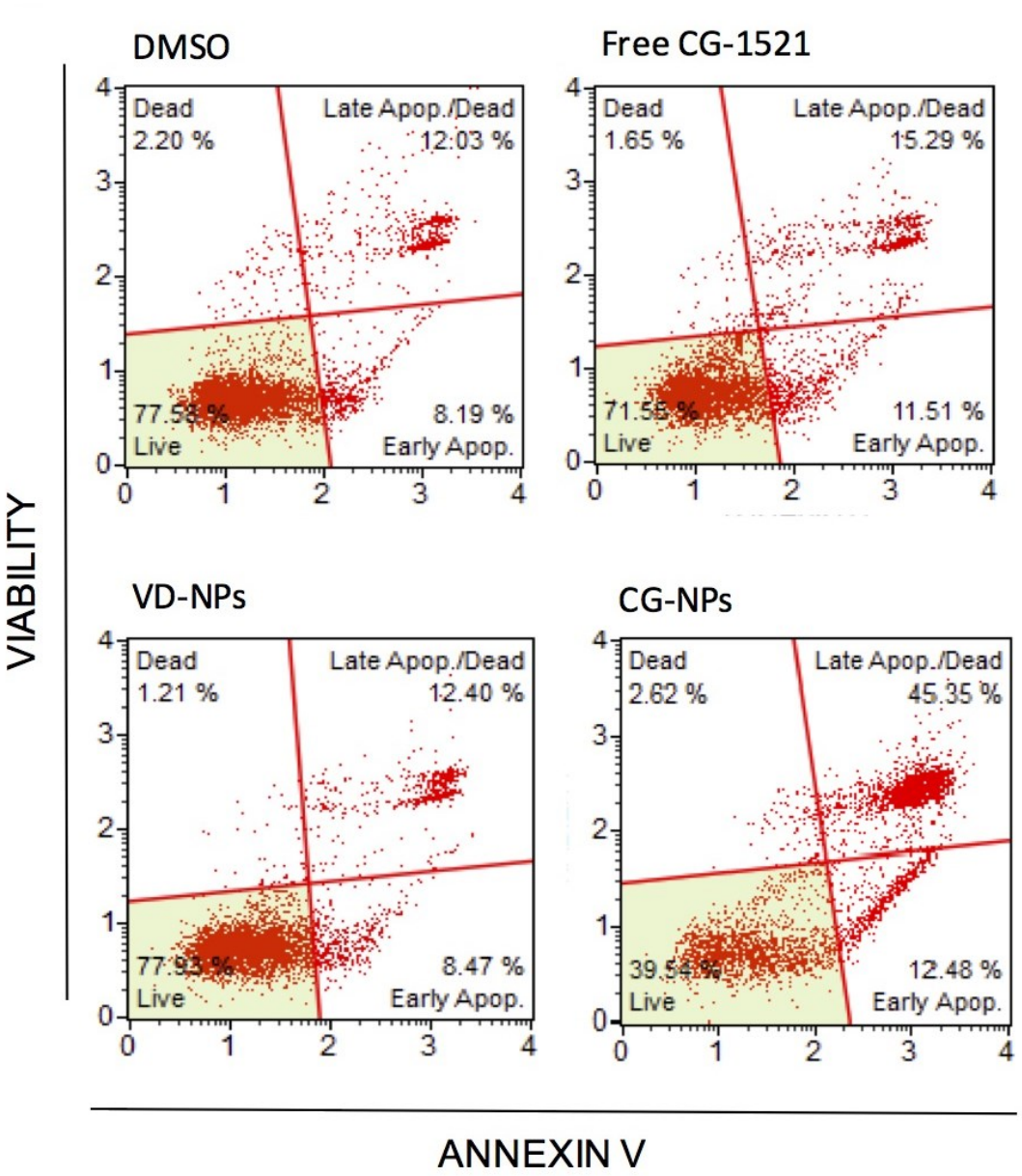

Figure 4.15. Apoptotic profiles of MCF-7 cells treated with free CG-1521 and CG-NPs -72h

4.2.3. Evaluation of the Cell Cycle with Muse Cell Analysis System

Cell cycle analysis was conducted to measure cell proportions in each phase of MCF-7 cells' cycles after exposed to free CG-1521 along with CG-NPs (Fig. 5). The significant increase was observed in the cell popupation arrested in G1 phase of cells treated with encapsulated drug, CG-NPs, in comparision with cells population treated with CG-1521 alone.

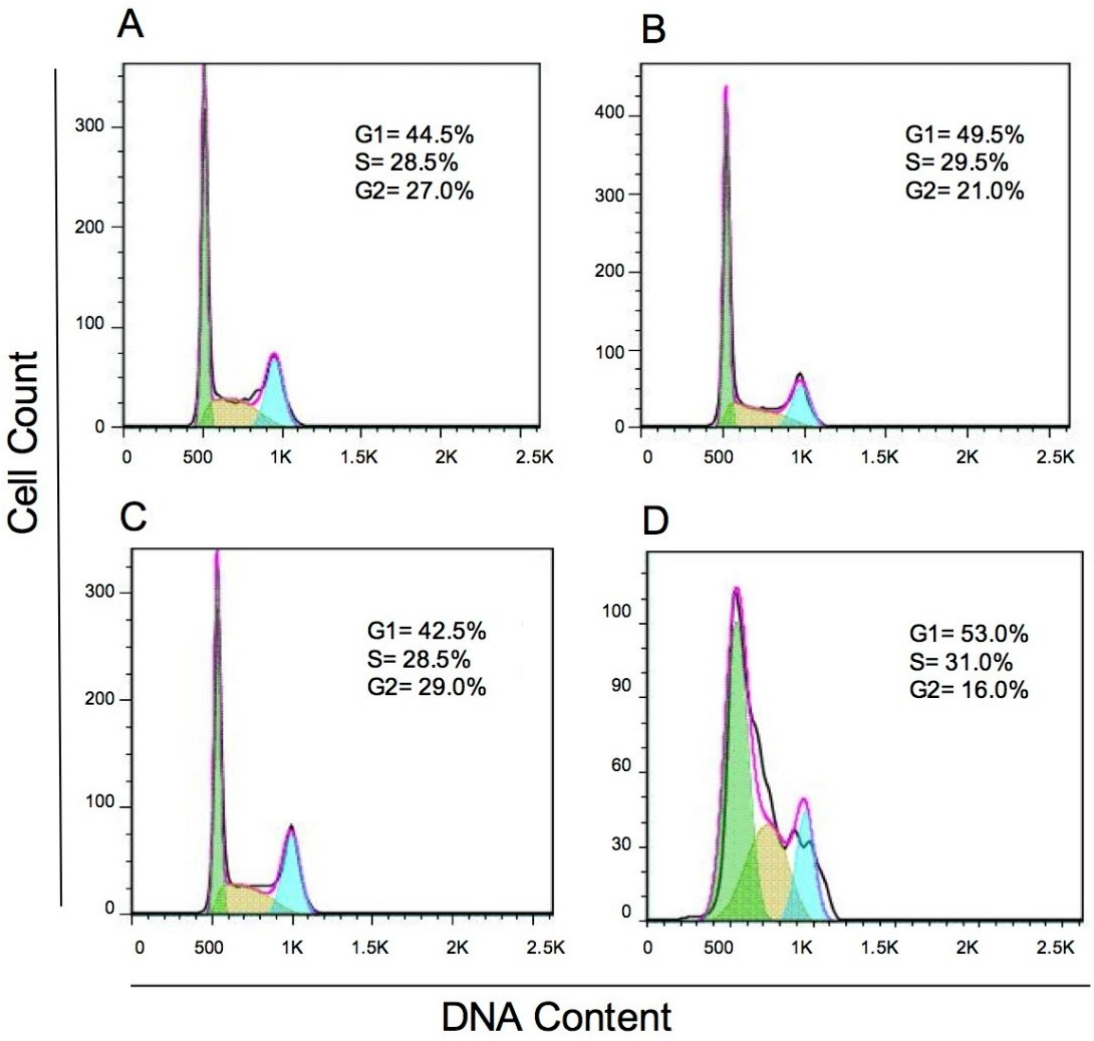

Figure 4.16. Cell cycle kinetics of MCF-7 cells after 72h treatment with CG-1521 and CG-NPs

4.2.4. Evaluation of DNA Fragmentation by Flow Cytometry

DNA fragmentation of MCF-7 cells that interacted with free drug and encapsulated drug was investigated using the TUNEL assay. Figure 4.17 shows the DNA fragmentation leve in apoptotic MCF-7 cells treated with free and encapsulated drug. The DMSO and void NPs used as control groups in the study. There is a significant increase in propidium iodide positive cells (second quadrant) treated with encapsulated drug (Q2 – 9.29%) compared to those treated with free drug (Q2 – 3.40%), demonstrating that at equivalent

concentrations (1.5 μM), CG-NPs are more potent to induce the apoptosis than free CG-1521.

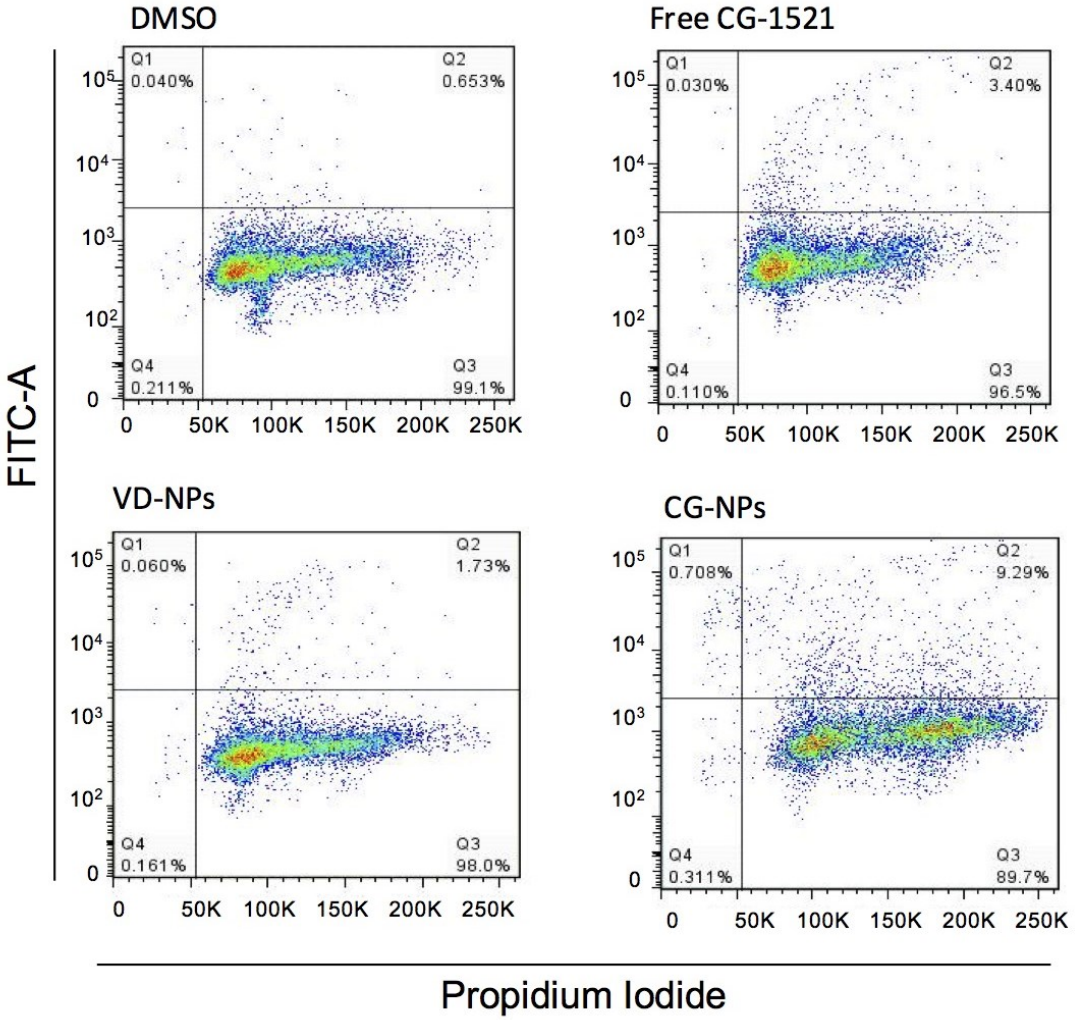

Figure 4.17. The effect of free and encapsulated CG-1521 on DNA fragmentation in MCF-7 cells-72h

4.2.5. Comparison of *In Vitro* Cytotoxicity Capacities of Folic Acid–Bound Nanoparticles in Different Cell Lines

In vitro cytotoxic effects of Folic Acid-modified formulations of nanoparticles were investigated using MCF-7 and MDA-MB-231 cell lines. The cell lines express different folate receptor levels on their surfaces. The study where the crystal violet assay was applied shows that Folic Acid-attached nanoparticles in MCF-7 cells do not increase the cell death capacity of nanoparticles.

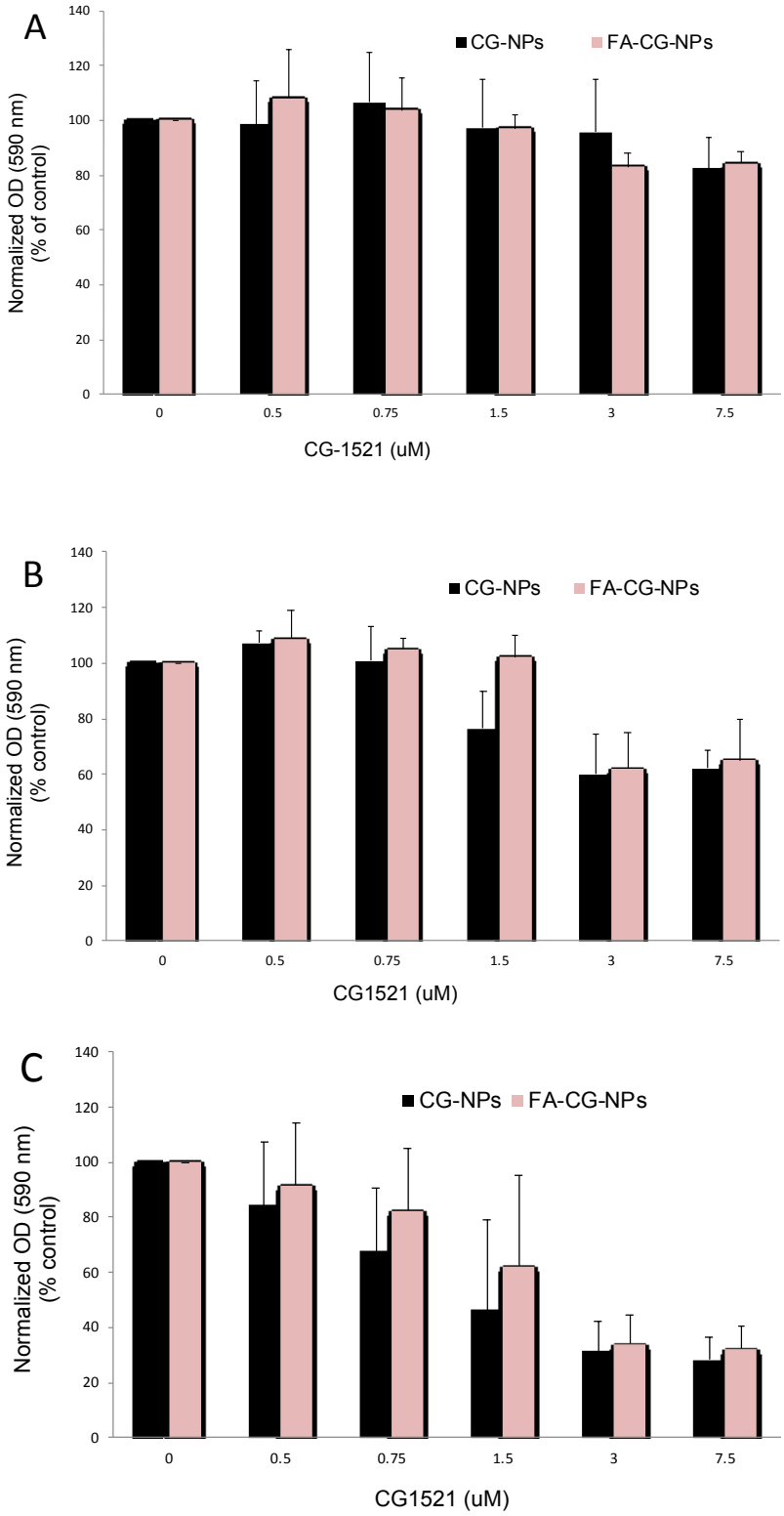

Figure 4.18. Cytotoxicity of Folic Acid modified nanoparticles on MCF-7 (A) 24h (B) 48h and (C) 72h

However, the study with the MDA-MB-231 cell line, which is more aggressive

and expresses more folate receptors [142], shows that modified nanoparticles are slightly effective in the first 24 hours, but they are not significantly effective in the 72-hour treatment compared to the unmodified formulation.

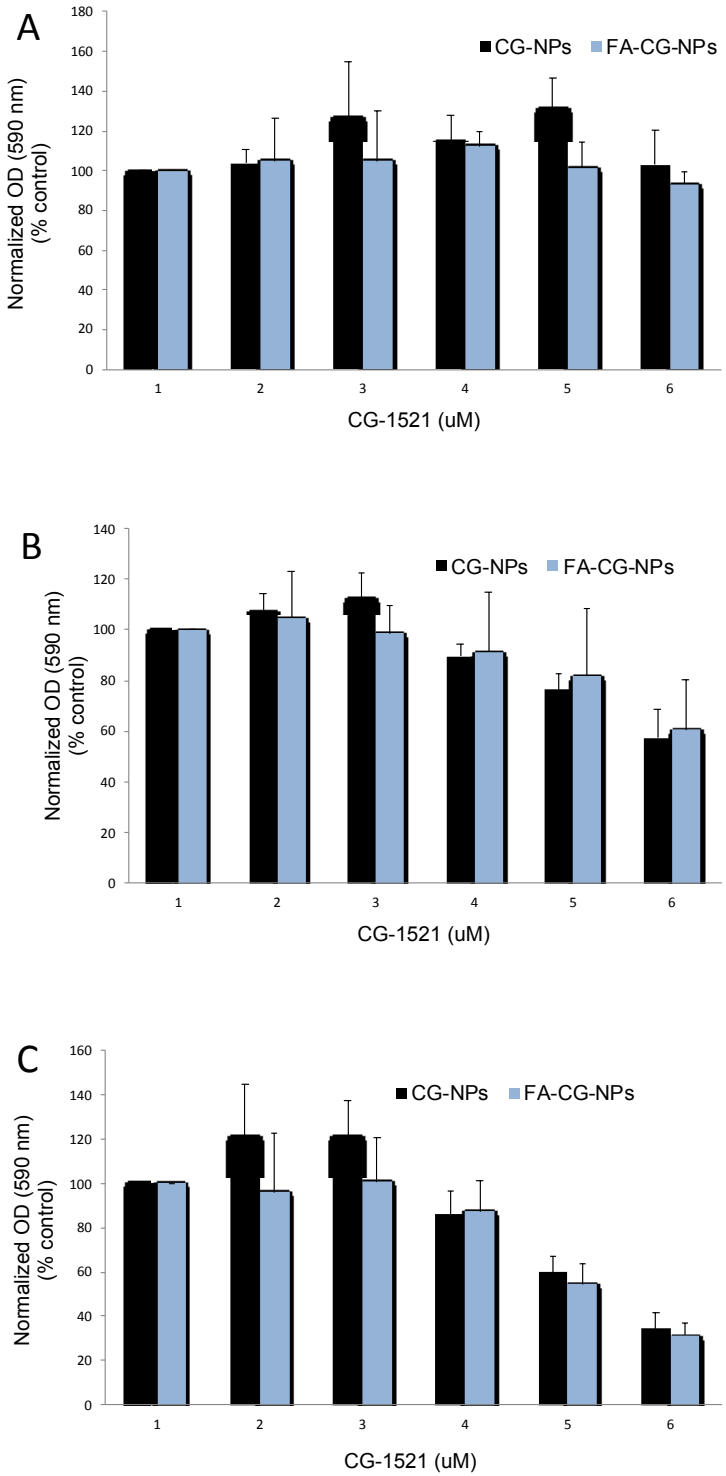

Figure 4.19. Cytotoxicity of Folic Acid modified nanoparticles on MDA-MB-231 cells; (A) 24h (B) 48h and (C) 72h

4.3. Cellular Uptake by Confocal Microscope

The cellular uptake of Rhodamine-6G labeled nanoparticle was evaluated using confocal microscopy. It was observed that the Rhodamine 6G fluorescent–labeled nanoparticles that interacted with MCF-7 cells for 12 hours were able to accumulate around the nuclei of cells and were effectively taken up by the cells (Figure 4.20).

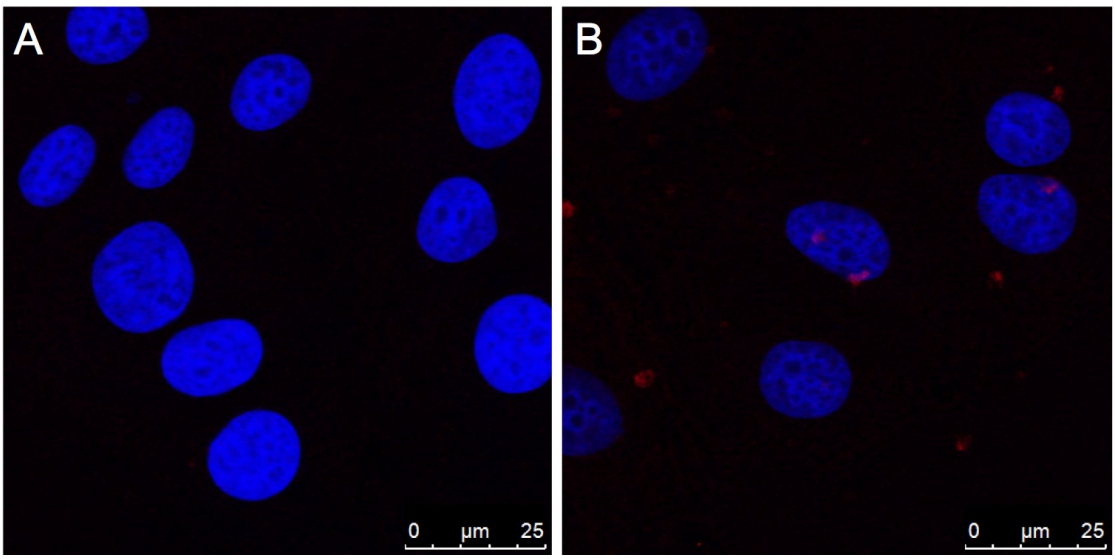

Figure 4.20. Cellular uptake of Rhodamine 6G-labeled nanoparticles

4.4. Evaluation of Biological Mechanisms of Drug-Loaded Nanoparticles

The biological mechanisms of free drug and drug-loaded nanoparticles, mRNA levels of various transcripts related to cell death/apoptosis, the cell cycle as well as spindle formation were measured by q-PCR after treatments.

In the Figure 4.21, the Bnip3 gene expression of cell death pathway was significantly downregulated after treated with both the free drug and drug loaded nanoparticles (at equivalent drug concentrations) compared to that of the control groups. However, there was no significant change in the expression level of the BNIP3L gene. The expression of the Gdf15 gene involved in the apoptosis process was significantly upregulated after interactions with CG-NPs

for 48h. While the expression of the Survivin gene responsible for promoting cell proliferation and inhibiting apoptosis was downregulated at a significant level by CG-NPs, the 48-hour interaction with the free drug showed a minimal effect on the regulation of Survivin.

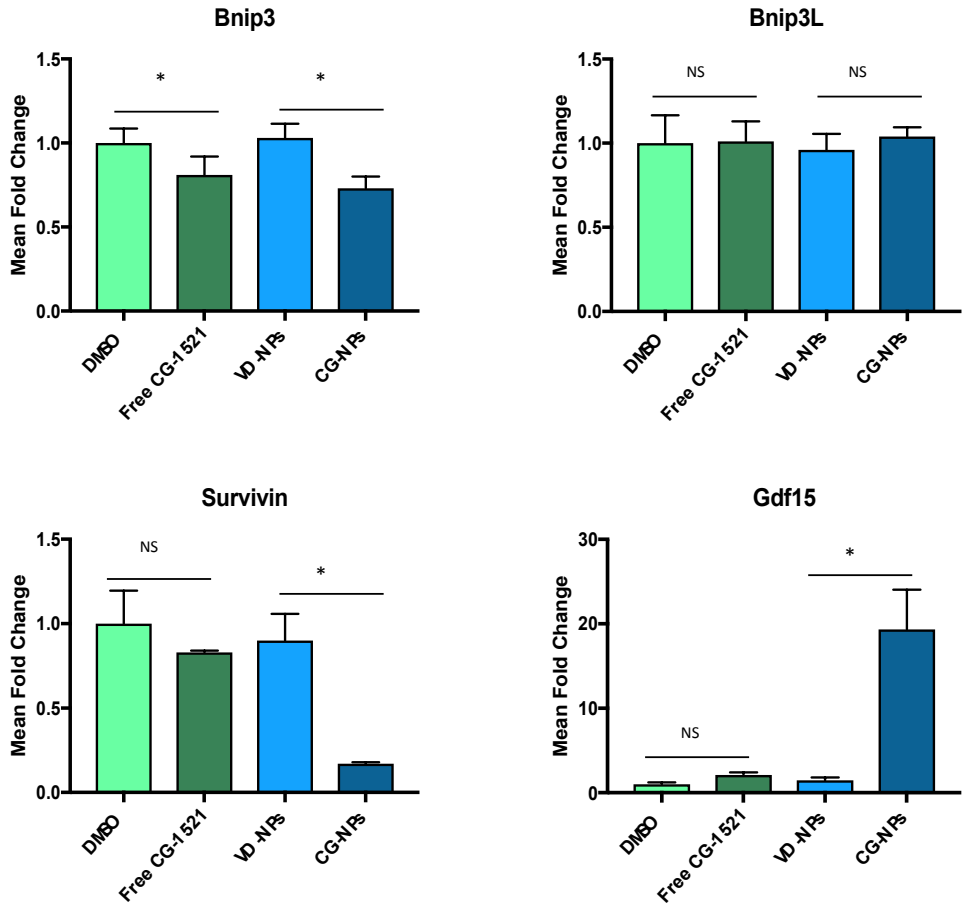

Figure 4.21. mRNA level of p53 target genes involved in cell death/apoptosis

Figure 4.22 shows that the expression levels of p21, p21B (p21 variant) and Cdc25a transcripts involved in the activity of the p53 gene, and the cell cycle (G1-S transition) are upregulated at a significant level after treatment with free drug and drug loaded nanoparticles. However, the expression level of the Cyclin D1 gene did not show any significant change after either treatment. The expression of Cyclin B1, one of the genes responsible for the G2-M transition of the cell cycle, was downregulated significantly after both free drug and

nanoparticle interactions. The mRNA level of the Gadd45a transcript responsible for G2-M transition increased after interaction with CG-NPs. However, the treatment with free CG-1521 did not change mRNA level of Gadd45a significantly.

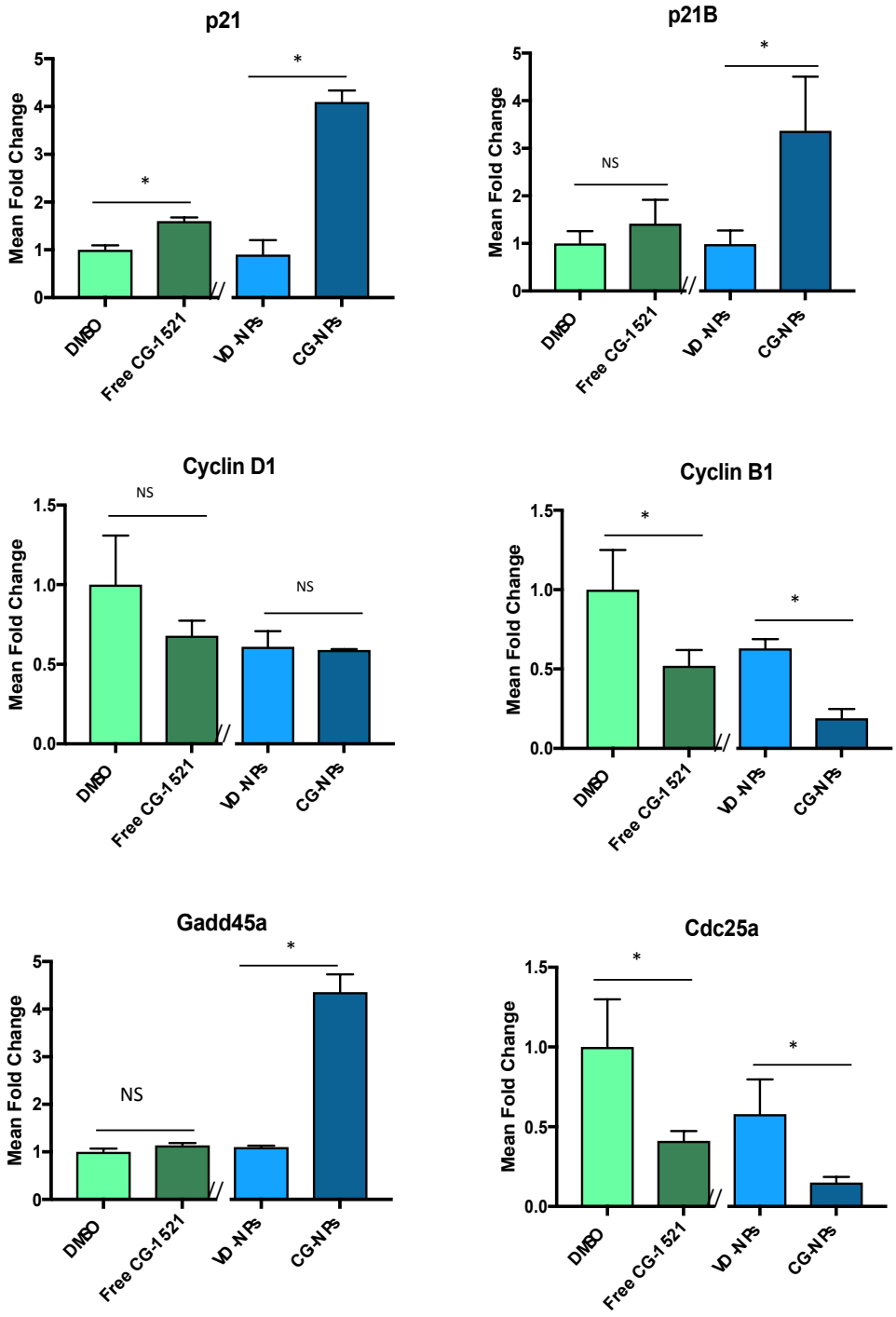

Figure 4.22 mRNA level of p53 target genes involved in cell cycle

Transcript levels of 3 different genes (Stk6, Plk1, Kntc2) responsible for the formation of spindle and centrosomes in the cell were investigated after interaction with free CG-1521 and CG-NPs (Figure 4.23). Stk6 and Plk1 genes levels downregulated with a close fold change after the treatments. Nevertheless, while the expression of Kntc2 gene was downregulated by the 48-hour nanoparticles interaction, the free drug did not cause a change significantly in the expression level of Kntc2.

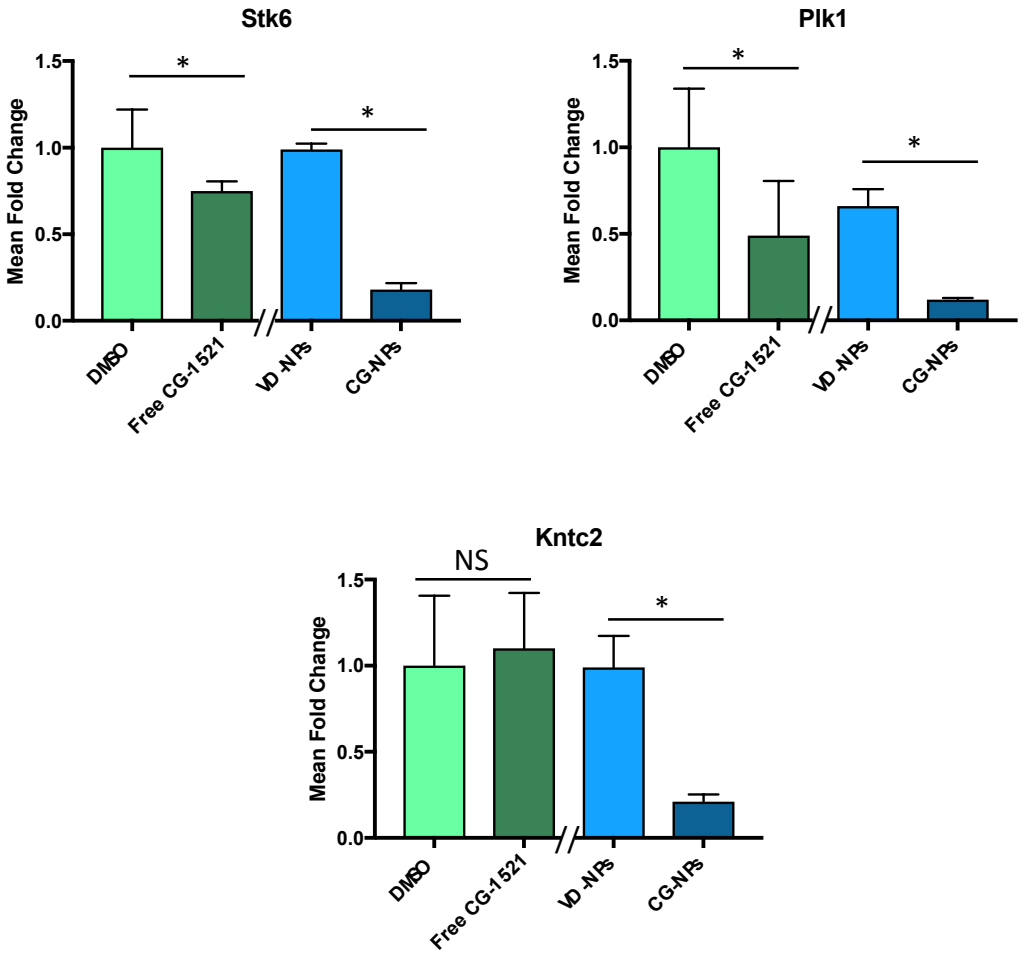

Figure 4.23 mRNA level of p53 target genes involve in spindle formation

The results confirmed that treatments by the free or encapsulated drug have the same mechanism on the expressions of majority of transcripts involved in cell cycle, apoptosis, and spindle formation pathways.

5. CONCLUSION

- Many histone deacetylase inhibitors show promising anti-tumor properties in various types of cancer in *in vitro* and *in vivo* models. However, the clinical use of such anticancer drugs, especially those that are hydrophobic, is limited due to problems such as rapid elimination from the body and systemic toxicity. So far, there are limited studies have examined the transport of HDAC inhibitors by a nano-based platform for use in cancer.

  Tran et al., investigated PLGA based nanoformulations for the delivery of HDACi family member vorinostat for both colorectal and prostate cancer [143]. In another report, Bahhaj et al., studied the potential of polyethylene oxide-norborne macromonomer based delivery system for HDACi produgs in mesothelioma [144]. Wang wt al., investigated the nanoparticles based on polymer-lipid conjugates for the delivery of two different HDACi vorinostat and quisinostat to study their potential as radiosensitizers in xenografs models in prostate and colorectal cancers [145].

  The studies outlined here is the the first report using polymeric starch nanoparticles for the delivery of CG-1521 inhibitor in the treatment of breast cancer.
- The synthesis process of nanoparticles yielded narrow size distribution (180 nm) with narrow PDI (0.138) that can benefit from increased permeability and retention of the tumor site. This fundamental feature gives the particles an optimal ability in intravenous applications. The encapsulation of CG-1521 did not cause a significant change in size (202 nm) distribution. The slightly negative zeta potential (-16.2 mV) of nanoparticles provides electrokinetic stability and prevents aggregation. In addition, previous studies have shown that nanoparticle surfaces with low negative or neutral zeta potential values decrease protein adsorption, and their uptake is inhibited by non-specific cells [146]. Although positively charged particles have been shown to have better cellular uptake *in vitro* and selectively bind to tumor-associated epithelial cells, it is advantageous if the particles are neutral or anionic until they reach the tumor area. It is known that the

neutral or anionic particles have more extended circulation and that their retention by the liver and spleen is lower [147].

- SEM and AFM images indicate that nanoparticles have spherical topography and have a homogeneous distribution. These properties allow the nanoparticles facilitate cellular uptake and make them more stable in the endosome after the endocytosis process [148, 149].
- *In vitro* drug release from nanoparticles is one of the most critical factors affecting the bioutilization of the drug. For this purpose, the release studies of CG-1521 from nanoparticles at the different pH condition were investigated. Rapid dissociation of drug molecules adsorbed on the outer surface of nanoparticles and intensive diffusion to the media causes a burst release of drug. This rapid release is followed by a slower release due to drug molecules passing slowly to the media because of the polymer matrix erosion and degradation. It has been observed that a lower pH increases the degradation rate of the starch-based polymer matrix, thus accelerating the rate of drug release significantly [150].
- Several studies show that drug release in more acidic environment inhibits premature release of the encapsulated drug after injection into a body, which thus promotes the release of the nanotransporter in the acidic microenvironment of the tumor (by EPR effect) [151].
- *In vitro* cytotoxicity studies in the MCF-7 cell line indicated that the cytotoxic potential of the encapsulated drug was much higher than that of the free drug. When the free drug molecules diffuse through the cell membrane, the uptake of the encapsulated drug into the cell is via the endocytosis mechanism. This mechanism slows down the therapeutic activity of the drug and increases its bioutilization and reduces the systemic toxicity of the accumulated drug with the EPR effect [152].
- Subsequent apoptosis studies supported the induction capacity of the encapsulated drug for cytotoxicity. Apoptosis process is controlled by multiple genetic mechanisms [153]. The reactions shown against various cancer agents predominantly cause cell death through the mechanism of apoptosis [154]. Annexin V binds to phospholipids and they are transferred to cells' surface from the inner surface of the cells during early apoptosis [155]. Phosphatidylserines are detected by fluorescence-labeled annexin V,

and non-apoptotic (annexin V negative) cells and cells of different phases of apoptosis are distinguished from each other. In the early phase of apoptosis, while plasma membranes do not allow the dyes such as propidium iodide (PI) or 7-AAD used for detecting viability, they allow Annexin-V dying of cells. Whereas, in the late phase of apoptosis or due to losing the integrity of cell membrane because of the cell death, cells are dyed with both FITC-labeled Annexin-V and propidium iodide dye. Annexin V dead cell assay allows for the quantitative analysis of live, early, and late apoptosis and dead cells populations using a Muse cell analyzer. In this study, it has been shown that the encapsulated drug formulation induces apoptosis at a significant level compared to the free drug. Thus, the advantage of the encapsulation process by increasing the therapeutic effect of the drug has been demonstrated. The obtained results are also consistent with previous cell viability results, indicating that unmodified starch may be a suitable carrier for histone deacetylase inhibitors.

- Another phenomenon in which the cytotoxic potentials of nanoparticles are examined is an investigation of suppressing cell accumulations collecting in specific phases of the cell cycle. The cell cycle is a process controlled by various mechanisms including DNA replication and cell division. Cell division occurs in two main phases containing DNA synthesis (S) and mitosis (M) and intermediate phases (G1 and G2) [156]. In normal cells, various interactions that regulate cell proliferation perceive conditions promoting cell growth and send signals to molecules responsible for cell division. The deregulation of this pathway is detected by specific cells, and the normal cell division process is blocked [157]. The loss or irregularity of the functions of these signaling mechanisms leads to the formation of a tumor [158]. During the cell cycle analysis performed, the number of cells arrested in S/G2 phases of cells interacted with nanoparticles is greater than the number of the arrested cells in S/G2 phases of free drug-induced cells. The arresting of the cell cycle in these phases confirms that the cells go apoptosis and thus inhibit cell proliferation.
- Nuclear DNA fragmentation is another biochemical-based differential feature of apoptosis and has been studied by the TUNEL test. The result of the TUNEL experiment was that the drug-containing particles being at the

same concentration as the loaded nanoparticles were found to be more effective in terms of DNA fragmentation activation than the free drug. The scatter diagram of DNA breaks shows that the nanoparticle interaction causes a threefold increase in the PI-positive cell population (Q2-9.29%), approximately as compared to the free drug interaction (Q2-3.30%). Several factors, such as the increased intracellular bioutilization by EPR and the drug solubility of CG-1521 play an essential role in this effect.

- Folate represents an essential and complex factor in DNA replication and cell proliferation. When neoplastic lesions begin to develop, tumor cells also provide intracellular uptake of the reduced form of folate (as opposed to healthy cells), promoting DNA replication and enhancing proliferation [159]. Folate receptors continue to be one of the primary targets in the development of new cancer diagnosis and treatment methods, since they supply both specific and prognostic information. In this study, we compared the therapeutic response of CG-1521-loaded nanoparticles conjugated with Folic Acid interacting with MCF-7 (luminal type, ER+, PR+, and HER2+) and MDA-MB-231 (basal B type, ER-, PR- and HER2+) subgroup of different breast cancer cells unmodified nanoformulation. The obtained data demonstrate that using the modified formulation in the MCF-7 cell line, the drug did not cause a specific increment in the cell's death capacity. Since the expression level of folate receptors in MCF-7 cell line was defined as both folate receptor (FR)positive [160] and FR-negative [161] in different studies, we will plan to use Western Blot to determine folate receptors level in MCF-7 in future studies. Shorter time periods (4-6 hours) and higher concentrations in cell studies will also be used to examine the effectiveness of the modification. MDA-MB-231 cells, which are triple negative, more aggressive, and display higher FR expression [162], were slightly sensitive to modified nanoparticles than unmodified nanoparticles, but statistical studies have shown that sensitivity level is not significant.
- The investigated biological mechanism of drug-loaded particles has been shown to have a trend similar to that of the free drug as a result of 48 hours of treatment. To verify that the drug encapsulation does not change the molecular pathways associated with cell cycle and apoptosis. We selected a cohort of genes that had been studied previously and found to be

sensitive to free CG-1521 in MCF-7 [163]. The effect of free drug and encapsulated drug on the expression of these genes that involve in the stabilization of p53 were compared. The chort of genes also contain some transcripts that regulated p53-independently by CG-1521 in inflammatory breast cancer [164]. The majority of transcripts's expressions in response to free CG-1521 and encapsulated CG-1521 in nanoparticles represent a concordance with the exceptions of three genes. While free CG-1521 does not modulate the expression of three genes (Gdf15, Gadd45a and Kntc2), encapsulated CG-1521 have different effect on these genes' expressions. The encapsulated formulation of CG-1521 induces the Gadd45a and Gdf15 transcripts but repress the Kntc2 gene expression significantly. Since this gene expression study conducted in a single time point (48 hours), we could not determine the underlying differences in these three transcripts' expressions. This could be a difference in molecular pathways that are involved or a difference in time points of repression/induction of these genes. Since these transcripts are involve in arrest of G2/M transition and spindle formation, proving that encapsulated form of CG-1521 increases the G2/M related cell death. In brief, in which the effects of the nanoformulation of the drug in the same group of genes were examined, it was found that the expressions of most of the genes (except Gdf15, Gadd451, and Kntc2) were incongruent in interaction with free drug and drug-loaded nanoparticles. Expression levels of specific genes involved in multiple pathways in a different time and concentration intervals will be investigated in future studies.

In conclusion, a polysaccharide-based carrier was designed and characterized for the transport of the CG-1521 in this study. The nanoparticles were modified with Folic Acid as targeting moiety to increase the specifity of delivery of drug. The encapsulation of the drug resulted in a stable and sustained release of the drug and increased bioavailability. Thus, the therapeutic effect of the drug is increased by nanoencapsulation compared to free drug. The data obtained are quite promising for future studies to determine the biological activity of the nanoformulation of CG-1521 in *in vivo* tumor models.

6. REFERENCES

[1] National Cancer Institute, https://seer.cancer.gov/statfacts/html/breast.html, 2021.

[2] Urbinati G, Marsauda V, Plassata V, Fattal E, Lesieura S, Renoir JM., Liposomes loaded with histone deacetylase inhibitors for breast cancer therapy, *International Journal of Pharmaceutics*, 397: 184–193, **2010.**

[3] Fana T, Lic M, Wub X, Lia M, Wu Y., Preparation of thermoresponsive and pH-sensitivity polymer magnetic hydrogel nanospheres as anticancer drug carriers, *Colloids and Surfaces B: Biointerfaces*, 88: 593–600, **2011.**

[4] Wanga F, Lib L, Liuc B, Chenc Z, Li C. Hyaluronic acid decorated pluronic P85 solid lipid nanoparticles as a potential carrier to overcome multidrug resistance in cervical and breast cancer, *Biomedicine & Pharmacotherapy*, 86: 595–604, **2017.**

[5] Lin G, Zhang H, Huang L. Smart polymeric nanoparticles for cancer gene delivery, *Mol. Pharm.* 12: 314–321, **2015.**

[6] Patel T, Zhou J, Piepmeier JM, Saltzman WM., Polymeric nanoparticles for drug delivery to the central nervous system, *Adv. Drug Deliv. Rev.* 64: 701–705, **2012.**

[7] Meng L, Huang W, Wang D, Huang X, Zhu X, Yan D., Chitosan-based nanocarriers with pH and light dual response for anticancer drug delivery, *Biomacromolecules,* 14: 2601–2610, **2013.**

[8] Kataoka K, Harada A, Nagasaki Y, Block copolymer micelles for drug delivery: design, characterization and biological significance, *Adv. Drug Deliv. Rev.* 47: 113–131, **2001.**

[9] Farokhzad, OC Langer R, Nanomedicine: Developing Smarter Therapeutic and Diagnostic Modalities. *Adv. Drug Delivery Rev.* 58: 1456–1459, **2006.**

[10] Gryparis EC, Hatziapostolou M, Papadimitriou E, Avgoustakis K., Anticancer activity of cisplatin-loaded PLGA-mPEG nanoparticles on LNCaP prostate cancer cells. *Eur J Pharm Biopharm.* 67:(1) 1–8, **2017.**

[11] Mobasseri R, Karimi K, Tian L, Naderi-Manesh H, Ramakrishna S. Hydrophobic lapatinib encapsulated dextran-chitosan nanoparticles using a toxic solvent free method: fabrication, release property & *in vitro* anti-cancer activity, *Materials Science and Engineering C* 74: 413–421, **2017.**

[12] Elsabahya M, Karen L. Wooley. Design of polymeric nanoparticles for biomedical delivery applications, Chem Soc Rev. 41(7): 2545–2561., **2012.**

[13] Osterberg E, Bergstrom K, Holmberg K, Schuman TP, Riggs JA, Burns, Vanalstine JM, Harris JM., Protein-rejecting ability of surface-bound dextran in end- on and side-on configurations-comparison to Peg, *Journal of Biomedical Materials Research,* 29 (6): 741–747, **1995.**

[14] Marques AP, Reis RL, Hunt JA., The biocompatibility of novel starch-based polymers and composites: *in vitro* studies, *Biomaterials,* 23 (6): 1471–1478, **2002.**

[15] Seyed Heydar Mahmoudi Najafi, Maryam Baghaie, Alireza Ashori , Preparation and characterization of acetylated starch nanoparticles as drug carrier: Ciprofloxacin as a model, *International Journal of Biological Macromolecules,* 87 ,48–54, **2016.**

[16] Pang, SC, Chin, SF, Nadirah, A, Tay SH, Yazid SNAM, Fabrication of Polysaccharide-Based Nanoparticles as Drug Delivery Nanocarriers. *ECS Trans.* 66: 5–32., **2015.**

[17] El-Naggar ME, El-Rafie MH, El-sheikh MA, El-Feky GS, Hebeish A. Synthesis, characterization, release kinetics and toxicity profile of drug-loaded starch nanoparticles. *Int. J. Biol. Macromol.* 81:718–729., **2015.**

[18] Wu X, Chang Y, Fu Y, Ren L, Tong J, Zhou J. Effects of non-solvent and starch solution on formation of starch nanoparticles by nanoprecipitation. *Starch/Staerke,* 68: 258–263., **2016.**

[19] Pandolfi PP., Transcription therapy for cancer. Oncogene. 20: 3116–27., **2001.**

[20] Richon V M, Emiliani S, Verdin E, Webb Y, Breslow R, Rifkind RA, and Marks PA., A class of hybrid polar inducers of transformed cell differentiation inhibits histone deacetylases. *Proc. Natl. Acad. Sci.* USA, 95: 3003–3007., **1998.**

[21] Lane AA, Chabner BA, Histone Deacetylase Inhibitors in Cancer Therapy, *Journal of Clinical Oncology*, 27 (32): 5459-5468., **2009.**

[22] Marks PA, Richon VM, Rifkind RA Histone deacetylase inhibitors: inducers of differentiation or apoptosis of transformed cells. *J. Natl. Cancer Inst.* 92: 1210–1216., **2000.**

[23] de Ruijter AJ, Kemp S, Kramer G, Meinsma RJ, Kaufmann JO, Caron HN, van Kuilengberg AB., The novel histone deacetylase inhibitor BL1521 inhibits proliferation and induces apoptosis in neuroblastoma cells. *Biochem. Pharmacol.* 68:1279–1288., **2004.**

[24] Chatterjee N, Wang W-LW, Conklin T, Chittur S, Tenniswood M., Histone deacetylase inhibitors modulate miRNA and mRNA expression, block metaphase, and induce apoptosis in inflammatory breast cancer cells. *Cancer Biology & Therapy.* 7: 658-671., **2013.**

[25] Roy S, Packman K, Jeffrey R, Tenniswood M. Histone deacetylase inhibitors differentially stabilize acetylated p53 and induce cell cycle arrest or apoptosis in prostate cancer cells. *Cell Death Differ.* 12(5): 482-91., **2005.**

[26] Elaut G, Torok G, Vinken M, Laus G, Papeleu P, Tourwe D, Rogiers V. Major phase I biotransformation pathways of Trichostatin a in rat hepatocytes and in rat and human liver microsomes. *Drug Metab. Dispos.* 30: 1320–1328., **2002.**

[27] Vanhaecke T, Papeleu P, Elaut G, Rogiers V. Trichostatin A-like hydroxam- ate histone deacetylase inhibitors as therapeutic agents: toxicological point of view. *Curr. Med. Chem.* 11: 1629–1643., **2004.**

[28] Maeda H, Fang J, Inutsuka T, Kitamoto Y. Vascular permeability enhancement in solid tumor: various factors, mechanisms involved and its implications, *Int. Immunopharmacol.* 3: 319–328., **2003.**

[29] Moghimi SM, Szebeni J. Stealth liposomes and long circulating nanoparticles: critical issues in pharmacokinetics, opsonization and protein-binding properties. *Prog. Lipid Res*. 42: 463–478., **2003.**

[30] Kim, B. Y., Rutka, J. T., Chan, W. C., Nanomedicine, The New England Journal of Medicine, 363, 25, 2434–2443, **2010.**

[31] Doane, T. L., Burda, C., The unique role of nanoparticles in nanomedicine: imaging, drug delivery and therapy, Chemical Society Reviews, 41, 7, 2885–2911, **2012.**

[32] Vanna Sanna Nicolino Pala Mario Sechi, Targeted therapy using nanotechnology: focus on cancer, International Journal of Nanomedicine 9, 467–483, **2014.**

[33] Lammers, T., Kiessling, F., Hennink, W. E., Storm G. Drug targeting to tumors: principles, pitfalls and (pre-) clinical progress, *Journal of Controlled Release*, 161, 2, 175–187, **2012.**

[34] (a) De Jong, W. H., Borm, J.A., Drug Delivery and Nanoparticles:Applications and hazards, *International Journal of Nanomedicine*, 3, 2, 133-149, **2008.** (b) Gürsoy, A., *Kontrollü Salım Sistemleri*, Kontrollü Salım Sistemleri Derneği Yayını,1.Baskı, İstanbul, 299-301, **2002.**

[35] Zhang, L., Gu. F. X., Chan, J. M., Wang, A. Z., Langer, R. S., Farokhzad, O.C. Nanoparticles in medicine: therapeutic applications and developments, *Clinical Pharmacology & Therapeutics*, 83, 5, 761–769, **2008.**

[36] Ferrari, M., Cancer nanotechnology: opportunities and challenges. *Nature Reviews Cancer*, 5, 3, 161–171, **2005.**

[37] Davis, M. E., Chen, Z. G., Shin, D. M., Nanoparticle therapeutics: an emerging treatment modality for cancer, *Nature Reviews Drug Discovery*, 7, 9, 771–782, **2008.**

[38] Lammers, T., Kiessling, F., Hennink, W. E., Storm, G., Nanotheranostics and image-guided drug delivery: current concepts and future directions, *Molecular Pharmacology*, 7, 6, 1899–1912, **2010.**

[39] Bangham, A. D., Standish, MM., Watkins, JC., Diffusion of univalent ions across the lamellae of swollen phospholipids, *Journal of Molecular Biolology*, 13, 1, 238–252. **1965.**

[40] Torchilin, VP., Recent advances with liposomes as pharmaceutical carriers, *Nature Reviєw Drug Discovery*, 4, 2, 145–160, **2005.**

[41] Xiaoyang Xu, William Ho, Xueqing Zhang, Nicolas Bertrand, and Omid Farokhzad, Cancer nanomedicine: from targeted delivery to combination therapy, *Trends in Molecular Medicine*, 21,3, 223-32, **2015.**

[42] Shi, J., Xiao, Z., Kamaly, N., Farokhzad OC. Self-assembled targeted nanoparticles: evolution of technologies and bench to bedside translation, *Accounts of Chemical Research*, 44, 10, 1123–1134, **2011.**

[43] Makadia, HK., Siegel, SJ., Poly lactic-co-glycolic acid (PLGA) as biodegradable controlled drug delivery carrier, *Polymers (Basel),* 3, 3, 1377–1397, **2011.**

[44] Couvreur, P., Couarraze, G., Devissaguet, J., Puisieux, F., Nanoparticles: preparation and characterization, In *Microencapsulation: Methods and Industrial Application*, S. Benita(Ed.), Marcel Dekker, New York, 183–211, **1996.**

[45] Ire`ne Brigger, Catherine Dubernet, Patrick Couvreur, Nanoparticles in cancer therapy and diagnosis, Nanoparticles in cancer therapy and diagnosis, Advanced Drug Delivery Reviews 54 631–651, **2002.**

[46] Prasad Rao, J., Geckeler, K.E., Polymer nanoparticles: Preparation techniques and size-control parameters, *Progress in Polymer Science,* 36, 7, 887–913, **2011.**

[47] Sajid, H.A., Rehman, K., Chen S., Natural and Synthetic Polymers as Drug Carriers for Delivery of Therapeutic Proteins, *Polymer Reviews*, **2015.**

[48] Muhammad Sajid Hamid Akash, Kanwal Rehman & Shuqing Chen, Natural and Synthetic Polymers as Drug Carriers for Delivery of Therapeutic Proteins, Volume 55, 3, 371-406, **2015.**

[49] Acharya S., Sahoo S. K., PLGA nanoparticles containing various anticancer agents and tumour delivery by EPR effect, *Advanced Drug Delivery Review*, 63, 170–183, **2011.**

[50] West, C. P., Lumsden, M. A., Lawson, S., Williamson J., Baird, D. T., Shrinkage of uterine fibroids during therapy with goserelin (Zoladex): a luteinizing hormone-releasing hormone agonist administered as a monthly subcutaneous depot, *Fertility and Sterility*, 48, 1, 45–51, **1987.**

[51] Sethi, R., Sanfilippo, N., Six-month depot formulation of leuprorelin acetate in the treatment of prostate cancer, *Clinical Intervention in Aging*, 4, 259–267, **2009**.

[52] Crawford, E. D., Phillips, J. M., Six-month gonadotropin releasing hormone (GnRH) agonist depots provide efficacy, safety, convenience, and comfort, *Cancer management and research*, 3, 201–209, **2011.**

[53] Anwunobi, AP., Emeje, MO., Recent Applications of Natural Polymers in Nanodrug Delivery, *Journal of Nanomedicine and Nanotechnology*, 4,2, **2011.**

[54] Geresh S., Gdalevsk, GY., Gilboa I, Voorspoels, J., Remon, J.P.,Kost, J., Bioadhesive grafted starch copolymers as platforms for peroral drug delivery: a study of theophylline release, *Journal of Control Release*, 94, 391-399, **2004.**

[55] Lavina, M., Rajabi-Siahboomi, A.R., The influence of excipients on drug release from hydroxypropyl methylcellulose matrices, *European Journal of Pharmaceutical Sciences*, 93, 2746-2754, **2004.**

[56] Yamini, K., Chalapathi, V., Lakshmi Narasimha Reddy, N., Lokesh K.V., Praveen Kumar Reddy, S., Formulation of diclofenac sodium tablets using tapioca starch powder- A promising binder, *Journal of Applied Pharmaceutical Science*, 1, 125–127, **2011.**

[57] Malafaya, B.P., Stappers, F., Reis, R.L., Starch-based microspheres produced by emulsion crosslinking with a potential media dependent responsive behavior to be used as drug delivery carriers, *The Journal of Materials Science: Materials in Medicine,* 17, 371–377, **2006.**

[58] Heller, J., Pangburn SH, Roskos, K.V., Development of enzymatically degradable protective coatings for use in triggered drug delivery systems: derivatized starch hydrogels, *Biomaterials* 11, 345-350, **1990.**

[59] Wu, C., Zhongyan, W., Zhi, Z., Jang, T., Zhang, J., Development of biodegradable porous starch foam for improving oral delivery of poorly water soluble drugs, *International Journal of Pharmaceutics*, 403, 162–169, **2011.**

[60] Santander-Ortega, M.J., Stauner, T., Loretz, B., Ortega-Vinuesa, JL., Bastos- González, D., et al., Nanoparticles made from novel starch derivatives for transdermal drug delivery, *Journal of Control Release,* 141, 85–92, **2010.**

[61] Mahkam, M., Modified Chitosan Cross-linked Starch Polymers for Oral Insulin Delivery, *Journal of Bioactive and Compatible Polymers*, 25, 406–418, **2010.**

[62] El-Feky, G.S., El-Rafie, M.H., El-Sheikh MA, El-Naggar, M.E., and Hebeish, A., Utilization of Crosslinked Starch Nanoparticles as a Carrier for Indomethacin and Acyclovir Drugs, *Journal of Nanomedicine and Nanotechnology*, 6:1, **2015.**

[63] American Cancer Society, Global Cancer Facts & Figures. https://www.cancer.org/content/dam/cancer-org/research/cancer-facts-and-statistics/annual-cancer-facts-and-figures/2021/cancer-facts-and-figures-2021.pdf, *American Cancer Society*, **2021.**

[64] Chu, E., DeVita, V.T., Physicians' Cancer Chemotherapy Drug Mannual, *Jones& Bartlett Learning*, **2015.**

[65] Makkouk, A., Weiner, G.J., Cancer immunotherapy and breaking immune tolerance: new approaches to an old challenge, *Cancer Research*, 75, 5–10, **2015.**

[66] Cowen. R.L., Garside E.J., Fitzpatrick B., Papadopoulou M.V., K.J.Williams, Genetherapy approaches to enhance bioreductive drug treatment, *The British Journal of Radiology*, 81, 45–56, **2008.**

[67] Vanneman, M., Dranoff, G., Combining immunotherapy and targeted therapies in cancer treatment, *Nature Reviews Cancer*, 12, 237–251, **2012.**

[68] Zhang, M., Garbuzenko, O.B., Reuhl, K.R., Rodriguez, L., Minko, T., Two-in- one: combined targeted chemo and gene therapy for tumor suppression and prevention of metastases, *Nanomedicine,* 7, 185–197, **2012.**

[69] Sawyers, C., Targeted cancer therapy, *Nature*, 432, 294-297, **2004.**

[70] Bora, G., Yurter Erdem, H., Epigenetik Hastalıklar ve Tedavi Yaklaşımları, *Hacettepe Tıp Dergisi*, 38, 48–54, **2007.**

[71] Egger, G., Liang, G., Aparicio, A., Jones, AP., Epigenetics in human disease and prospects for epigenetic therapy, *Nature*, 63, 429, 457-63, **2004.**

[72] Robertson, DK., DNA methylation and human disease, *Nature Review Genetics*, 6, 597–610, **2005.**

[73] Kazakov, D. V., Burg, G., and Kempf, W., Clinicopathological spectrum of mycosis fungoides, *Journal of the European Academy of Dermatology and Venereology*, 18, 4,397–415, **2004.**

[74] Rodd, A. L., Ververis, K., Karagiannis T. C., Current and Emerging Therapeutics for Cutaneous T-Cell Lymphoma: Histone Deacetylase Inhibitors, *Lymphoma*, **2012.**

[75] Grant, A. P., A tale of histone modifications, *Genome Biology*, 2, 1–6, **2001.**

[76] Annabelle L. Rodd,1, 2 Katherine Ververis,1, 2 and Tom C. Karagiannis, Current and Emerging Therapeutics for Cutaneous T-Cell Lymphoma: Histone Deacetylase Inhibitors, Lymphoma Volume **2012**, Article ID 290685, 10 pages doi:10.1155/2012/290685

[77] Delcuve, G. P., Khan, D. H., Davie, J. R., Role of HDACIs in Epigenetic Regulation: Emerging Paradigms From Studies With Inhibitors, *Clinical Epigenetics*, 12, 4:5, **2012.**

[78] Dokmanovic, M., Clarke, C., Marks, P. A., Histone Deacetylase Inhibitors: Overview & Perspectives, *Molecular Cancer Research*, 5, 982–983, **2007.**

[79] Zhou, W., Zhu, W. G., The changing face of HDAC inhibitor depsipeptide, *Current Cancer Drug Targets*, 9, 1, 91–100, **2009.**

[80] Kim, H. J., Rowe. M., Hong. J. S., Chen, P. S., Chuang, D. M., Histone deacetylase inhibitors exhibit anti- inflammatory and neuroprotective effects in a rat permanent ischemic model of stroke: multiple mechanisms of action, *The Journal of pharmacology and experimental therapeutics*, 321, 3, 892–901, **2007.**

[81] Acharya, M. R., Sparreboom, A., Venitz, J., Figg, W. D., Rational Development of Histone Deacetylase Inhibitors as Anticancer Agents: A Review, Molecular Pharmacology, 68, 917–932, **2005.**

[82] Di-Fei Wang, Paul Helquist, Norbert L. Wiech, and Olaf Wiest, Toward Selective Histone Deacetylase Inhibitor Design: Homology Modeling, Docking Studies, and Molecular Dynamics Simulations of Human Class I Histone Deacetylases, *J. Med. Chem.*, 48, 6936-6947, **2005.**

[83] Roy, S., Packman, K., Jeffrey, R., and Tenniswood, M., Histone deacetylase inhibitors differentially stabilize acetylated p53 and induce cell cycle arrest or apoptosis in prostate cancer cells, *Cell Death and Differentiation*, 12,5, 482–91, **2005.**

[84] Urbinati, G., Marsaud, V., Plassat, V., Fattal, E., Lesieur, S., Renoir, J.M., Liposomes loaded with histone deacetylase inhibitors for breast cancer therapy, *International Journal of Pharmaceutics* , 15, 397, 184-93, **2010.**

[85] Knutson, A.K., Welsh, J., Taylor, T., Roy, S., Wang, W.L.W. and Tenniswood, M. Comparative Effects of Histone Deacetylase Inhibitors

on p53 Target Gene Expression, Cell Cycle and Apoptosis in MCF-7 Breast Cancer Cells. Oncology Reports. 27:849–853.2012

[86] Farokhzad, O.C. and Langer, R., Impact of nanotechnology on drug delivery, *ACS Nano*, 3, 16–20, **2009**.

[87] Matsumura, Y. Maeda, H., A New Concept for Macromolecular Therapeutics in Cancer Chemotherapy: Mechanism of Tumoritropic Accumulation of Proteins and the Antitumor Agent Smancs, *Cancer Research*, 46, 6387–6392, **1986**.

[88] Carmeliet, P., Jain, R. K., Angiogenesis in cancer and other diseases, *Nature*, 407, 249–257, **2000.**

[89] Danquah, M. K., Zhang, X. A., Mahato R. I., Extravasation of polymeric nanomedicines across tumor vasculature, *Advance Drug Delivery Reviews*, 63, 623–639, **2011.**

[90] Xu, X., Ho W., Zhang, X., Bertrand, N., Farokhzad, O., Cancer nanomedicine: from targeted delivery to combination therapy, *Trends in molecular medicine*, 21, 4, **2015.**

[91] Weiss G. J., Chao J., Neidhart J. D., Ramanathan R. K., Bassett D., Neidhart J. A., Choi C. H., Chow W., Chung V., Forman S. J., Garmey E, Hwang J, Kalinoski DL, Koczywas M, Longmate J, Melton RJ, Morgan R, Oliver J, Peterkin JJ, Ryan JL, Schluep T, Synold TW, Twardowski P, Davis ME, Yen Y., First-in-human Phase 1/2a trial of CRLX101, a cyclodextrin-containing polymer–camptothecin nanopharmaceutical in patients with advanced solid tumor malignancies. *Invest. New Drugs,* 31, 986–1000, **2013.**

[92] Alexis, F. et al., Nanoparticle technologies for cancer therapy. Handb. Exp. Pharmacol. 197, 55–86, **2010.**

[93] Che-Ming J. Hu, Li Zhang, Santosh Aryal, Connie Cheung, Ronnie H. Fang, and Liangfang Zhang,Erythrocyte membrane-camouflaged polymeric nanoparticles as a biomimetic delivery platform. Proc. Natl. Acad. Sci. U.S.A. 108, 10980–10985, **2011.**

[94] Bertrand N, Wu J, Xu X, Kamaly N, Farokhzad OC., Cancer nanotechnology: the impact of passive and active targeting in the era of modern cancer biology. Adv. Drug Deliv. Rev. 66, 2–25, **2014.**

[95] Michael K. Danquah a, Xin A. Zhang b, Ram I. Mahato, Extravasation of polymeric nanomedicines across tumor vasculature. Adv. Drug Deliv. Rev. 63, 623–639, **2011.**

[96] Alexandre Albanese, Peter S. Tang, and Warren C.W. Chan, The effect of nanoparticle size, shape, and surface chemistry on biological systems. Annu. Rev. Biomed. Eng. 14,1-16, **2012.**

[97] Davis, M.E., The first targeted delivery of siRNA in humans via a self-assembling, cyclodextrin polymer-based nanoparticle: from concept to clinic. Mol. Pharm. 6, 659–668, **2009.**

[98] Mark E. Davis Jonathan E. Zuckerman, Chung Hang J. Choi, David Seligson, Anthony Tolcher Christopher A. Alabi, YuRn Yen, Jeremy D. Heidel& Antoni Ribas, Evidence of RNAi in humans from systemically administered siRNA via targeted nanoparticles. Nature 464, 1067–1070, **2010.**

[99] Hrkach J, Von Hoff D, Mukkaram Ali M, Andrianova E, Auer J, Campbell T, De Witt D, Figa M, Figueiredo M, Horhota A, Low S, McDonnell K, Peeke E, Retnarajan B, Sabnis A, Schnipper E, Song JJ, Song YH, Summa J, Tompsett D, Troiano G, Van Geen Hoven T, Wright J, LoRusso P, Kantoff PW, Bander NH, Sweeney C, Farokhzad OC, Langer R, Zale S., Preclinical development and clinical translation of a PSMA-targeted docetaxel nanoparticle with a differentiated pharmacological profile. Sci. Transl. Med. 4, 128ra139, **2012.**

[100] L. Nobs, F. Buchegger, R. Gurny and E. Allemann, Bioconjugate Chem., Biodegradable Nanoparticles for Direct or Two-Step Tumor Immunotargeting, *Bioconjugate Chem.*,17, 139–145, **2006.**

[101] L. Nobs, F. Buchegger, R. Gurny and E. Allemann, Poly (lactic acid) nanoparticles labeled with biologically active Neutravidine for active targeting, Eur. J. Pharm. Biopharm., 58, 483–490, **2004.**

[102] J. Willuda, A. Honegger, R. Waibel, P. A. Schubiger, R. Stahel, U. Zangemeister-Wittke and A. Pluckthun, High Thermal Stability Is Essential for Tumor Targeting of Antibody Fragments: Engineering of a Humanized Anti-epithelial Glycoprotein-2 (Epithelial Cell Adhesion Molecule) Single-Chain Fv Fragment, Cancer Res., 59, 5758–5767, **1999.**

[103] V. Cortez-Retamozo, N. Backmann, P. D. Senter, U. Wernery, P. De Baetselier, S. Muyldermans and H. Revets, Efficient Cancer Therapy with a Nanobody-Based Conjugate, Cancer Res., 64, 2 853–2857, **2004.**

[104] C. H. Choi, C. A. Alabi, P. Webster and M. E. Davis, Mechanism of active targeting in solid tumors with transferrin-containing gold nanoparticles, Proc. Natl. Acad. Sci. U. S. A., 107, 1235–1240, **2010.**

[105] T. P. Thomas, R. Shukla, A. Kotlyar, B. Liang, J. Y. Ye, T. B. Norris and J. R. Baker, Jr., Dendrimer−Epidermal Growth Factor Conjugate Displays Superagonist Activity, Biomacromolecules, 9, 603–609,**2008.**

[106] B. Cui, C. Wu, L. Chen, A. Ramirez, E. L. Bearer, W. P. Li, W. C. Mobley and S. Chu, One at a time, live tracking of NGF axonal transport using quantum dots, Proc. Natl. Acad. Sci. U. S. A., 104, 13666–13671, **2007.**

[107] F. X. Gu, R. Karnik, A. Z. Wang, F. Alexis, E. Levy-Nissenbaum, S. Hong, R. S. Langer and O. C. Farokhzad, Targeted nanoparticles for cancer therapy, Nano Today, 2, 14–21, **2007.**

[108] R. Brissette, J. K. Prendergast and N. I. Goldstein, Identification of cancer targets and therapeutics using phage display, Curr. Opin. Drug Discovery Dev., 9, 363–369, **2006.**

[109] D. N. Krag, G. S. Shukla, G. P. Shen, S. Pero, T. Ashikaga, S. Fuller, D. L.Weaver, S. Burdette-Radoux and C. Thomas, Selection of tumor-binding ligands in cancer patients with phage display libraries, Cancer Res., 66, 7724–7733, **2006.**

[110] J. S. Desgrosellier and D. A. Cheresh. Integrins in cancer: biological implications and therapeutic opportunities. Nat. Rev. Cancer, 10, 9–22, **2010.**

[111] D. S. Wilson and J. W. Szostak, *In vitro* selection of functional nucleic acids. Annu. Rev. Biochem., 68, 611–647, **1999.**

[112] C. Tuerk and L. Gold, Science, Systematic evolution of ligands by exponential enrichment: RNA ligands to bacteriophage T4 DNA polymerase., 249, 505–510, **1990.**

[113] J. Guo, X. Gao, L. Su, H. Xia, G. Gu, Z. Pang, X. Jiang, L. Yao, J. Chen and H. Chen, Aptamer-functionalized PEG-PLGA nanoparticles for enhanced anti-glioma drug delivery, Biomaterials, 32, 8010–8020, **2011.**

[114] A. P. Drabovich, M. V. Berezovski, M. U. Musheev and S. N. Krylov, Anal. Chem., Selection of smart small-molecule ligands: the proof of principle**,** 81, 490–494, **2009.**

[115] M. Talekar, J. Kendall, W. Denny and S. Garg, Targeting of nanoparticles in cancer: drug delivery and diagnostics.Anti-Cancer Drugs, 22, 949–962, **2011.**

[116] A. R. Hilgenbrink and P. S. Low, Folate receptor-mediated drug targeting: from therapeutics to diagnostics, J. Pharm. Sci., 94, 2135–2146, **2005.**

[117] F. Gu, L. Zhang, B. A. Teply, N. Mann, A. Wang, A. F. Radovic- Moreno, R. Langer and O. C. Farokhzad, Precise engineering of targeted nanoparticles by using self-assembled biointegrated block copolymers, Proc. Natl. Acad. Sci. U. S. A., 105, 2586–2591, **2008.**

[118] M. Hashida, M. Nishikawa, F. Yamashita and Y. Takakura, Cell-specific delivery of genes with glycosylated carriers, Adv Drug Delivery Rev., 52, 187–196, **2001.**

[119] X. Li, H. Zhou, L. Yang, G. Du, A. S. Pai-Panandiker, X. Huang and B. Yan, Enhancement of cell recognition *in vitro* by dual-ligand cancer targeting gold nanoparticles, Biomaterials, 32, 2540–2545, **2011.**

[120] J. M. Bergen, H. A. von Recum, T. T. Goodman, A. P. Massey and S. H. Pun, Gold nanoparticles as a versatile platform for optimizing physicochemical parameters for targeted drug delivery, Macromol. Biosci., 6, 506–516, **2006.**

[121] Valencia, Pedro M; Pridgen, Eric M; Perea, Brian; Gadde, Suresh; Sweeney, Christopher; Kantoff, Philip Wayne; Bander, Neil H; Lippard, Stephen J; Langer, Robert S.; Karnik, Rohit; Farokhzad, Omid Cameron, Synergistic cytotoxicity of irinotecan and cisplatin in dual-drug targeted polymeric nanoparticles. Nanomedicine 8, 687–698, **2013.**

[122] Liang Ma, Manish Kohli, and Andrew Smith, Nanoparticles for combination drug therapy. ACS Nano 7, 9518–9525, **2013.**

[123] E. Kluza, D. W. van der Schaft, P. A. Hautvast, W. J. Mulder, K. H. Mayo, A. W. Griffioen, G. J. Strijkers and K. Nicolay, Synergistic targeting of alphavbeta3 integrin and galectin-1 with heteromultivalent paramagnetic liposomes for combined MR imaging and treatment of angiogenesis**,** Nano Lett., 10, 52–58, **2010.**

[124] Real time PCR handbook, Life Technologies, **2012**.

[125] Maria Feoktistova, Peter Geserick, and Martin Leverkus, Crystal Violet Assay for Determining Viability of Cultured Cells, Cold Spring Harb Protoc; **2016.**

[126] Veerle Vandersickel a, Jacobus Slabbert b, Hubert Thierens a, Anne Vral, Comparison of the colony formation and crystal violet cell proliferation assays to determine cellular radiosensitivity in a repair deficient MCF10A cell line, Radiation Measurements 46 72-75, **2011.**

[127] Khan A, Gillis K, Clor J, Tyagarajan K, Simplified evaluation of apoptosis using the Muse cell analyzer, Postepy Biochem. 58(4):492-6, **2012.**

[128] Weiqiang Zhou, Xiuyan Feng, Han Han, Shanchun Guo, Guangdi Wang, Synergistic e ects of combined treatment with histone deacetylase inhibitor suberoylanilide hydroxamic acid and TRAIL on human breast cancer cells, Sci. Rep. 6, 28004, **2016.**

[129] EMD Millipore Protocols, Precise and Accurate Counts and Viability Measurements Across Multiple Cell Lines Using the Muse Cell Count & Viability Assay, *BioTechniques*, 52, 3, 200–203, **2012.**

[130] Wyllie AH, et al. Cell Death: The significance of apoptosis. Int Rev Cytol. 68:251-306, **1980.**

[131] Rudin CM, Thompson CB. Apoptosis and disease: Regulation and clinical relevance of programmed cell death. Ann Rev Med. 48:267-281, **1997.**

[132] Fadok VA, et al. Exposure of phosphatidylserine on the surface of apoptotic lymphocytes triggers specific recognition and removal by macrophages. J Immunol. 148:2207-2216, **1992.**

[133] Khan A., Gillis K., Clor J., Tyagarajan K., Simplified evaluation of apoptosis using the Muse cell analyzer, Postepy Biochem. ;58(4):492-6, **2012.**

[134] Vermeulen K, Van Bockstaele DR, Berneman ZN. The cell cycle: a review of regulation, deregulation and therapeutic targets in cancer. Cell Prolif. 36:131–149, **2003.**

[135] Alberts B, Johnson A, Lewis J, et al. Molecular Biology of the Cell. 4th edition. New York: Garland Science; **2002.**

[136] Michael Brown and Carl Wittwer, Flow Cytometry: Principles and Clinical Applications in Hematology, Clinical Chemistry 46:8(B), 1221–1229, **2000.**

[137] Li, X. and Z. Darzynkiewicz, Labeling DNA strand breaks with BrdUTP. Detection of apoptosis and cell proliferation. Cell Prolif. 28:572-579, **1995.**

[138] Miechel L.T. Zweers, Dirk W. Grijpma, Gerard H.M. Engbers, Jan Feijen, The preparation of monodisperse biodegradable polyester nanoparticles with a controlled size, J Biomed Mater Res B Appl Biomater., 66(2):559-66, **2003.**

[139] Budhian A, Siegel SJ, Winey KI. Haloperidol-loaded PLGA nanoparticles: systematic study of particle size and drug content. Int J Pharm., 336:367–375, **2007.**

[140] Navneet Sharma, Parshotam Madan, Senshang Lin, Effect of process and formulation variables on the preparation of parenteral paclitaxel-loadedbiodegradable polymeric nanoparticles: A co-surfactant study, Asian Journal of Pharmaceutical Sciences 11, 404–416, **2016.**

[141] J. Zhang, S. Rana, R.S. Srivastava, R.D.K. Misra, On the chemical synthesis and drug delivery response of folate receptor-activated, polyethylene glycol-functionalized magnetite nanoparticles, Acta Biomaterialia. 4 ,40–48, **2008.**

[142] Reinhard Meier, Tobias D. Henning, Sophie Boddington, Sidhartha Tavri, Sandeep Arora, Guido Piontek, Martina Rudelius, Claire Corot, Heike E. Daldrup-Link, Breast Cancers: MR Imaging of Folate-Receptor Expression with the Folate-Specific Nanoparticle P1133, Radiology: Volume 255: Number 2, **2010.**

[143] Tran TH, Choi JY, Ramasamy T, et al. Hyaluronic acid-coated solid lipid nanoparticles for targeted delivery of vorinostat to CD44 overexpressing cancer cells, Carbohydr Polym. 114:407–415, **2014.**

[144] El Bahhaj F, Denis I, Pichavant L, et al. Histone deacetylase inhibitors delivery using nanoparticles with intrinsic passive tumor targeting properties for tumor therapy. Theranostics. 6(6):795‑807, **2016.**

[145] Wang EC, Min Y, Palm RC, et al. Nanoparticle formulations of histone deacetylase inhibitors for effective chemoradiotherapy in solid tumors. Biomaterials. 51:208–215, **2015.**

[146] Elvin Blanco, Haifa Shen1, Mauro Ferrari, Principles of nanoparticle design for overcoming biological barriers to drug delivery, Nature Biotechnology, 33:9, 941-951, **2015.**

[147] Yamamoto Y, Nagasaki Y, Kato Y, Sugiyama Y, Kataoka K. Long-circulating poly (ethylene glycol)-poly (d, l-lactide) block copolymer micelles with modulated surface charge. J. Control. Release 77: 27–38, **2001.**

[148] Zhang XQ, Xu X, Bertrand N, Pridgen E, Swami A, Farokhzad OC. Interactions of nanomaterials and biological systems: Implications to personalized nanomedicine, Advanced Drug Delivery Reviews 64:1363–1384, **2012.**

[149] Yanes RE, Tarn D, Hwang AA, Ferris DP, Sherman S, Thomas CR, Lu J, Pyle AD, Zink JI, Tamanoi F., Involvement of Lysosomal Exocytosis in the Excretion of Mesoporous Silica Nanoparticles and Enhancement of the Drug Delivery Effect by Exocytosis Inhibition. Small 9, 697–704, **2013.**

[150] Braz L, Rodrigues S, Fonte P, Grenha A, Sarmento B., Mechanisms of chemical and enzymatic chitosan biodegradability and its application on drug delivery, Biodegradable Polymers: Processing, Degradation and Applications, Nova Science Publishers, New York, USA. 325-364, **2011.**

[151] Dai J, Lin S, Cheng D, Zou S, Shuai X., Interlayer-crosslinked micelle with partially hydrated core showing reduction and pH dual sensitivity for pin-pointed intracellular drug release. Angew Chem Int Ed, 50:9404e8, **2011.**

[152] Sun Y, Zou W, Bian S, Huang Y, Tan Yb, Liang J, Fan Y, Zhang X. Bioreducible PAA-g-PEG graft micelles with high doxorubicin loading for targeted antitumor effect against mouse breast carcinoma. Biomaterials, 34:6818-28, **2013.**

[153] Brodie C, Blumberg PM, Regulation of cell apoptosis by protein kinase c delta. Apoptosis 8(1): 19–27, **2003.**

[154] Herbst RS, Khuri FR., Mode of action of docetaxel–a basis for combination with novel anticancer agents. Cancer Treat. Rev. 29: 407–415, **2003.**

[155] Swami R, Singh I, Jeengar MK, Naidu V-GM, Khan W, Sistla R., Adenosine conjugated lipidic nanoparticles for enhanced tumor targeting, International Journal of Pharmaceutics 486: 287–296, **2015.**

[156] Vermeulen K, Van Bockstaele DR, Berneman ZN, The cell cycle: a review of regulation, deregulation and therapeutic targets in cancer, Cell Prolif. 36: 131–149, **2003.**

[157] Hartwell LH, Kastan MB. Cell cycle control and cancer, Science 266:1821-1828, **1994.**

[158] Evan GI, Vousden KH. Proliferation, cell cycle and apoptosis in cancer, Nature 411: 342-348, **2001.**

[159] Salazar, M.D., Ratnam, M., The folate receptor: What does it promise in tissue-targeted therapeutics? Cancer Metastasis Rev., 26:141. **2007.**

[160] Tavassolian F, Kamalinia G, Rouhani H, Amini M, Ostad SN, Khoshayand MR, Atyabi F, Tehrani MR, Dinarvand R. Targeted poly (L-γ-glutamyl glutamine) nanoparticles of docetaxel against folate over-expressed breast cancer cells, Int J Pharm.,467(1-2):123-38, **2014.**

[161] Haimei Chen, Richard Ahn, Jeroen Van den Bossche, David H. Thompson, and Thomas V. O'Halloran, Folate-mediated intracellular drug delivery increases the anticancer efficacy of nanoparticulate formulation of arsenic trioxide, Mol Cancer Ther., 8(7): 1955–1963, **2009.**

[162] Reinhard MeierTobias D. Henning, Sophie Boddington, Sidhartha Tavri, Sandeep Arora, Guido Piontek, Martina Rudelius, Claire Corot, Heike E. Daldrup-Link, Breast Cancers: MR Imaging of Folate-Receptor Expression with the Folate-Specific Nanoparticle P1133, Radiology, 255:2, 527-535, **2010.**

[163] Knutson, A.K., Welsh, J., Taylor, T., Roy, S., Wang, W.L.W. and Tenniswood, M. Comparative effects of histone deacetylase inhibitors on p53 target gene expression, cell cycle and apoptosis in MCF-7 breast cancer cells. Oncol. Rep., 27:849–853, **2012.**

[164] Chatterjee N, Wang WLW, Conklin T, Chittur S, Tenniswood M. Histone deacetylase inhibitors modulate miRNA and mRNA expression, block metaphase, and induce apoptosis in inflammatory breast cancer cells. Cancer Biology & Therapy7:658–671, **2013.**

SUPPLEMENTARY FIGURES and TABLES

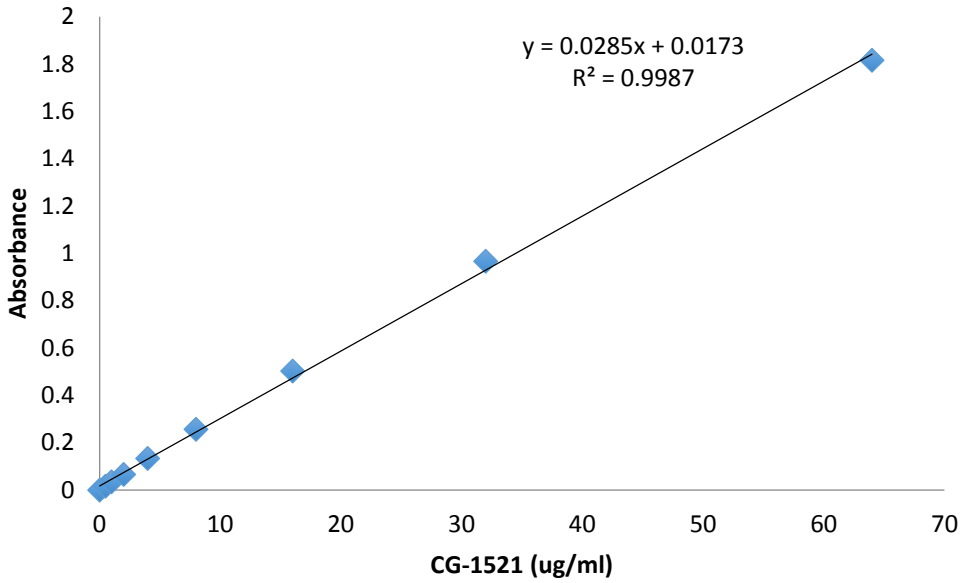

Figure 1. Calibration curve of CG-1521

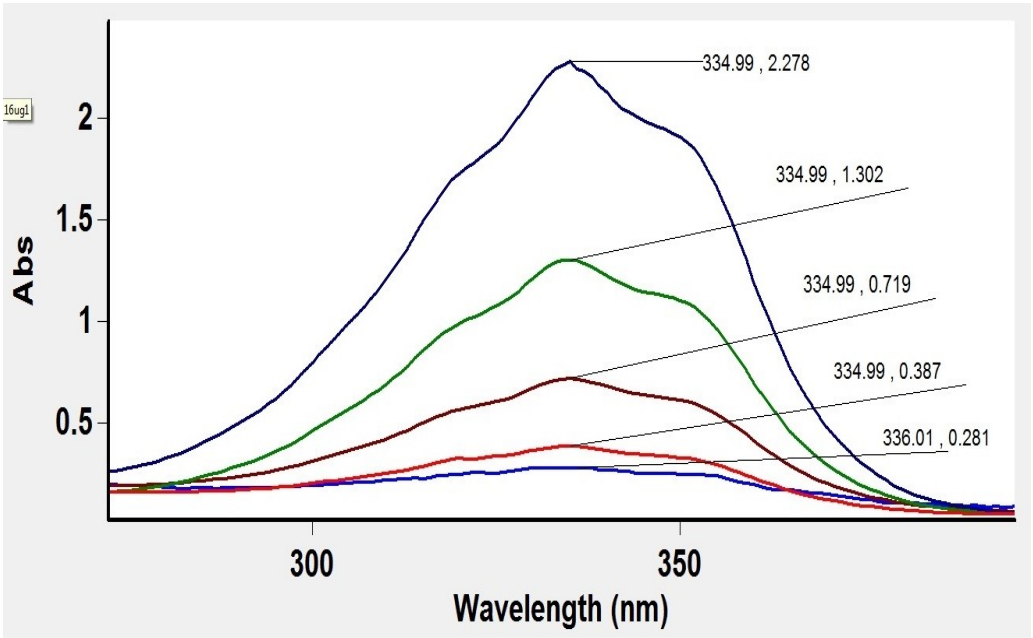

Figure 2. UV-Vis absorption spectra of the CG-1521

Table 1. The effect of formulation parameters on nanoparticle size distribution

Sample	Starch Concentration (%)	PVA Concentration (%)	Homogenization Rate (rpm)	Particle Size (nm)	Polydisperity Index (PDI)
1*	2	2	24000	180.0	0.138
2	3	2	24000	205.1	0.182
3	4	2	24000	455.0	0.354
4	2	0.5	24000	561.6	0.546
5	2	1	24000	347.7	0.322
6	2	2	12000	363.0	0.381
7	2	2	6000	512.8	0.478

EKLER

EK 1: Publications Related to the Thesis

Esma Alp, Fehmi Damkaci, Eylem Güven, Martin Tenniswood, Starch nanoparticles for delivery of histone deacetylase inhibitor CG-1521 in breast cancer treatment, International Journal of Nanomedicine, 14:1335–1346, 2019.

EK 2: Presentation Related to the Thesis

Esma Alp, Martin Tenniswood, Eylem Güven, Fehmi Damkaci, Starch nanoparticles for delivery of histone deacetylase inhibitor CG-1521 in breast cancer treatment, Applied Pharmaceutical Nanotechnology, October 4, 2017, Broad Institute of Harvard and MIT, Cambridge, MA.